A Mechanistic Investigation Into the Photochemistry of an Iron(0) Complex in C-Cl, C-H, and C-F Bond Activation

A DISSERTATION
SUBMITTED TO THE FACULTY OF
UNIVERSITY OF MINNESOTA
BY

Emily Jane Pelton

IN PARTIAL FULFILLMENT OF THE REQUIREMENTS
FOR THE DEGREE OF
DOCTOR OF PHILOSOPHY

David A. Blank, Co-advisor
Kristopher McNeill, Co-advisor

August 2013

Acknowledgements

To my advisors, David Blank and Kris McNeill: Thank you for supporting me for the past five years. You have offered me opportunities that have expanded my horizons, encouraged me to follow my interests and passions, and through all of it have provided me considerable insight and support to reach my goals. I have learned so much from both of you that I will keep with me forever.

To my Blank group boys: You welcomed me into your group, complete with musical theater soundtracks and a glovebox, and have made the past three years an exciting and entertaining place to work and learn. Our group parties, wing challenges, and informal discussions have made every day a blast, and I will miss each of you. I was thinking about leaving one of my *Glee* posters behind for you to remember me, but I thought better of it.

To the McNeill group, especially KT and EEM: My first two years of graduate school were as incredible as they were because you taught and trained me and gave me insight into the grad school experience from so many views. I especially enjoyed our coffee adventures and trip to San Franscisco, and I will especially remember all the fun we had in lab together.

To the Lu group, who, without any obligation to do so, welcomed me into their group and literature club meetings, offered insight into research problems, and always listened: You will never know how often you saved my day and how generous you all were with your time and energy. I am forever thankful that I was lucky enough to interact with you as often as I did. Maybe I will donate a *Glee* poster to you.

To my friends: Without you, I would not have been able to make it through a single day of grad school, much less five years. Words cannot express how meaningful each one of you has been to me throughout this entire experience, and I will forever be grateful for your support, understanding, and insight. I give special thanks to the ladies of Tit for Tat Brewery for being exceptional women, scientists, and friends!

To E: Thank you for being awesome! You made me laugh and smile when I didn't want to, and you always reminded me that I could do it when I didn't think I could. I truly could not have accomplished this without your support and encouragement!

And finally, to my parents, Tim and Cindy, my sister, Ally, and my family: You all believed in me when I forgot to believe in myself and reminded me why I did this in the first place. You've been my people since the *very* beginning, and I thank you for being there when I needed you the most. I love you all.

Table of Contents

List of Tables

List of Figures

List of Schemes

List of Equations

List of Abbreviations

A	ampere
BBO	beta barium borate
br	broad
C	Celsius
cDCE	*cis*-dichloroethylene
CE	chlorinated ethylene
CERCLA	Comprehensive Environmental Response, Compensation, and Liability Act
cm	centimeter
CW	continuous wave
Cy	cyclohexyl
δ	chemical shift
d	doublet
DCE	dichloroethylene
dddd	doublet of doublet of doublet of doublets
dmpe	1,2-bis(dimethylphosphino)ethane
dmpm	dimethylphosphinomethane
ε	molar absorptivity
e^-	electron
Φ	quantum yield
FB	fluorobenzene
fs	femtosecond
fwhm	full width-half maximum
g	gram
GC	gas chromatography
GC-MS	gas chromatography-mass spectrometry
h	hour
h	Planck's constant
Hz	hertz
I	light flux
i.d.	interior diameter
J	coupling constant
k	rate constant
kcal	kilocalorie
kHz	kilohertz
L	liter
λ	wavelength
LED	light-emitting diode
LFP	laser flash photolysis
M	molar
m	meter
m	multiplet
mΔOD	change in milliabsorbance units
Me	methyl
mg	milligram

MHz	megahertz
min	minute
μJ	microjoule
μL	microliter
mL	milliliter
mM	millimolar
μm	micrometer
mm	millimeter
μmol	micromole
mmol	millimole
mol	mole
mPa	millipascal
mTorr	millitorr
mV	millivolt
μW	microwatt
mW	milliwatt
m/z	mass-to-charge ratio
ν	frequency
Nd:YAG	neodymium-doped yttrium aluminum garnet
nm	nanometer
NMR	nuclear magnetic resonance
Np	2-naphthyl
NPL	National Priorities List
ns	nanosecond
Ω	ohm
OAc	acetate
PCE	perchloroethylene
PFOA	perfluorooctanoic acid
PFOS	perfluorooctanesulfonic acid
Ph	phenyl
phen	1,10-phenanthroline
ppm	parts per million
PRB	permeable reactive barrier
ps	picosecond
Q	quality-factor
s	second
s	singlet
SHE	standard hydrogen electrode
t	time
t	triplet
^{t}Bu	*tert*-butyl
TCE	trichloroethylene
tDCE	*trans*-dichloroethylene
THF	tetrahydrofuran
$^{t}SiP_3$	tris(dimethylphosphinomethyl)tertbutylsilane

UV	ultraviolet
V	volt
VC	vinyl chloride
Vis	visible
v/v	volume to volume
W	watt
ZVI	zero-valent iron
1,1-DCE	1,1-dichloroethylene

Chapter 1

Introduction

1.1 Halogenated organics in the environment

In recent years, a variety of halogenated compounds have been employed for myriad household and industrial uses. Halogenated hydrocarbons have been introduced into common application as components of dry cleaning solvents and household cleaners, among others;[1, 2] although these compounds are effective in consumer products, their introduction has had a considerably negative environmental impact.[3] Many of these chemicals have been detected in groundwater systems due to improper disposal or chemical runoff,[4, 5] and once in these water systems, halogenated compounds can undergo a variety of reactions.[6] Both the chemicals themselves and the products of such reactions can be hazardous to human and ecosystem health.

One particular subclass of halogenated hydrocarbons that is known to pose a considerable risk to organisms is chlorinated ethylenes (CEs). According to the U.S. Environmental Protection Agency, vinyl chloride (VC), trichloroethylene (TCE), and tetrachloroethylene (PCE) are ranked 4th, 16th, and 33rd, respectively, among the most hazardous materials found at sites on the U.S. National Priorities List (NPL).[7] These compounds, along with the three dichloroethylene (DCE) species, have been implicated in the occurrence of a variety of health effects in exposed workers, such as increased risk of liver cancer,[8, 9] spontaneous abortion,[10, 11] and scleroderma.[12-14]

In addition to chlorinated hydrocarbons, fluorinated hydrocarbons have been gaining in use and thus have also been detected in humans throughout the world. The source of these organofluorine compounds in people has been linked to occupational exposure[15] and natural sources.[16, 17] Studies have linked exposure to fluorinated organics to cancer and death in rats and monkeys,[17] but fewer studies have been conducted to

examine the long-term effects of fluorinated organics to humans. However, detection of fluorinated organics in human serum from a variety of populations has led to increased awareness of the potential health effects of these compounds.[18] Because these compounds have been detected in a variety of aquatic systems, most commonly from runoff from insecticides and pesticides,[19] it is important to study how these compounds can be removed from these systems to help mitigate their effects on human populations.

1.2 Current remediation technologies

CEs and fluorinated organics are known to persist in groundwater systems, posing a continual threat to the industries, people, and organisms that depend on them.[1, 2, 20] As such, discovering and developing remediation mechanisms is important. Several metalloproteins, including cobalamin,[21-23] hematin,[24] and cytochrome P450,[25, 26] have been shown to dechlorinate and defluorinate organic compounds in the environment and have been employed in biological remediation. These proteins typically include a macrocyclic structure and a metal center that serves as an active site for reaction with CEs and fluorinated substrates (Figure 1.1).[24]

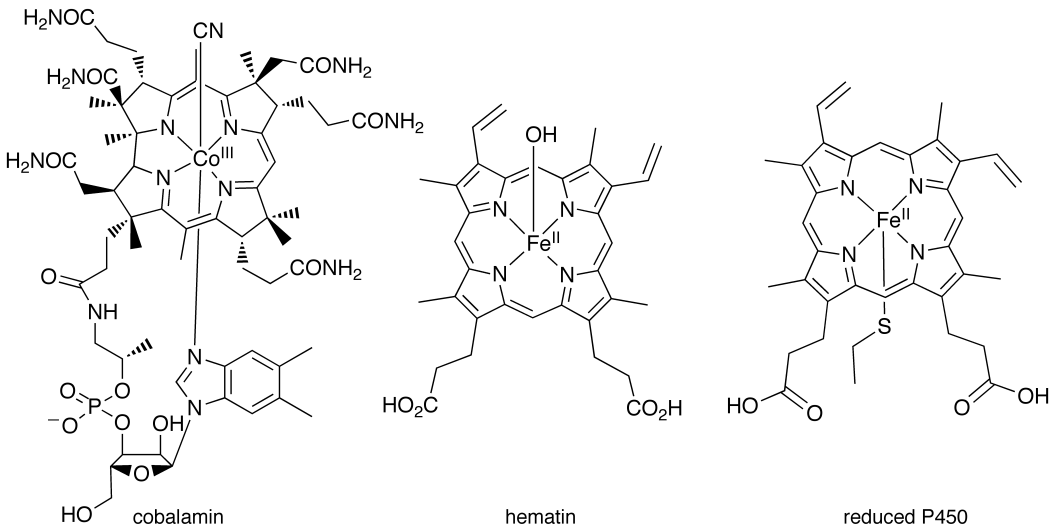

Figure 1.1. Active sites of proteins employed in biological remediation processes.

The majority of mechanistic studies of these proteins have focused on catalytic reductive dehalogenation as the primary degradation pathway.[24, 27] For instance, cobalamin, a Co-corrin protein, reductively defluorinates perfluorooctane sulfonate (PFOS) in the presence of Ti^{III} citrate, a common reductant in biological systems.[23] Similarly, hematin, an Fe-porphyrin protein, has been shown to catalyze the reaction of TCE sequentially to *cis*-DCE (cDCE) and VC in the presence of Ti^{III} citrate.[24] Conversely, cytochrome P450, another Fe-porphyrin protein, has been shown to oxidatively dehalogenate both fluorinated and chlorinated pollutants.[26, 28] With these different approaches to dehalogenation, biological remediation applications are available for employment in an array of environments.

In addition to biological remediation mechanisms, physically engineered methods of dehalogenation continue to be active areas of research. In 1980, the U.S. passed the Comprehensive Environmental Response, Compensation, and Liability Act (CERCLA) that established Superfund sites, which are locations throughout the U.S. known to have

significant groundwater contamination.[1] To decontaminate these groundwater systems, pump-and-treat methods were employed at the majority of sites.[29] Pump-and-treat methods work by pumping contaminated groundwater from the water table into a well, treating the water with air stripping, sorption to activated carbon, or a noble metal catalyst, and then pumping the cleaned water back into the ground (Figure 1.2).[30-33] In the early 1990s, the groundwater systems at Superfund sites that employed pump-and-treat remediation mechanisms were found to still fall short of the standards for drinking water set forth by CERCLA.[28] Additionally, pump-and-treat methods are extremely energy-intensive, as they require energy to both pump in contaminated water and discharge treated water and the presence of H_2 gas.[31] As such, permeable reactive barriers (PRBs) were introduced as alternatives to pump-and-treat methods.

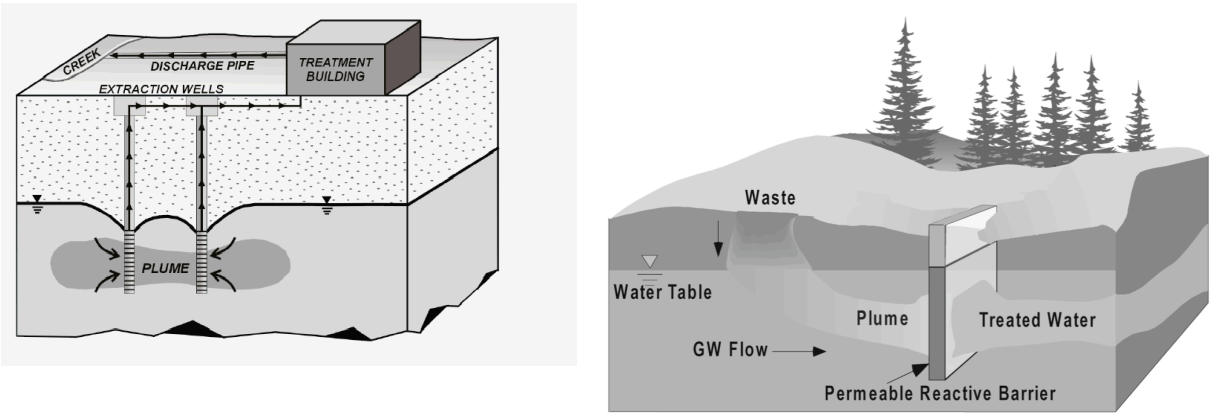

Figure 1.2. Illustrations of a pump-and-treat approach (left)[34] and of an installed PRB (right).[35]

PRBs are zones of reactive materials that are installed downstream of a hydraulic gradient and perpendicular to the natural flow of groundwater (Figure 1.2). By constructing these barriers downstream, contaminated groundwater is passively transported through the reactive media, eliminating the need for the active transport

inherent to pump-and-treat methods. The reactive medium employed in the majority of PRBs is zero-valent iron (ZVI); in addition to its low cost and abundance, an advantage to using ZVI is that its reactivity allows for multiple common groundwater contaminants to be treated simultaneously.[36] For instance, a PRB in Elizabeth City, North Carolina, was installed to remove both TCE and Cr from the groundwater.[37] The ZVI employed in the system was found to be effective against these contaminants in both laboratory tests and field studies;[36] the ability of a single metal to treat two completely different contaminants is unparalleled.

1.3 Fe^0 model system studies with fluorinated organics

Because zero-valent iron has been used in groundwater remediation, it is important to study the role of Fe^0 in dehalogenation of fluorinated organics. Few studies have examined this process in depth, likely due to the general inertness of the C-F bond.[38] The majority of studies have focused on the reaction of PFOS in aquatic systems, as it is ubiquitous in aquatic environments and has been detected in a variety of organisms.[17, 38] The principal goal of these defluorination studies is to generate F^- as a final product, as reaction with Ca^{2+} in water treatment is known to generate environmentally benign CaF_2.[39] Hori *et al*. found that the degradation of PFOS in subcritical water occurred in the presence of Fe^0 powder to generate F^- ions in aqueous solution, while no degradation occurred without iron.[40] Subsequent studies of more bioaccumulative perfluorinated substrates also demonstrated that addition of Fe^0 to subcritical water showed generation of F^-.[41] In these studies, the fluorinated substrate adsorbed to the metal surface, a process that plays an important role in groundwater remediation in PRBs.[36] Reductive defluorination was determined to be the primary mechanism for these reactions,[38] but

because few studies have specifically examined the role of any Fe^0 species in defluorination of groundwater contaminants, more investigation is necessary to evaluate the reaction between Fe^0 and fluorinated substrates.

1.4 Fe^0 model system studies with CEs

Due to its frequent use as an active component of PRBs, zero-valent iron has been studied extensively for its reaction with CEs. The majority of these studies have focused on employing bulk iron, a common component of PRB installations.[37, 42] Studies of the bulk iron-CE reaction have been evaluated in multiple systems, including batch and column experiments,[42-44] as well as field studies,[36, 45] rendering the efficacy of Fe^0 for dechlorination of CEs to be generally accepted. In these studies, Fe^0 has been shown to react with all six CE congeners to initially form lower-chlorinated CEs[46] and chlorinated acetylenes.[47, 48] These intermediate species react further with Fe^0 to give final products ethylene, ethane, acetylene, and C_4 products (Figure 1.3).[46]

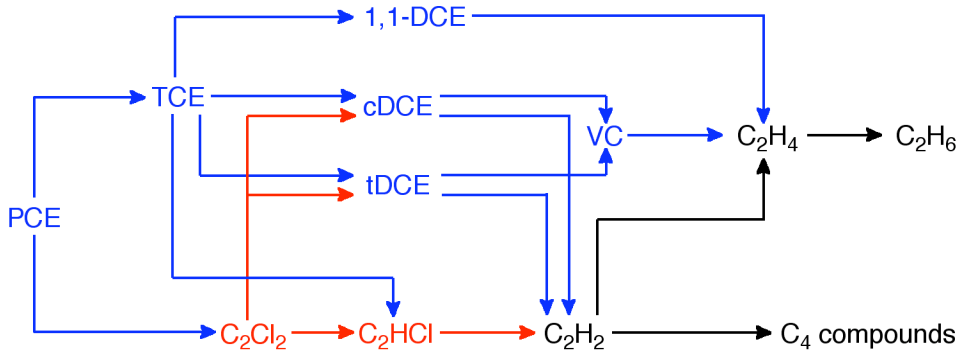

Figure 1.3. Reported transformations of CEs (adapted from ref. 46) The blue pathways are transformations from CEs, red pathways are transformations from chlorinated acetylenes, and black pathways are transformations from hydrocarbons.

These findings justify the widespread use of Fe^0 in PRBs: not only does Fe^0 remove CEs, but the chlorinated intermediates generated are eliminated as well, yielding non-chlorinated, and therefore less hazardous, final products.

1.4.1 Proposed mechanisms

While the studies in the literature have agreed on the extensive applicability of Fe^0 in the dechlorination of CEs, several uncertainties have been presented in the literature, necessitating further investigation. The major question pertains to the mechanism of degradation, as no single proposed mechanism has gained widespread acceptance. Several mechanisms have been proposed for the fundamental dechlorination of CEs by Fe^0 (Scheme 1.1).

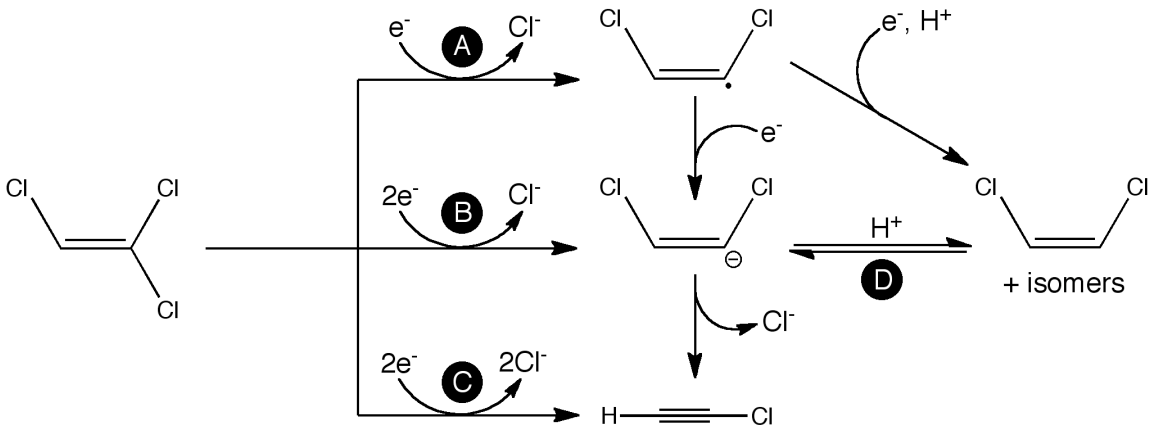

Scheme 1.1. Proposed mechanisms for the dechlorination of CEs by Fe^0.[46, 48] Pathways **A-C** refer to the dechlorination of TCE. **A** and **B** are the 1- and 2-electron hydrogenolysis pathways, respectively, and **C** is the *vic*-Cl_2-elimination pathway. **D** is the proposed deprotonation pathway of cDCE.

The most commonly proposed mechanisms are hydrogenolysis (**A** and **B**) and *vic*-Cl_2-elimination (**C**), known commonly in environmental science literature as "reductive elimination," although it is not the same as the pathway by the same name known in organometallic transformations.[46] A third pathway, deprotonation (**D**), is also proposed to be a possible route for dechlorination of CEs, although this pathway is not possible with PCE, which has no hydrogens available. Deprotonation would generate the same products as *vic*-Cl_2-elimination pathways. In collecting and analyzing data that supports

or challenges a particular mechanism of degradation, it is important to understand that a single mechanistic pathway may not apply to all CEs dechlorinated by Fe^0.

One contentious issue among research groups is the effect that the degree of chlorination has on the rate of degradation. Several studies have found that increasing the degree of chlorination increases the rate of degradation by Fe^0.[42, 49, 50] If the dechlorination mechanism proceeds via hydrogenolysis, it is predicted that more highly chlorinated CEs will react faster than less chlorinated CEs. This prediction is based on reduction potentials, as it is easier to reduce a compound with a lower potential (Table 1.1).

Table 1.1. Structures and reduction potentials of CEs.[51]

	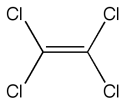	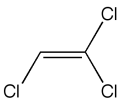	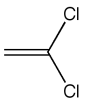	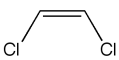	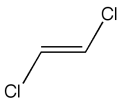	
CE	PCE	TCE	1,1-DCE	cDCE	tDCE	VC
reduction potential vs. SHE (mV)	-598	-674	-802	-955	-1012	-1141

However, other studies have provided evidence to the contrary and support a *vic*-Cl_2-elimination pathway, concluding that the rate of degradation *decreases* with increased degree of chlorination.[45, 46]

Most studies evaluating the dechlorination of CEs by Fe^0 have focused on heterogeneous systems. While studying the behavior of bulk iron is most applicable to assessment of PRBs, the heterogeneity of these systems introduces several complications for fundamental understanding of the reaction between Fe^0 and CEs, such as sorption, surface area, and reactive sites. For instance, sorption of a CE to the iron surface, the first step in a heterogeneous reaction,[46] is unique to each CE congener.[52, 53] These

differences can be readily considered and accounted for if the reaction being studied is solely between the parent CE and Fe^0; however, as stated previously, the byproducts of these reactions are often lower chlorinated CEs. Without accounting for these additional sorption processes, the overall reactivity observed and reported may be skewed.[46] Thus, it is essential to account for processes to accurately characterize and measure the observed reactivity.

As clearly evidenced by the previous discussion, the specific mechanistic details of the reactions between Fe^0 and CEs have yet to be settled, making it more difficult to optimize ZVI as a powerful groundwater remediation tool. However, by using an analogous homogeneous system, in which complicating effects of sorption processes and surface chemistry are eliminated while the dechlorination pathways are maintained, a greater mechanistic insight will be obtained for the system as a whole. This approach also offers opportunity for increased control over reaction conditions and permits new and additional characterization techniques to be employed while probing the reaction mechanism and identifying intermediates.

1.4.2 Homogeneous Fe^0 model systems

There are relatively few Fe^0 complexes reported in the literature that have been shown to activate sp^2 C-Cl bonds. For instance, $Fe_2(CO)_9$ has been shown to oxidatively insert into the C-Cl bond of chlorobutadienes.[54] Formally an Fe^0 species, an Fe center of the carbonyl compound inserts into the C-Cl bond to form a relatively stable Fe^{II} complex. A similar approach was employed by Shi *et al.* through the use of a P ligand-supported Fe^0 complex, $Fe(PMe_3)_4$, that activates aryl C-Cl bonds.[55] While the researchers claimed that the complex was an Fe^0 analogue, it is unlikely that the 16-e^-

complex was the only species being studied. The authors use $Fe(PMe_3)_4$ as the Fe^0 source, but considering the electron deficiency of this complex, it is unlikely that this was the species measured on a gram scale. Instead, the 16-e$^-$ Fe^0 complex was likely in equilibrium with an activated, 18-e$^-$ Fe^{II} complex, $Fe(PMe_3)_3(PMe_2CH_2)H$[56, 57] (Scheme 1.2).

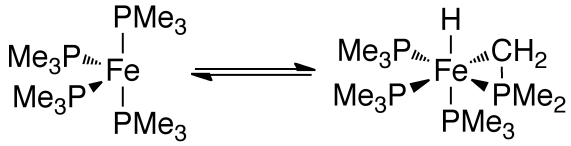

Scheme 1.2. Equilibrium of $Fe(PMe_3)_4$ with the activated ligand complex.

The activation of intramolecular C-H bonds by an Fe complex supported by phosphorus ligands has much precedence in the literature, especially for ligands that have P-methyl moieties.[58, 59] This equilibrium persists even at -80°C;[58] thus, it cannot be decisively known if the aryl C-Cl activation observed is due to the reaction with the Fe^0 species or the activated Fe^{II} complex. Perhaps the use of more sterically crowded P ligands would limit the activation of the ligand by the Fe center and offer an opportunity to study the reaction between the Fe^0 complex and the aryl C-Cl bond alone.

While the $Fe(PMe_3)_4$ complex may be in equilibrium with an activated-ligand, Fe(II) complex, there has been evidence that a reactive 16-e$^-$ Fe^0 species can be generated from an 18-e$^-$ Fe^{II} complex. Specifically, thermolysis of $(dmpe)_2FeNpH$ (dmpe = 1,2-bis(dimethylphosphino)ethane; Np = 2-naphthyl) has been shown to generate a highly reactive, 16-e$^-$ intermediate, $(dmpe)_2Fe$, and neutral naphthalene.[56, 57] The intermediate then undergoes oxidative insertion with a substrate to generate a more stable, 18-e$^-$ complex. The intermediate generated from the naphthyl complex has been well studied

for its ability to activate a variety of C-H bonds,[56, 57, 60, 61] but the studies with C-Cl bonds have been limited.[60] By generating the Fe^0 species as an intermediate, the reactivity of the species can be manipulated by monitoring the temperature of the reaction, allowing for increased control of the reactant and substrate.

Of the Fe^0 species studied for C-Cl bond activation, the majority of the complexes have been supported by P ligands, likely due to the stabilizing interaction of the P ligand with the electron-rich metal center. The π-acid character of the phosphine ligands allows for stabilization with the Fe^0 center through backbonding. In addition to PMe_3 and dmpe ligands, dimethylphosphinomethane (dmpm) and tris(dimethylphosphinomethyl)tertbutylsilane ($^tSiP_3$) have also been shown to stabilize Fe^0 centers, and such complexes have been found to activate C-Cl bonds.[62] One such complex, $^tSiP_3$(dmpm)Fe, employs both ligands and has been shown to dechlorinate the CE-like 1,2-dichloro-3,3,3-trifluoropropene.[63] The active species is a five-coordinate, 18-e^- Fe^0 complex and is considerably different from the four-coordinate $Fe(PMe_3)_4$ and $(dmpe)_2Fe$ species. Dechlorination is proposed to occur via dissociation of one of the P ligand arms, forming a reactive 16-e^- species that can oxidatively insert into the C-Cl bond of the substrate to generate an 18-e^- Fe(II) species. This Fe(II) species then undergoes β-elimination to generate $^tSiP_3$(dmpm)$FeCl^+Cl^-$ and 3,3,3-trifluoropropyne, supporting a deprotonation or *vic*-Cl_2-elimination pathway.[63]

1.5 $(dmpe)_2FeH_2$ as an Fe^0 model system

The model system selected for the study of CE and fluorobenzene dehalogenation by Fe^0 employs a similar approach to the $(dmpe)_2$FeNpH system. A well-characterized Fe(II) complex, $(dmpe)_2FeH_2$, has been shown to generate a highly reactive, 16-e^-

intermediate, $(dmpe)_2Fe$, and H_2 gas when exposed to UV light.[57, 61, 64] Formally an Fe^0 species, $(dmpe)_2Fe$ has been shown to activate C-O, C-X, and sp, sp^2, and sp^3 C-H bonds to form Fe(II) species.[60, 61] Due to its previously observed proclivity to oxidatively insert into C-X bonds, it is likely that a similar insertion mechanism will be observed in reactions of $(dmpe)_2Fe$ and CEs and fluorobenzenes. But, because this complex has been shown to activate C-H bonds, while C-Cl or C-F activation is preferred in reactions aimed at the dehalogenation of substrates, investigation into the mechanism of reaction between $(dmpe)_2Fe$ and halogenated substrates is necessary to validate the applicability of this model. The preference for insertion into the vinyl C-Cl bond versus an sp^2 C-H bond is predicted: first, the bond strength of a C-Cl bond is less than that of an sp^2 C-H bond (91 versus 110 kcal/mol),[65] so C-Cl insertion is more energetically favorable. Also, reactions of $(dmpe)_2Fe$ with methyl iodide have shown formation of a $(dmpe)_2Fe(CH_3)I$ complex instead of a $(dmpe)_2Fe(CH_2I)H$ complex, supporting the prediction that C-X activation is more energetically favorable than C-H activation.[60] However, for the aryl C-X activation examined in the reaction with fluorobenzenes, the aryl C-F bond is stronger than the C-H bond (127 versus 113 kcal/mol).[65] The use of an Fe^0 model system may offer increased insight into the C-F activation, however energetically unfavorable, because bulk Fe^0 has been shown to defluorinate aryl C-F bonds.[66]

This model system has a number of advantages. First, $(dmpe)_2FeH_2$ is a well-studied system that has been employed extensively in C-H activation.[61, 64, 67] These detailed studies offer considerable insight into the types of reactions the complex undergoes, although there have been no studies focusing on the reaction with CEs or fluorobenzenes. Second, because the complex photochemically generates the transient

intermediate $(dmpe)_2Fe$, several spectroscopic methods become available for use: specifically, the reactive intermediate can be monitored by laser flash photolysis (LFP) and ultrafast laser spectroscopy. In the early 1990s, Whittlesey *et al.* conducted a series of LFP experiments that probed $(dmpe)_2Fe$ and its reactivity with a variety of substrates.[68] A third advantage to employing $(dmpe)_2Fe$ as a model system is that the Fe^0 species can be generated at specific and selected times. Such controlled generation allows for more regulation of what species can interact with the Fe^0 species and at what time. Additionally, controlling the time at which the Fe^0 species is generated allows for greater accuracy in kinetic studies.

There are some disadvantages to employing $(dmpe)_2Fe$ as a model system for Fe^0 in PRBs. First, while the fundamental reaction between Fe^0 and halogenated substrates can be studied by this model system, the reaction of Fe^0 with aqueous substrates cannot be, as $(dmpe)_2Fe$ is very air- and moisture-sensitive; thus, the effects of aquation on CE and fluorobenzene degradation cannot be studied with this model system. Second, $(dmpe)_2Fe$ is not a structural model for Fe^0. Because the Fe^0 species generated is a 16 e^- complex, it is a highly reactive species. Iron metal, on the other hand, is still Fe^0 but does not have the same reactivity because it is in its elemental state. Also, the inherent properties of bulk iron are not represented by a small molecule containing a single iron atom. These differences may be manifested in the reactivity of $(dmpe)_2Fe$ compared to Fe^0 in PRBs. Even though these differences are considerable, there are no better models that present themselves, and they are not predicted to adversely affect the study of the fundamental reaction with Fe^0 and CEs or fluorobenzenes.

1.6 Photochemistry of $(dmpe)_2FeH_2$

A common spectroscopic technique employed in physical inorganic experiments, laser flash photolysis (LFP) was developed in the 1960s for the study of reactive intermediates. While several experimental setups have been used in LFP studies, one of the most common employs pump-probe and time-resolved absorbance spectroscopies.[69] In general, the sample is prepared in a closed, transparent reaction vessel and the vessels placed into the observation cell. The pump, which in these original experiments was a Nd:YAG laser, is the source of the flash of light required to initiate the generation of the intermediate species and is filtered to select the wavelength and duration of the pump pulse.[69] The probe portion of the setup is typically a lamp that emits white light, such as a Xe arc lamp.[70] By varying the time delay between the pump pulse and the probe, the time required to generate the intermediate species can be determined. The use of a laser as the pump allows for access to time scales on the order of nano- to picoseconds.

Once the intermediate is generated, it is monitored by time-resolved absorbance spectroscopy experiments. The intermediate absorbs some or all of the light emitted by the probe, and its absorbance at a particular wavelength is detected.[69] Typically, the wavelength at which absorbance is measured is the λ_{max} for the species of interest. A kinetic trace can be collected by monitoring the decay of the intermediate over time, allowing for the lifetime of the intermediate to be calculated. Fitting these decays to integrated rate laws allows for determination of the rate constant for the studied reaction.[69]

As described previously, $(dmpe)_2Fe$ is generated by the photolysis of $(dmpe)_2FeH_2$. While several types of light and photochemical reaction conditions have

been shown to initiate the formation of this reactive intermediate, LFP offers several advantages for use in this system. First, LFP allows for the generation and subsequent monitoring of the reactive intermediate, the species that actually reacts with the CEs of interest, rather than the precursor species. LFP is unique in this regard, as other spectroscopic and analytical techniques cannot detect the 16-e^- intermediate due to its short lifetime. Second, this technique allows for kinetic data to be collected for reactions that occur on very short time scales. For instance, monitoring the reaction by NMR allows for time scales in the millisecond range, but, as previously mentioned, the lifetime of $(dmpe)_2Fe$ when pulsed by a laser is in the nanosecond range. Third, the kinetic traces generated by LFP analysis can be fit to combinations of different integrated rate laws, allowing for reactions of the parent CE and possible daughter CEs to be distinguished in analysis. Finally, the LFP-induced generation of $(dmpe)_2Fe$ has been well studied. In 1993, Whittlesey *et al.* published an extensive study of LFP-induced reactions of the intermediate with C-H bonds; this study offers considerable insight into the behavior of $(dmpe)_2Fe$ under LFP conditions.[68] This study concluded that $(dmpe)_2Fe$ was generated instantaneously and reacted on microsecond timescales, the limits of their experiment.[68]

While advantages exist to studying the photochemistry of $(dmpe)_2FeH_2$ with LFP, examining this iron complex on the ultrafast timescale can offer increased insight into the dynamics of the reaction. In order to study the reaction between Fe^0 and halogenated substrates, it is necessary to understand the fundamental generation of the formally Fe^0 $(dmpe)_2Fe$ upon irradiation with light and what happens when it reacts with C-X bonds. Whittlesey *et al*. were able to resolve generation of $(dmpe)_2Fe$ within 30 ns,[68] but the dynamics of the "trigger step", or release of H_2 from the iron center, remain largely

unknown. Examining this fundamental process on the ultrafast timescale will allow for increased understanding of the dynamics of generation of the Fe^0 model on the femto- and picosecond timescales.

1.7 Scope of thesis

The objective of this dissertation is the investigation of the photochemical generation of an Fe^0 model complex and its subsequent reactivity with C-Cl and C-F bonds. In the second chapter, the photochemical generation and ultrafast dynamics of an Fe^0 model complex is presented. The rate of H_2 escape in solvents of various viscosities, as well as the effect of H_2 versus D_2 release, is also discussed, as is the yield of geminate recombination of the Fe^0 complex and H_2 within the solvent cage. The third chapter employs the photochemically generated Fe^0 species to dechlorinate CE substrates. A mechanistic investigation was conducted, and a hydrogenolysis pathway was observed. Additionally, increased chlorination of the CE substrates was observed to lead to faster rates of dechlorination by the Fe^0 system. Finally, in the fourth chapter, C-F activation of fluorobenzene substrates by the parent Fe^{II} complex is presented. C-F activation was observed to occur via electron transfer within the solvent cage. Competitive C-H activation of nonperfluorinated substrates was observed when light was introduced into the system, similar to the oxidative addition mechanism mediated by the previously investigated Fe^0 species.

Chapter 2

Investigation of the ultrafast dynamics of $(dmpe)_2FeH_2$ and $(dmpe)_2FeD_2$ in pentane and tetradecane

2.1 Overview

The ultrafast dynamics of $(dmpe)_2FeH_2$ and $(dmpe)_2FeD_2$ were investigated using pump-probe laser spectroscopy. Irradiation at 266 nm generates 16-e^-, $(dmpe)_2Fe$, a reactive intermediate that absorbs at 400 nm, in less than 100 fs. Recombination of H_2 and D_2 with $(dmpe)_2Fe$ was observed to occur in approximately 3 ps in both pentane and tetradecane, consistent with recombination time scales observed with other small molecules. Recombination yields of H_2 and D_2 were larger in tetradecane than in pentane, consistent with solvent cage effects. In the same solvent, more D_2 recombined than did H_2, due to the mass effect of the dissociated group.

2.2 Introduction

The photodissociation and subsequent recombination of molecules in solution is important in developing a deeper understanding of the unique properties of these compounds. The seminal studies of this field came from the evaluation of I_2 dynamics in solution, especially the cage effect.[71, 72] Wood and Rabinowitch examined the photodissociation of I_2 and found that some I atoms recombined within the same solvation shell, limiting the number of I atoms that remain dissociated in solution. This observation was defined as the cage effect – the geminate recombination of dissociated atoms or molecules within a solvent cage.[72] In its most basic form, the cage effect has been described as a hole or space in the solvent matrix[73] where dissociated atoms or molecules are trapped and can more readily react before random or impulsive motion allows for reactive species to escape the solvent cage.[74]

The dynamics of atoms or molecules within a solvent cage and understanding the photolytic preparation of reactive intermediates can lend insight into the reactivity of photodissociated species. For instance, the rate and amount of geminate recombination within the solvent cage can offer insight into the fundamental processes occurring on very fast time scales. The geminate recombination rate of photodissociated I atoms from I_2 is 10-15 ps in CCl_4,[75] while larger molecules, such as Mo-Mo dimers, recombine in 5 ps.[76] Similarly, the recombination yield of species within the cage vary based on the species photodissociating, as values from 30% recombination for $Cr(CO)_6$ to 75% for ICN have been reported.[77, 78]

In addition to differences in the rates and yields of geminate recombination, the effect of the solvent on photodissociated species in solution is an important area of study.

Early studies by Booth *et al*. found that species recombine more quickly with increasing solvent viscosity,[79] and recent studies by Oelkers *et al*. have found that the efficiency of cage escape of Mo-Mo dimers decreases as solvent viscosity increases.[76]

While many studies have focused on the photodissociation dynamics of molecular dissociation products, such as those from photolysis of I_2 or Mo-Mo dimers, there has been increased interest into the photodissociation of inert small molecules, such as CO, N_2, or O_2, from metal centers, especially when these processes allow for increased reactivity. The majority of these studies have focused on the photodissociation dynamics of CO from a variety of metal centers. Early studies by Joly and Nelson evaluated the ultrafast dynamics of photodissociation of CO from $M(CO)_6$ (M = Cr, Mo, W) and observed that, instead of the several $M(CO)_x$ fragments formed from photodissociation in the gas phase, only one CO dissociates from the metal center in solution.[80] This control of CO photodissociation (dissociation of only one CO instead of several) from the metal center allowed for increased investigation into the dynamics of the process.

Once the CO dissociates from the metal center, several processes have been observed to occur. The simplest is geminate recombination within the solvent cage, which Lian *et al*. found to occur on a fast timescale (< 300 fs) for Group 6 hexacarbonyls in alkane solvents.[81] Another process is association of a solvent molecule to the generated metal fragment. Studies by Joly and Nelson with Group 6 hexacarbonyl complexes found that no significant solvent effects occurred within 350 fs but that the $M(CO)_5$ fragment combines with solvent and persists on the nanosecond timescale.[80, 82] A third process is bond activation, typically of a ligand on the metal center. Bechara *et al*. found that, after photodissociation of a CO ligand from the Fischer carbene complex

$(OC)_5W=C(OMe)Ph$, the complex rearranges to activate the C-H bond of the Me group on a nanosecond timescale.[83]

While these processes have been well defined for metal carbonyl systems, less is known about the photodissociation of H_2 from metal centers, important in developing an understanding of the unique properties of these compounds. Several metal hydrides have been shown to photodissociate H_2 under UV irradiation in the solution state. $[IrClH_2(PPh_3)_3]$ releases H_2 over 35 minutes,[84] while $RhClH_2(PCy_3)_2$ releases H_2 over several hours.[85] Whittlesey *et al*. found that $(dmpe)_2FeH_2$ and $(dmpe)_2RuH_2$ photodissociated H_2 on the millisecond and microsecond timescales, respectively.[68, 86] However, very little is known about the photodissociation of H_2 from metal centers on the ultrafast (femtosecond and picosecond) timescale in solution state.

In this study, the photodissociation of H_2 from $(dmpe)_2FeH_2$ on the ultrafast timescale is discussed. $(dmpe)_2FeH_2$ (dmpe = 1,2-bis(dimethylphosphino)ethane) has been shown to activate C-H[68] and C-X bonds[87] upon UV irradiation. Previous studies have reported dynamics on the millisecond timescale,[68] but no studies have examined its ultrafast dynamics. For instance, studying the ultrafast dynamics of geminate recombination is important to understanding the initial steps in the photochemistry of $(dmpe)_2Fe$, presented in Chapters 3 and 4. For example, if H_2 and D_2 geminate recombination from the iron center are different, additional consequences to the standard isotope effect must be considered. The use of ultrafast laser spectroscopy offers insight into the dynamics of the photodissociation of small molecules, such as H_2, on the femto- and picosecond timescales and is employed in this study.

2.3 Experimental

2.3.1 General considerations

All chemicals were purchased from chemical suppliers and used as received. Pentane (BDH) and tetradecane (Sigma Aldrich) were dried prior to use. Syntheses of $(dmpe)_2FeH_2$ (**1**) and $(dmpe)_2FeD_2$ (**1-D$_2$**) were conducted under anhydrous and anaerobic conditions using proper glovebox and Schlenk line techniques following previously reported methods (Chapter 3).[87] UV/Vis absorbance data was collected with an OLIS Cary 14 spectrophotometer, accompanying software, and 2 mm quartz cuvettes.

2.3.2 Laser system

Ultrafast measurements were taken using a home-built, amplified ultrafast Ti:sapphire laser system.[88] Briefly, a 200 mW, 85 MHz pulse train is produced by a mode-locked oscillator pumped by 2.7 W from a CW Nd:YVO_4 laser (Spectra Physics, Millenia Pro). Selected pulses are amplified at 1 kHz by a home-built regenerative amplifier pumped with a Q-switched Nd:YAG laser (Spectra Physics, Empower 15). After compression, the 810 nm pulses have an energy of ~400 μJ and are 60 fs fwhm, assuming a Gaussian profile. Excitation pulses were created by first frequency doubling of the laser fundamental using a 1 mm BBO crystal to create 405 nm light. Then, the 405 nm light was added to the 810 nm in a second 1 mm BBO crystal to create the sum frequency 266 nm light. The white light probe was generated by sending 810 nm light through a constant-motion, 1 mm CaF_2 window (350-810 nm). The instrument response time was calculated to be ~300 fs.

2.3.3 Sample preparation

Stock solutions of **1** were prepared in pentane, tetradecane, or a 50:50

pentane:tetradecane mixture in volumetric flasks to concentrations of ~10^{-5} M in a nitrogen-filled glovebox. Solutions of **1-D_2** in pentane or tetradecane were prepared in a similar manner. Aliquots of stock solutions were placed in 2 mm quartz cuvettes, fitted with a small stir bar, and sealed with Teflon caps and Parafilm for UV/Vis and ultrafast studies.

2.3.4 Laser experiments

General considerations. All experiments were conducted with a pump pulse of 150 μW, unless otherwise noted, with a beam waist of 100 μm. Samples were stirred using a small motor (Thor Labs) directly below the laser crossing to minimize bleaching of the sample. Samples were shielded from light except during data collection. The pump light was 266 nm; probe light was either a white light continuum (380-810 nm) or a single color (405 nm) beam. With the exception of sample stability studies, the sample was exposed to laser irradiation for no longer than 30 minutes.

Sample stability studies. Samples were mounted and exposed to light at a 2 ps pump-white light probe delay. The sample was exposed for 50 seconds and shuttered for 10 seconds, for a total of two hours. The loss of signal was measured as a function of laser exposure time.

Full frequency experiments. Samples were mounted and exposed to various pump-white light probe delays. After irradiation, transmitted white light was columnated and sent through a 10 cm lens, where it was focused onto a dispersive grating. The light was incident on a 256 pixel Si-diode array (Hamamatsu). For pentane and tetradecane, the first sample was run from -5 ps to 5 ps, and the second sample was run from 2.5 to 900 ps with additional -5 ps and -3 ps background scans. For the 50:50 mixture, the

second sample was run from 2.5 to 500 ps with additional background scans.

Power dependence studies. Samples were mounted and exposed to light at -5, 0, 5, 50, and 300 ps pump-white light probe delays at various pump powers. Full frequency spectra were collected at each delay, averaging 5000 scans per delay. Scans of each sample were collected consecutively in triplicate.

Single color experiments. Samples were mounted and exposed to various pump-single color probe delays with a pump power of 100 μW. The 400 nm probe light was columnated and sent through a 10 cm lens, where it was focused onto a Thor Labs DET210 Si-photodiode fitted with a 400 nm filter (10 nm fwhm). Each sample was run consecutively in triplicate.

2.4 Results and Discussion

Because **1** and **1-D_2** are extremely light-sensitive, special considerations had to be taken to ensure sample stability. In the static cell, photobleaching was observed after short (<5 minutes) periods of laser exposure. To mitigate these effects, samples were stirred at constant speed by a small stir bar and stirring setup, allowing for the irradiated portion of the sample to be constantly refreshed.

Even with stirring, though, it was necessary to determine the usable lifetime of individual samples of **1** in various solvents. To evaluate this, full frequency spectra at 2 ps were collected for 50 seconds, followed by 10 seconds of darkness, repeated for two hours. The full frequency signal at 400 ± 5 nm decayed over time for each solvent (Figure 2.1). After 10 minutes, pentane decayed at a rate of 3.33×10^{-7} mΔOD/s. The 50:50 mixture decayed at a rate of 1.50×10^{-8} mΔOD/s after 10 minutes, and in tetradecane the rate of decay was 4.72×10^{-8} mΔOD/s after 10 minutes. Because the first 10 minutes of all further experiments were spent optimizing the experimental setup for the individual sample, only the effect of laser exposure after 10 minutes was important for correction.

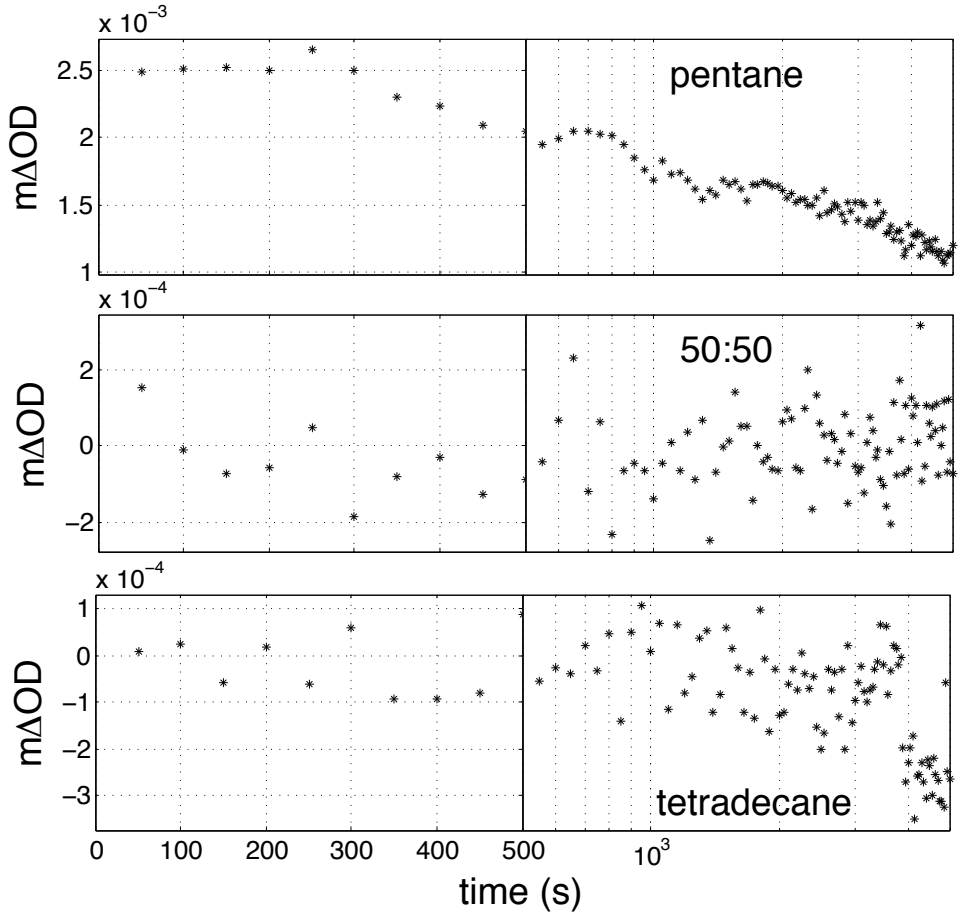

Figure 2.1. Observed signal at 400 ± 5 nm from **1** in various solvents as a function of laser exposure time. All samples were run at a pump power of 150 μW.

Samples of **1** were prepared in neat pentane, neat tetradecane, and a 50:50 v/v mixture of pentane and tetradecane. Full frequency spectra were collected at either 100, 150, or 200 μW for each solvent, and no appreciable shape change occurred. In neat pentane, the spectra collected at 0, 5, 50, and 300 ps showed a maximum absorbance at 375 nm (Figure 2.2). With increased power, the measured signal increased linearly, but the shape of the spectrum did not change between 300 and 500 nm. Similar spectra were observed for **1** in the 50:50 mixture (Figure 2.3) and in neat tetradecane (Figure 2.4), and again no shape change was observed upon increased power.

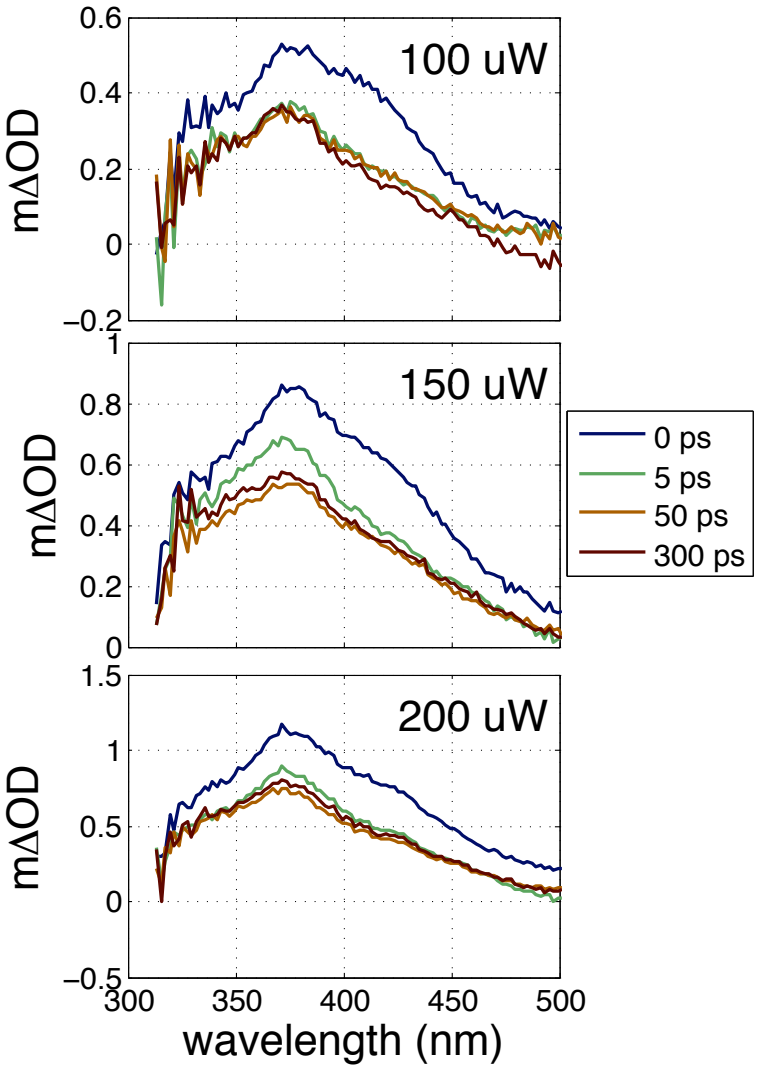

Figure 2.2. Power dependence of **1** in pentane. All scans were background subtracted using a -5 ps trace.

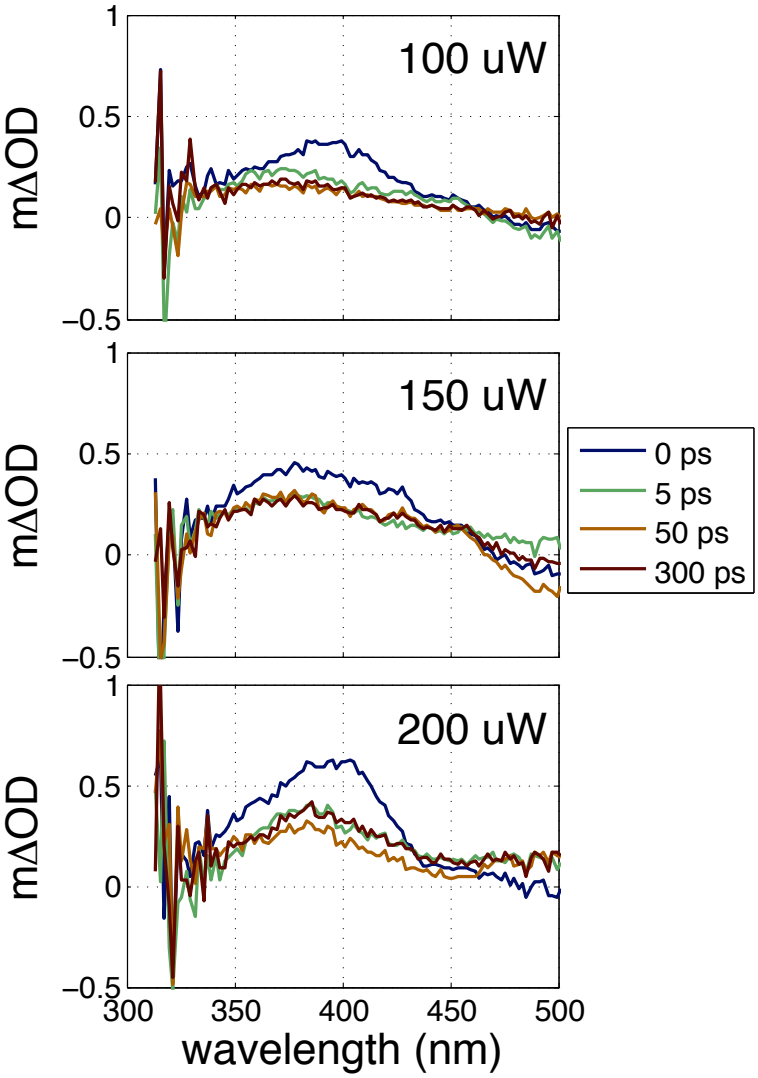

Figure 2.3. Power dependence of **1** in 50:50 pentane:tetradecane. All scans were background subtracted using a -5 ps trace.

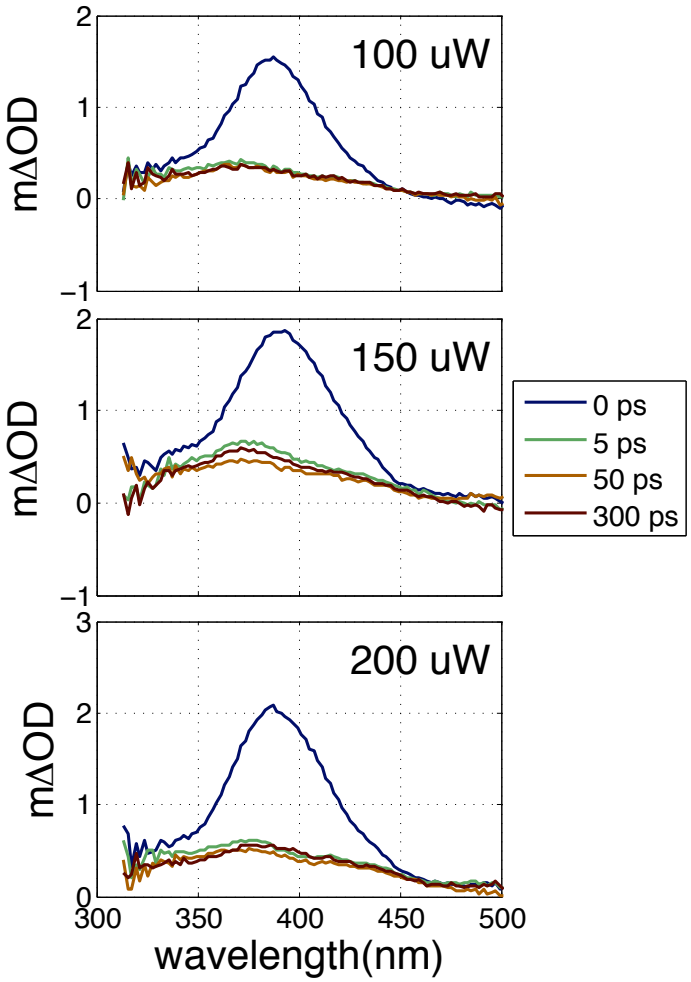

Figure 2.4. Power dependence of **1** in tetradecane. All scans were background subtracted using a -5 ps trace.

Full frequency spectra of **1** in various solvents were also collected from 0 to 500 ps (Figure 2.5). All spectra were frequency corrected and corrected for laser exposure, based on the stability studies conducted. Additionally, the spectra were corrected for absorbance by correcting all scans at 400 nm based on the single color fit for **1** in each solvent. In both pentane and tetradecane, a species with an absorbance at 375 nm appeared upon excitation at 266 nm, and this species decays over 900 ps. In the 50:50 mixture, a species with an absorbance maximum at 410 nm appeared upon excitation with 266 nm light and decays over 500 ps. Integration of single colors from the full

frequency data showed similar dynamics over time from 360 to 430 nm for **1** in all solvents, indicating no change in the spectrum over this time period.

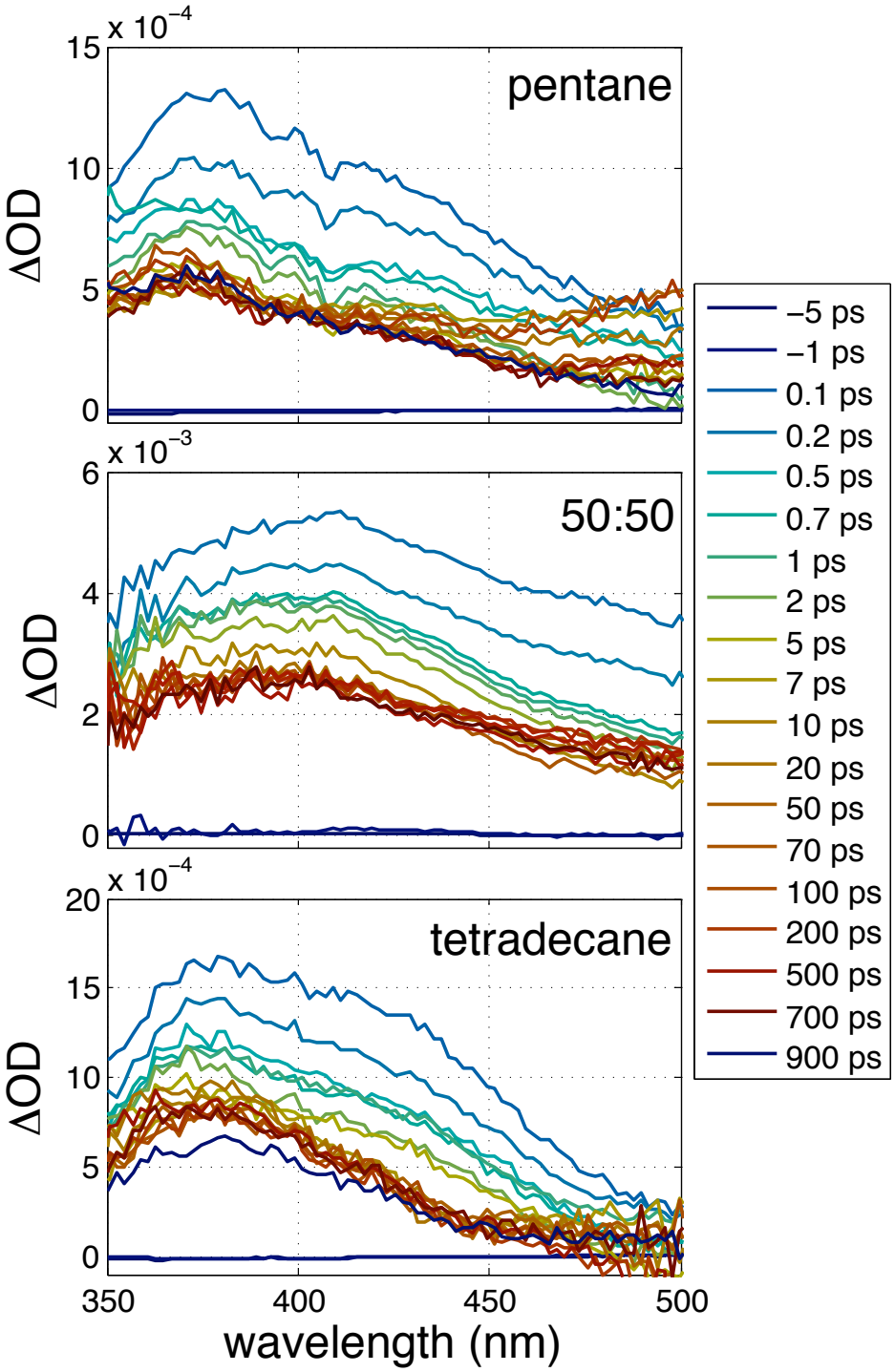

Figure 2.5. Full frequency spectra for **1** in neat pentane, 50:50, and neat tetradecane. All spectra were frequency corrected, corrected for laser exposure, and scaled to single color traces at 400 nm.

In order to achieve higher sensitivity, single color traces of **1** in various solvents

were collected at 400 nm. Using a single color probe instead of white light minimized the noise and allowed for scans to be conducted quickly, lessening any laser exposure effects. The single color traces of **1** in various solvents are shown in Figure 2.6. The data was background subtracted and corrected for the absorbance of each sample, because samples were created individually and each had a slightly different absorbance at 266 nm. The decay of **1** in various solvents was fitted to a 2-step exponential decay model and incorporated an instrument response (338 fs fwhm) and inputted solvent response function. The 2-step exponential decay model is defined in Equation 2.1, where A, B, and C are signal amplitudes and the decay processes τ_1 and τ_2 are assumed to be first order.

$$A \xrightarrow{\tau_1} B \xrightarrow{\tau_2} C \qquad \textbf{Equation 2.1}$$

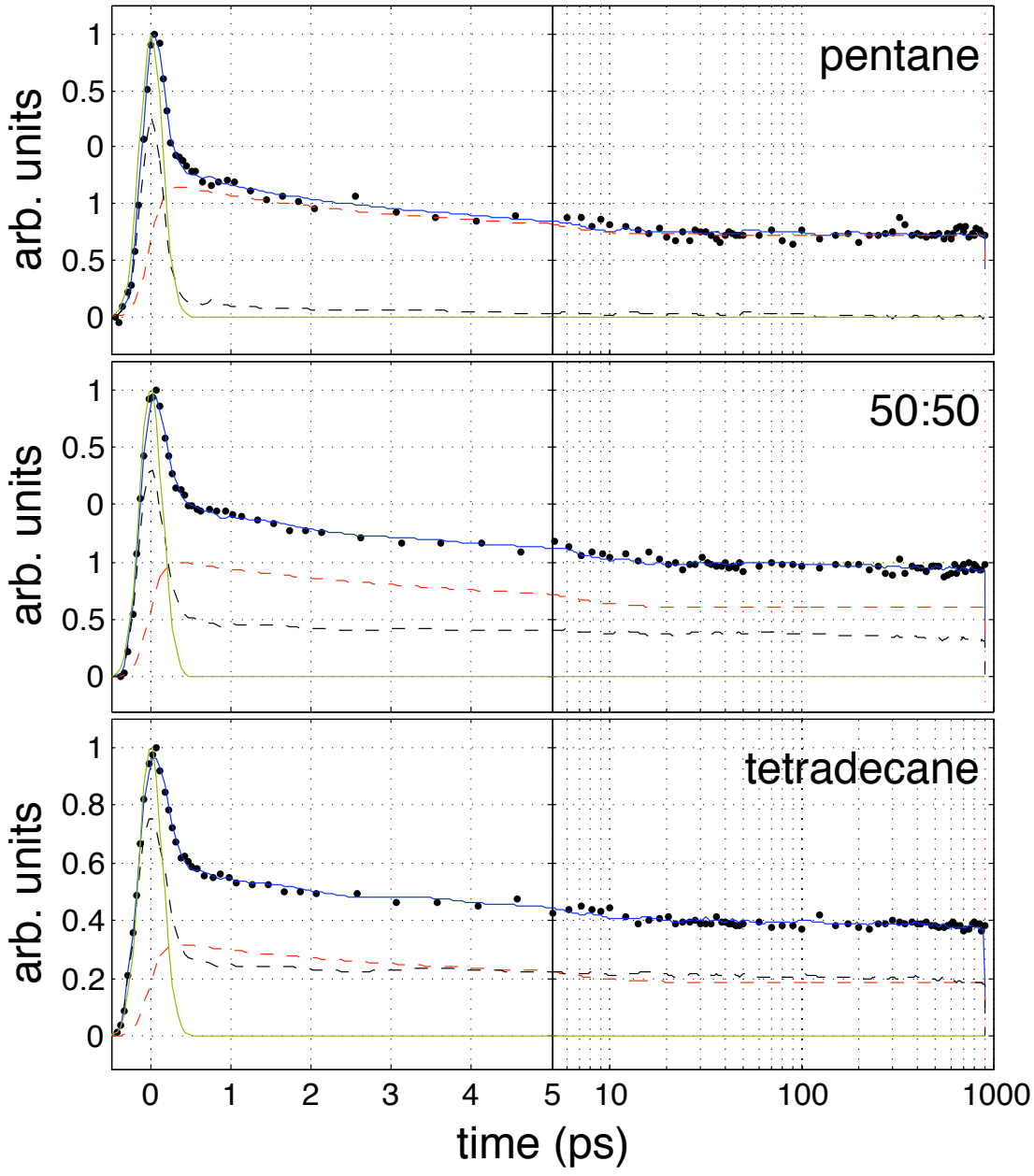

Figure 2.6. Single color traces of **1** in various solvents. Data was fit (blue) to a 2-step exponential model (red) with solvent background (black) and instrument response function (green). The data did not fit to a single exponential, a Heavyside function, or the combination of both a single exponential and a Heavyside function.

The parameters of the fits for **1** in pentane, tetradecane, and a 50:50 pentane:tetradecane mixture are summarized in Table 2.1. For all solvents, a species that

absorbs at 400 nm was generated within 100 fs (τ_1), the limit of the experimental time resolution. The amount of the species generated in each solvent, B, is greatest in neat pentane and smallest in neat tetradecane. In all solvents, this species decayed ($\tau_2 \approx 3$ ps) to a non-zero value, C. C represents the amount of the absorbing species that persists in the sample over 500 ps (900 ps for neat pentane and neat tetradecane).

Table 2.1. Fitting parameters for **1** in various solvents. Single-color data was fit to a 2-step exponential model with a solvent background. Errors were calculated to the 95th confidence interval.

solvent	solvent weight	A	τ_1 (fs)	B	τ_2 (ps)	C	% recombined
pentane	0.71 ± 0.02	0	1	0.49 ± 0.02	2.82 ± 0.6	0.29 ± 0.005	40.6 ± 1.3
50:50	0.75 ± 0.02	0	1	0.41 ± 0.02	3.85 ± 0.9	0.24 ± 0.006	41.4 ± 1.0
tetradecane	0.78 ± 0.02	0	1	0.33 ± 0.02	3.67 ± 0.9	0.18 ± 0.006	43.6 ± 0.9

The photogenerated species that absorbs at 400 nm is $(dmpe)_2Fe$ (**2**),[68] which is generated in less than 100 fs (Scheme 2.1). After generation, some **2** undergoes geminate recombination ($\tau_2 \approx 3$ ps) to reform **1**, while the rest persists for the duration of the experiment. No other loss processes of **2** are observed over nearly 1 ns. Geminate recombination has been reported to occur on timescales anywhere from several hundred femtoseconds to a few picoseconds,[76, 77] and the observed value of 3 ps reported here is consistent with these findings. A $\tau = 3$ ps for pentane, tetradecane, and a 50:50 mixture of both is also consistent with previous findings, which have found that the solvent itself does not have a large effect on the timescale of geminate recombination but does have an effect on the amount of recombination observed.[77]

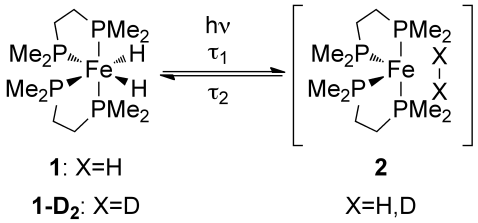

Scheme 2.1. Proposed generation of **2** from irradiation of **1** or **1-D$_2$** in alkane solvents.

B is the initial signal from **2**, and C is the signal from **2** that persists at long times; thus, the percentage of **2** that has recombined can be calculated from the difference between B and C, as a function of B (Table 2.1). The least amount of **1** is reformed in pentane (40.6%), while the most **1** is reformed in tetradecane (43.6%). This observation is consistent with the prediction that increased viscosity of the solvent will lead to increased recombination of **2** and H_2.[79] Tetradecane has a viscosity of 2.13 mPa·s at 25°C, while pentane has a viscosity of 0.22 mPa·s at 25°C;[89] H_2 can travel away from **2** more quickly in pentane than it can in tetradecane. Thus, it is expected that less **1** reforms in pentane than in tetradecane, because more H_2 has escaped the cage, leaving less H_2 available to recombine.

To better understand the escape of H_2 from the Fe center, the same experiments were conducted with $(dmpe)_2FeD_2$ (**1-D$_2$**), allowing for the release of D_2 upon irradiation. Single color traces of **1-D$_2$** in neat pentane and in neat tetradecane were collected over 900 ps (Figure 2.7), and the data was fit to a 2-step exponential model and incorporated an input solvent response and instrument response (338 fs fwhm).

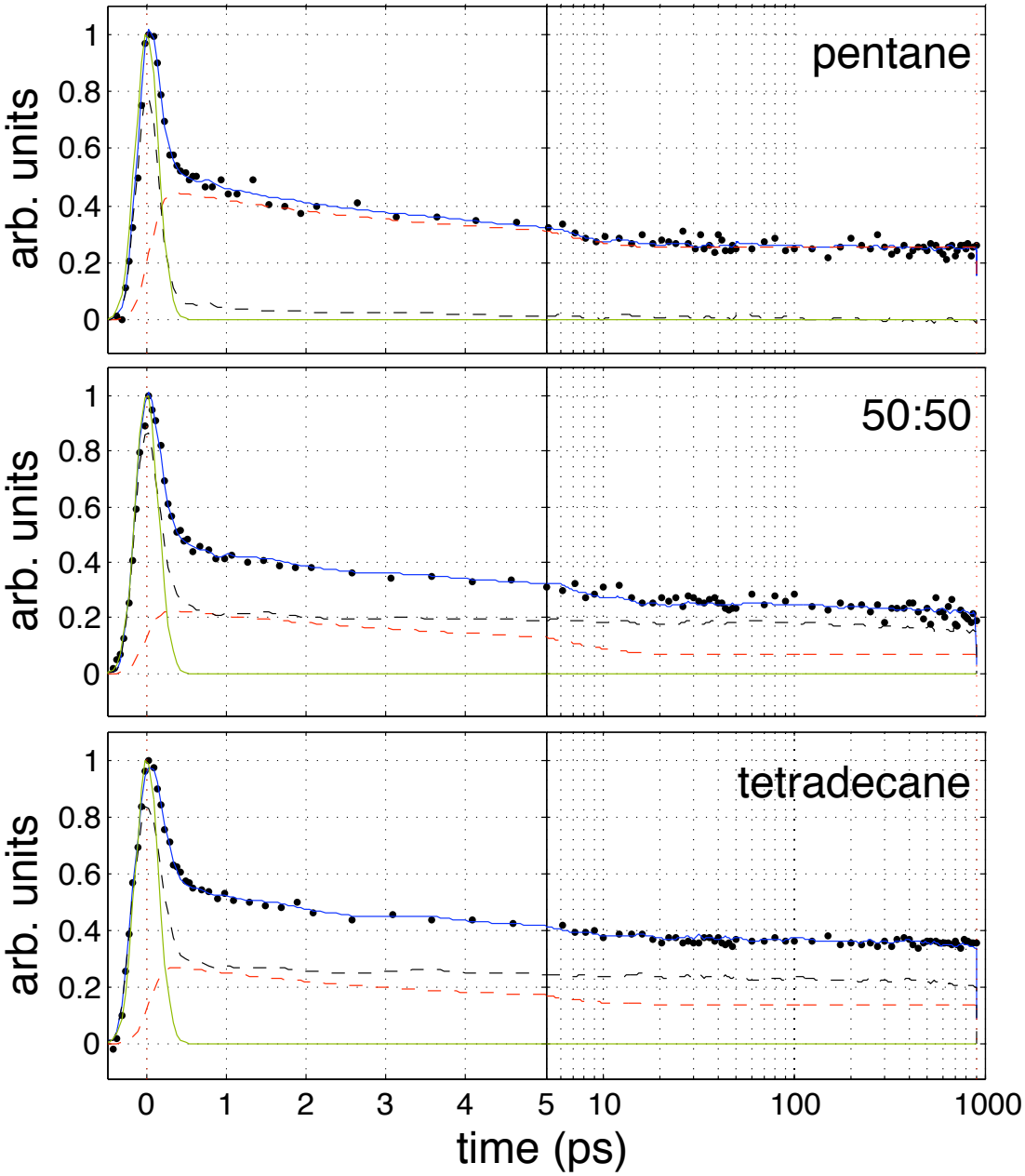

Figure 2.7. Single color traces of **1-D$_2$** in various solvents. Data was fit (blue) to a 2-step exponential model (red) with solvent background (black) and instrument response function (green). The data did not fit to a single exponential, a Heavyside function, or the combination of both a single exponential and a Heavyside function.

The parameters for the fit of **1-D$_2$** in each solvent are summarized in Table 2.2. Similar to the dynamics observed with **1**, **2** is generated within 100 fs and decays with a τ_2 of ~3 ps, and more **1-D$_2$** was reformed in tetradecane than in pentane, owing to the

difference in viscosity between the two solvents. The most notable difference between **1** and **1-D$_2$** is the amount of recombination: more recombination is observed upon release of D_2 from **1-D$_2$** than H_2 from **1**. This observation is consistent with previous findings that relate the amount of recombination with the mass of the dissociated fragment.[77] Within the solvent cage, a lighter molecule gains more of the kinetic energy after photodissociation – in this case, H_2 would be predicted to gain more of the kinetic energy compared to D_2, as momentum is conserved. In comparing the recombination of either H_2 or D_2 with **2**, H_2 has more kinetic energy and is thus less likely to undergo geminate recombination.

Table 2.2. Fitting parameters for **1-D$_2$** in various solvents. Single-color data was fit to a 2-step exponential model with a solvent background. Errors were calculated to the 95th confidence interval.

solvent	solvent weight	A	τ_1 (fs)	B	τ_2 (ps)	C	% recombined
pentane	0.78 ± 0.02	0	1	0.48 ± 0.02	3.65 ± 0.8	0.25 ± 0.006	46.7 ± 0.8
tetradecane	0.84 ± 0.02	0	1	0.29 ± 0.02	3.16 ± 0.8	0.14 ± 0.007	52.0 ± 0.7

While the observed timescales for geminate recombination of both **1** and **1-D$_2$** in all studied solvents were all approximately 3 ps, the amount of observed recombination varied based on solvent and on the photodissociated product. To our knowledge, this is the first study to evaluate the recombination of H_2 and D_2 to a metal center in the condensed phase. Recombination yields range from 30% for $Cr(CO)_6$[77] to 75% for ICN.[78] The recombination rates observed in this study (40-50%) are consistent with these studies.

Within the time covered by the experiments, we assert that **2** is a long-lived intermediate that persists for nearly 1 ns in neat solvent. Several possible competing

processes could be conceived but are not consistent with these findings. The first is association of a solvent molecule to **2** (identified as **2-solvent**). Whittlesey *et al.* observed a transient with an absorbance at 410 nm in alkane solvents on the microsecond timescale. Based on reactivity and low temperature matrix studies, they assigned this transient to be either **2** or **2-solvent**. Kowalska *et al.* found that coordination of solvent molecules to a reactive intermediate proceeded on a timescale of a few nanoseconds,[90] far slower than the dynamics reported here. Additionally, C-H activation of the solvent is not observed, as that occurs on a timescale of 200 ns.[91] Thus, solvent association and/or activation is not predicted to occur, and **2** is the absorbing species that persists over 1 ns.

2.5 Conclusion

The ultrafast dynamics of $(dmpe)_2FeH_2$ and $(dmpe)_2FeD_2$ were investigated and found to generate the 16-e^- intermediate $(dmpe)_2Fe$ within 100 fs upon irradiation at 266 nm. This intermediate then recombined with H_2 or D_2 with $(dmpe)_2Fe$ in ~3 ps in both pentane and tetradecane, consistent with recombination time scales observed with other small molecules. However, ~40% of these intermediates do not recombine, and $(dmpe)_2Fe$ persists over 1 ns. This yield is dependent on both the type of molecule dissociated (H_2 or D_2) and the viscosity of the solvent. Recombination yields of H_2 and D_2 were larger in tetradecane than in pentane, consistent with solvent cage effects and the effect of solvent viscosity. In the same solvent, more D_2 recombined than did H_2, due to the mass effect of the dissociated group. These absorbance, geminate recombination rates and yields, and the effect of varied metal substituent studies have allowed for increased understanding of the ultrafast dynamics of this 16-e^-, formally Fe^0, species. This is the first comparison of H_2 and D_2 geminate recombination from a metal center in the condensed phase, and future directions for study include evaluating the ultrafast dynamics of the complex in solvents of intermediate viscosity and reactivity, as well as adding reactive substrates to the reaction mixture to evaluate ultrafast reaction dynamics of the reactive intermediate.*

* Special thanks to Eric Nordland for assistance in conducting full frequency and single color experiments; to Tom Pundsack for help setting up the 266 nm light and data analysis; and to Dr. Jon Hinke for assistance in data collection and analysis.

Chapter 3

Dechlorination of chlorinated ethylenes facilitated by a photochemically generated iron(0) complex

In part from
Emily J. Pelton, David A. Blank, and Kristopher McNeill. *Dalton Transactions*, 2013, **42**, 10121-10128.

3.1 Overview

The reactivity of Fe^0 toward chlorinated ethylenes was examined using a photochemically generated, highly reactive Fe^0 complex. Irradiation of $(dmpe)_2FeH_2$ (dmpe = $Me_2PCH_2CH_2PMe_2$) with 360 nm light generated a 16-e^-, Fe^0 intermediate that reacted to dechlorinate chlorinated ethylene substrates in a stepwise fashion, consistent with a hydrogenolysis dechlorination pathway. The source of the hydrogen atoms in the hydrogenolysis were the hydride ligands of an additional equivalent of $(dmpe)_2FeH_2$, as evidenced by deuterium labeling experiments. The reaction was observed to be first-order in $(dmpe)_2FeH_2$, chlorinated ethylene substrate, and the intensity of 360 nm radiation. The rate of chlorinated ethylene substrate decay increased with increasing substrate chlorination in the order CH_2=CHCl < *cis*-CHCl=CHCl < *trans*-CHCl=CHCl < CCl_2=CHCl. A mechanism of reaction was proposed that accounts for the reaction kinetics, the observed intermediates, and the origin of hydrogen atoms incorporated into reaction products.

3.2 Introduction

The presence of chlorinated solvents in groundwater systems has led to the development of technologies to mitigate these hazardous and toxic compounds.[3, 92] One such remediation approach is permeable reactive barriers (PRBs) that employ zero-valent metals that react with chlorinated solvents to form lower chlorinated, less hazardous materials.[42, 45]

Several studies have endeavored to elucidate a mechanism for reaction between zero-valent iron (ZVI), a metal commonly used in PRBs, and chlorinated ethylenes (CEs), a class of chlorinated solvents known to contaminate groundwater systems. Some studies have demonstrated a hydrogenolysis mechanism,[42, 93, 94] replacing chlorine with hydrogen in a stepwise manner, while others have observed vicinal-Cl_2 elimination mechanisms that generate alkyne byproducts.[46, 95, 96] Additionally, some reports have found that an increase in chlorination leads to an increase in reaction rate,[49, 50] while others have found that lesser chlorinated substrates react fastest.[45, 46, 97] The discrepancies in these findings have been attributed to a variety of issues introduced by the heterogeneous experimental conditions employed.[46]

With this motivation, a phosphine-supported Fe complex can be employed to understand the fundamental reaction chemistry of well defined Fe^0 complexes and chlorinated ethylenes. Previously, a pentakis-phosphine-supported Fe complex was prepared and utilized to study the reaction between Fe^0 and CEs.[63, 98] While these 18 e^-, L_5Fe^0 complexes dissociate a phosphine arm to generate a 16 e^-, L_4Fe^0 reactive species that allow for C-Cl bond activation, previous studies have found that an L_4Fe^0 model can be generated without dissociation of the phosphine ligand. Whittlesey *et al*. reported the

photochemical generation of $(dmpe)_2Fe$ (dmpe = 1,2-bis(dimethylphosphino)ethane), formally an L_4Fe^0 species, from $(dmpe)_2FeH_2$ via release of H_2.[68] The reactive $(dmpe)_2Fe$ complex was shown to activate alkyl C-H bonds upon irradiation, and given that C-Cl bonds are weaker (85 kcal/mol) and generally more reactive than C-H bonds (100 kcal/mol),[65] the formally Fe^0 species is predicted to activate C-Cl bonds.

In this study, a photochemically generated, formally Fe^0 species was generated and shown to react with CEs. The effect of degree of chlorination on the rate of substrate decay was evaluated, as was the type of dechlorination pathway observed in the studied reaction. Based on the collected data, a mechanism for the reaction between the Fe^0 model system and CEs was proposed. While the use of a single iron complex and its reaction with CEs does not reflect the behavior between CEs and bulk ZVI, use of a model system allows for the determination of specific reaction parameters for the reaction between Fe^0 and CEs.

3.3 Experimental

3.3.1 General considerations

All experiments were conducted under anhydrous and anaerobic conditions using glovebox and Schlenk line techniques. All chemicals were purchased from Aldrich, Fluka, Merck, and Acros and used as received, unless otherwise noted. Solvents were dried prior to use.[99] Nuclear magnetic resonance (NMR) spectra were collected on Varian Inova VXR-300 MHz, Varian Inova VMX-400 MHz, and Varian Inova VI-500 MHz instruments. UV/Vis absorbance data were collected with OceanOptics CHEMUSB2 and OLIS Cary 14 spectrophotometers using quartz cuvettes. GC-MS data were collected on an Agilent 6890 GC system (Phenomenex ZB-624, 60 m x 0.32 mm i.d., 1.8 μm film thickness) with a 5973 mass selection detector, and data were analyzed with the accompanying software.

3.3.2 Synthesis

$(dmpe)_2FeCl_2$. The complex was prepared following reported methods.[64, 100] Briefly, $FeCl_2 \cdot 2$ THF (2.00 g, 7.36 mmol) was suspended in toluene, and to it was added bis(dimethylphosphino)ethane (dmpe; 2 mL, 14.8 mmol). The purple-green suspension was stirred for 2 h. The resulting mixture was filtered and washed with toluene. The solvent and volatile materials of the green filtrate were removed under vacuum to yield green crystals (1.18 g, 38% yield). ^{1}H NMR (C_6D_6) δ 1.97 (br s, 8H); 1.36 (s, 24H). $^{31}P\{^1H\}$ NMR (C_6D_6) δ 59.6 (s, 4P).

*$(dmpe)_2FeH_2$ (**1**).* The complex was synthesized following a modified procedure of Whittlesey *et al.*[68] In brief, a solution of $(dmpe)_2FeCl_2$ (363 mg, 850 μmol) in THF (20 mL) was prepared in a Schlenk flask, as was a separate suspension of $LiAlH_4$ (206

mg, 5.4 mmol) in THF (20 mL). Both Schlenk flasks were placed under an H_2 atmosphere, and the solution of the dichloride was transferred to the $LiAlH_4$ suspension via cannula. The reaction mixture was stirred under H_2 for ~2 h. All solvent and volatile materials were removed under vacuum. The resulting residue was extracted into pentane (3 x 5 mL) and filtered through a pipette filter into a foil-wrapped vial to avoid exposure to ambient light. The solvent was removed from the light yellow filtrate *in vacuo* to yield a pale yellow solid (200 mg, 66% yield). ^{1}H NMR (C_6D_6) δ 1.59 (br s, 10H); 1.435-1.354 (br d, 4H); 1.239 (s, 12H); 1.085 (br s, 6H); -13.629-14.140 (dddd, 2H). $^{31}P\{^1H\}$ NMR (C_6D_6) δ 77.2 (t, J = 26.5 Hz, 2P); 67.7 (t, J = 27.2 Hz, 2P). UV/Vis (pentane): λ_{max} 214 nm, ε_{214} 30900 L/mol·cm.

*$(dmpe)_2FeD_2$ (**1-d_2**)*. The complex was prepared similarly to **1** (*vide supra*). Briefly, a solution of $(dmpe)_2FeCl_2$ (515 mg, 1.21 mmol) in THF (20 mL) was prepared, as was a suspension of $LiAlD_4$ (718 mg, 17.1 mmol) in THF (20 mL). Both Schlenk flasks were placed under a N_2 atmosphere, and the dichloride solution was added to the $LiAlD_4$ suspension via cannula. The reaction was allowed to stir under N_2 for 2 h, shielded from ambient light then placed under vacuum to remove volatiles. The resulting residue was extracted into pentane and filtered. Volatile materials were removed *in vacuo* to yield a pale yellow solid (82 mg, 20% yield). The product contained approximately 16% of the dihydride complex, **1**, as evidenced by ^{1}H NMR. ^{1}H NMR (C_6D_6) δ 1.59 (br s, 10H); 1.435-1.354 (br d, 4H); 1.239 (s, 12H); 1.085 (br s, 6H); -13.629-14.140 (dddd, 0.32H). ^{2}H NMR (C_7H_8) δ -14.07 (br, 2H). $^{31}P\{^1H\}$ NMR (C_7H_8) δ 79.8 (br m, 2P); 69.7 (t, J = 27.2 Hz, 2P).

3.3.3 Construction of LED-based photoreactor

An LED-based photoreactor was constructed for use in photolysis experiments. Four 3 x 3 arrays, mounted onto plastic breadboards (RadioShack) and each consisting of nine 360 nm LEDs (The Fox Group, Inc.) and one 300 Ω resistor, were all serially wired. The breadboards were affixed in a rectangular orientation to a small plastic base to create a light source with a total of 36 LEDs driven at 4-5 V with a current of 0.1 A.

3.3.4 Actinometry studies

All actinometry experiments were conducted using the LED photoreactor while protected from extraneous light sources. For stability of the light source intensity, the photoreactor was allowed to run for at least 30 minutes prior to photolysis. Experiments were conducted in at least triplicate following the method developed by Montalti *et al*.[101]

Preparation of ferrioxalate actinometer solution. In the dark, $K_3Fe(C_2O_4)_3 \cdot 3\ H_2O$ (297 mg, 0.605 mmol) was dissolved in H_2SO_4 (50 mL, 0.050 M). The resulting yellow solution was stored in an amber bottle.

Preparation of 1,10-phenanthroline actinometer solution. A stock solution was prepared by dissolving 1,10-phenanthroline (phen; 1.00 g, 5.56 mmol) and $NaOAc \cdot 3\ H_2O$ (225 g, 1.65 mol) in H_2SO_4 (1.00 L, 0.50 M). The resulting colorless solution was stored in an amber bottle.

Actinometry experiments. Ferrioxalate solution (3 mL, 0.012 M) was placed into each of two crimp cap vials, each fitted with a small stir bar. For 30 s, one vial was stirred in the dark, and the other was stirred in the LED photoreactor (36 LEDs). Both vials were wrapped in foil (to prevent exposure to ambient light), and 1 mL from each vial was placed into a 1 cm plastic cuvette fitted with a small stir bar. An aliquot of phen solution

(0.5 mL, 0.1%) was added to each cuvette, and the cuvettes were sealed with Parafilm. A UV/Vis spectrum from 500-520 nm was collected at t = 0 min, using the dark cuvette as a background for the sample exposed to light. The cuvettes were stirred in the dark for 5 min, and another UV/Vis spectrum was collected. This process was repeated every 5 min for 1 h, then every 10 min for another hour. The absorbance at 510 nm was converted into photons/molecule·min using the literature method.[101]

3.3.5 GC-MS photolysis experiments

All photolysis experiments were conducted in the dark using the LED light source. The source was allowed to warm up for at least 30 minutes prior to photolysis. Experiments were conducted in at least triplicate unless otherwise noted.

General. In the glovebox, a solution of **1** in cyclohexane (250 μL, 15.7 μmol) was placed in a glass crimp cap vial fitted with a small stir bar. An aliquot of CE solution in cyclohexane (50 μL, 1.0 μmol) was added, and the vial was sealed. The final concentrations of **1** and the CE substrate were 52 mM and 3.3 mM, respectively. The vial was allowed to rest for five minutes in the dark. A headspace sample (200 μL) was removed from the vial (t = 0 min), and then the vial was placed into the light source (36 LEDs) for one minute. At the t = 1 min time point, the vial was removed from the light source, another headspace sample was removed, and then the vial was placed again into the light source. The process was repeated for time points t = 0, 1, 2, 4, 8, 15, 30, 45, and 60 min. Headspace samples were analyzed using GC-MS. Control experiments were conducted in the same way, but samples were not exposed to the light source.

Effects of light. The reaction between **1** (250 μL, 15.7 μmol) and CE substrates (50 μL, 1.0 μmol) was studied by the method described above. Experiments were conducted using 0, 9, 18, 27, or 36 LEDs.

Effects of [3]. The reaction between **1** and TCE (50 μL, 1.0 μmol) was studied using 36 LEDs by the method described above. Experiments were conducted using 0, 4.1, 7.9, 12.6, or 15.7 μmol **1**.

Effects of CE substrate. The reaction between **1** (250 μL, 15.7 μmol) and CE substrates (50 μL, 1.0 μmol) was studied using 36 LEDs by the method described above. Experiments were conducted using TCE, cDCE, and tDCE.

*Effects of **1-D$_2$***. The reaction between **1-D$_2$** (250 μL, 16.5 μmol) and TCE (50 μL, 1.0 μmol) was studied using 36 LEDs by the method described above.

Effects of cyclohexane-d_{12}. The reaction between **1** (250 μL, 15.7 μmol) and CE substrates (50 μL, 1.0 μmol) was studied using 36 LEDs by the method described above, but experiments were conducted in cyclohexane-d_{12} instead of cyclohexane in duplicate.

Effects of added gas. In the glovebox, a solution of **1** in cyclohexane (250 μL, 15.7 μmol) was placed in a glass crimp cap vial fitted with a small stir bar. An aliquot of CE solution in cyclohexane (50 μL, 1.0 μmol) was added, and the vial was sealed. H_2 (30 mL) or D_2 (28 mL) was bubbled into the solution in the vial, and after addition, the vial was allowed to rest for five minutes in the dark. Photolysis, headspace samples, and analysis were conducted following the method described above.

GC-MS analysis. All studies were conducted using headspace injections (200 μL) of crimp-capped vials containing the reaction mixture. The volume was injected into the column at 140°C, and the sample ran for 11.5 min. All spectra were collected in scan

mode, and peaks of interest were detected using extracted ion chromatograms set to detect parent m/z values. Detected m/z values were 130 for TCE, 96 for DCEs, and 62 for VC. GC retention times were used to identify the products and were compared to the retention times of known standards. cDCE, tDCE, and 1,1-DCE were all able to be separated using this method.

3.3.6 NMR photolysis experiments

All photolysis experiments were conducted in the dark using the LED light source. The source was allowed to warm up for at least 30 minutes prior to photolysis. Experiments were conducted at least in triplicate unless otherwise noted.

cDCE and tDCE. In the glovebox, an aliquot of DCE solution in cyclohexane-d_{12} (200 μL, 2.6 μmol) was added to an aliquot of a solution of **1** in cyclohexane-d_{12} (500 μL, 35.2 μmol) in a J-Young tube. The tube was sealed, removed from the glovebox, and kept away from light. A ^{1}H NMR spectrum was collected at t = 0 min, and then the tube was placed into the LED light source for one minute. At the t = 1 min time point, another ^{1}H NMR spectrum was collected, and the tube was placed again into the light source. The process was repeated for time points t = 0, 1, 2, 4, 8, 15, 30, 45, 60, and 75 min. Experiments were conducted in duplicate for tDCE.

VC. In the glovebox, an aliquot of cyclohexane-d_{12} (200 μL) was added to an aliquot of a solution of **1** in cyclohexane-d_{12} (500 μL, 35.2 μmol) in a J-Young tube. The tube was sealed, removed from the glovebox, placed into liquid N_2 to freeze the sample, and kept away from light. The frozen sample was placed under vacuum to remove headspace, and VC (58 mTorr, 2.4 μmol) was added to the frozen solution via a vacuum transfer. The solution was allowed to thaw to ambient temperature, away from light. A

^{1}H NMR spectrum was collected at t = 0 min, and then the tube was placed into the LED light source for one minute. At the t = 1 min time point, another ^{1}H NMR spectrum was collected, and the tube was placed again into the light source. The process was repeated for time points t = 0, 1, 2, 4, 8, 15, 30, 45, 60, and 75 min. The experiment was conducted in duplicate.

NMR analysis. Each ^{1}H NMR spectrum was integrated relative to a grease peak at 0.1 ppm. The bc command was employed to correct the baseline of each spectrum.

3.3.7 MATLAB fittings

CE growth and decay. Growth and decay k values were determined by globally fitting GC-MS or NMR data to kinetic models in MATLAB. The decay of TCE (k_T) was defined as the sum of k_1 and k_2. The growth of cDCE from TCE was defined as k_1, and the decay was defined as k_3. The growth of tDCE from TCE was defined as k_2, and its decay was defined as k_4.

$$[TCE]_t = [TCE]_0 e^{-(k_1+k_2)t} \quad \textbf{Equation 3.1}$$

$$[cDCE]_t = \frac{k_1[TCE]_0}{k_3-k_1-k_2}(e^{-(k_1+k_2)t} - e^{-k_3t}) \quad \textbf{Equation 3.2}$$

$$[tDCE]_t = \frac{k_2[TCE]_0}{k_4-k_1-k_2}(e^{-(k_1+k_2)t} - e^{-k_4t}) \quad \textbf{Equation 3.3}$$

Matrix approach to D incorporation. In order to determine the deuterium incorporation present in photoproducts, a matrix approach was chosen to convert ion intensities into the number of deuterium atoms present. Based on the ion intensities of the parent ion fragment of the species of interest, a theoretical matrix (A) was generated. This matrix was calculated by extrapolating the relative ion intensities of the fragment without deuterium to relative ion intensities of the fragment with a defined number of deuterium atoms (Table 3.1 and Table 3.2).

Table 3.1. Theoretical matrix (A1) containing relative ion intensities for the mass spectrum fragment 96 of DCE, which can contain up to two deuterium atoms. The fragment without deuterium consists of masses m/z 96 (100%), 97 (2.2%), and 98 (64.8%).

		number of D atoms		
		0 D	1 D	2 D
masses (m/z)	96	1	0	0
	97	0.022	1	0
	98	0.648	0.022	1
	99	0.014	0.648	0.022
	100	0.105	0.014	0.648
	101	0.002	0.105	0.014
	102	0	0.002	0.105
	103	0	0	0.002

Table 3.2. Theoretical matrix (A2) containing relative ion intensities for the mass spectrum fragment 62 of VC, which can contain up to three deuterium atoms. The fragment without deuterium consists of masses m/z 62 (100%), 63 (2.2%), 64 (32.4%), and 65 (0.7%).

		number of D atoms			
		0 D	1 D	2 D	3 D
masses (m/z)	62	1	0	0	0
	63	0.022	1	0	0
	64	0.324	0.022	1	0
	65	0.007	0.324	0.022	1
	66	0	0.007	0.324	0.022
	67	0	0	0.007	0.324
	68	0	0	0	0.007

For each deuterated product generated during a photolysis experiment, the integrated peak area for each m/z value in the parent ion fragment was extracted. The extracted area integrations were normalized to the highest mass to generate a "photolysis column vector" (B) (Table 3.3).

Table 3.3. "Photolysis column vector" (B1) containing relative ion intensities extracted from the mass spectrum for deuterated cDCE as a product of the reaction between **1-D_2** and TCE at 1 min.

	reaction product
masses (m/z)	relative peak areas
96	0.172
97	1
98	0.129
99	0.638
100	0.0170
101	0.0889
102	0
103	0

The number of deuterium atoms contained in the product is then calculated by weighting the theoretical matrix (A) so that it gives the vector with the extracted relative ion intensities of the mass fragment of the product (B); that is, the theoretical matrix (A) multiplied with a weighting vector (X) gives the photolysis column vector (B).

theoretical matrix (A) × weighting vector (X) = photolysis column vector (B)

$$AX = B$$

The weighting vector (X) can be calculated with the mldivide (\) function in MATLAB.

$$X = A \setminus B$$

The weighting vector (X) is the least-squares solution to the overdetermined system of equations AX = B. From the resulting weighting vector (X), the values were normalized to total 100% (Table 3.4).

Table 3.4. Weighting vector (X) calculated for deuterated cDCE as a product of the reaction between **1-D_2** and TCE, containing the percentage of the cDCE products containing a certain number of deuterium atoms.

	number of deuterium atoms		
	0 D	1 D	2 D
%	15.1	85.9	0

3.4 Results and Discussion

Following literature procedures, $(dmpe)_2FeH_2$ (**1**) was prepared in 66% yield from $(dmpe)_2FeCl_2$ and $LiAH_4$.[100] The pale yellow solid was isolated and characterized by ^1H and ^{31}P NMR and UV/Vis spectroscopy. The ^1H NMR spectra reveal a dddd splitting pattern of the two hydrides at δ -13.9 ppm, indicating that the hydrides are *cis* to each other. This is confirmed by the presence of two triplets at δ 77.2 and 67.7 ppm in the ^{31}P NMR spectra, indicating that the two P environments on the dmpe ligands are distinct. Previous studies have demonstrated that, upon exposure to light, the 18 e^- dihydride complex (**1**) generates a 16 e^- intermediate (**2**) (Scheme 3.1) that is capable of activating C-H and C-Cl bonds.[60, 68] Based on matrix isolation UV/Vis studies, the geometry of **2** is believed to be *cis*-divalent octahedral and not square planar.[68]

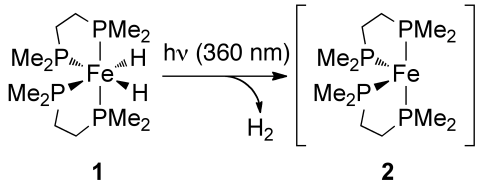

1 **2**

Scheme 3.1. Generation of 16 e^- intermediate **2** from reaction of **1** and hν.

The UV/Vis absorbance spectrum of **1** displayed a λ_{max} value at 214 nm, with limited absorbance at $\lambda > 400$ nm. For photolysis studies, a 360 nm LED light source was selected. The $\varepsilon_{360\ nm}$ value (2484 L/mol·cm) is considerably lower than maximum molar absorptivity value (30900 L/mol·cm at 214 nm). Irradiation at 360 nm in the LED photoreactor led to phototransformation on time scales that were convenient to follow by NMR spectroscopy and GC-MS analysis.

Reaction between **1** and CE substrates (TCE, cDCE, tDCE, and VC) was observed upon irradiation with 360 nm light, while no dark reaction was observed (Scheme 3.2). In contrast, perchloroethylene was found to react with **1** in the absence of light (data not shown) and was therefore not included in this study.

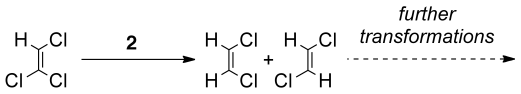

Scheme 3.2. Observed transformation of TCE with 16 e^- intermediate **2**.

The transformation pathways of the various CE substrates mediated by **1** and 360 nm light are summarized in Scheme 3.3. Dechlorination appeared to occur in a stepwise manner, such that TCE was dechlorinated to generate both cDCE and tDCE in approximately a 4:1 ratio with a mass balance of ~80%. Stepwise dechlorination was also observed for the photochemical reactions between **1** and cDCE and tDCE, with both substrates forming up to 20% VC by the end of each experiment. The reaction between **1** and VC also underwent stepwise dechlorination to yield ethylene. No 1,1-DCE or acetylene products were observed upon photolysis of **1** and any investigated CE substrate.

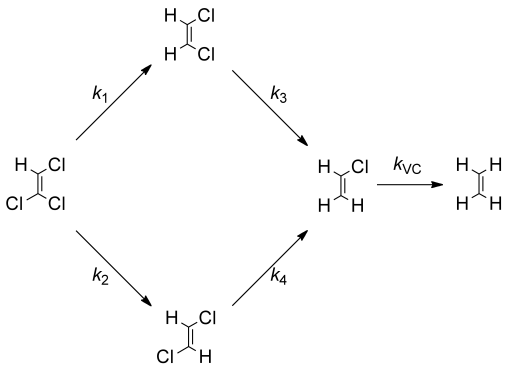

Scheme 3.3. Observed reaction pathways for the reaction of **1** with CE substrates and hν.

Photolysis of **1** with cDCE, tDCE, and VC also generated $(dmpe)_2Fe$-based photoproducts, including *trans*-$(dmpe)_2FeCl_2$, *trans*-$(dmpe)_2Fe(H)Cl$ (**3**), *trans*-$(dmpe)_2Fe(vinyl)Cl$, and *cis*-$(dmpe)_2Fe(vinyl)H$, observed by ^1H NMR.[64]

Because the reaction between **1** and CE substrates is predicated on the presence of light (and generation of reactive species **2**), the effect of the amount of light on the rate of reaction was investigated. The reaction of **1** with a CE and varying amounts of 360 nm light was studied over 60 minutes. The reaction was monitored by headspace samples analyzed by GC-MS. As the amount of light increased, the rate of CE substrate decay increased (Figure 3.1 and Figure 3.2), indicating that the reaction has a first-order dependence on the amount of 360 nm light present in the system.

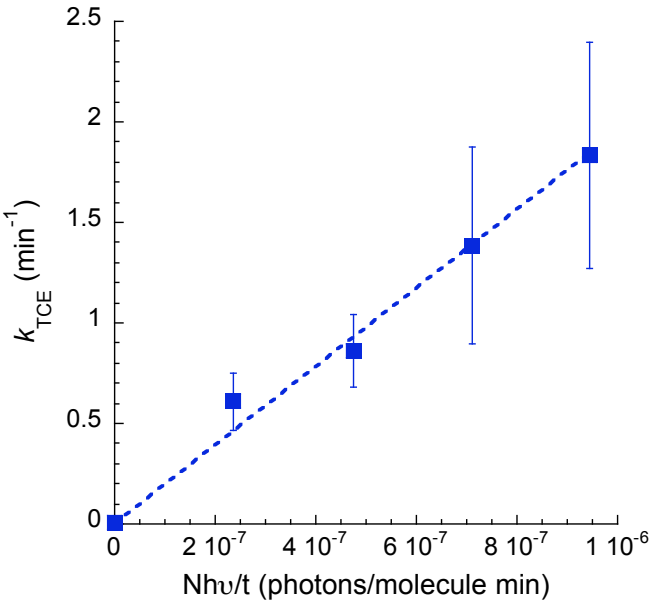

Figure 3.1. Dependence of k_{TCE} (■, R^2=0.99) values on amount of irradiation at 360 nm. Initial concentrations were 54 mM for **1** and 2.3-2.7 mM for TCE.

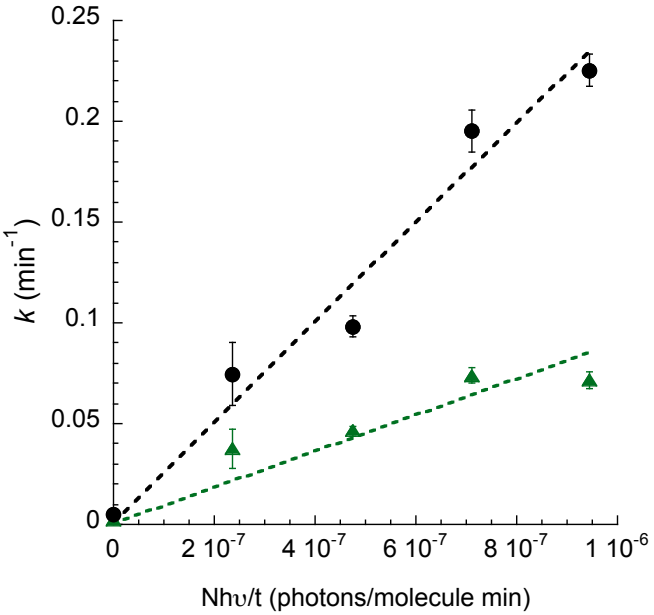

Figure 3.2. Dependence of k_{cDCE} (▲, R^2=0.90) and k_{tDCE} (•, R^2=0.97) values on amount of irradiation at 360 nm. Initial concentrations were 54 mM for **1**, 2.3-2.7 mM for cDCE, and 2.9-6.3 mM for tDCE.

With increased amounts of light, however, the relative rates of reaction remained approximately constant (Figure 3.3). This indicates that the amount of light does not affect the *relative* rates of CE decay between **1** and each CE substrate.

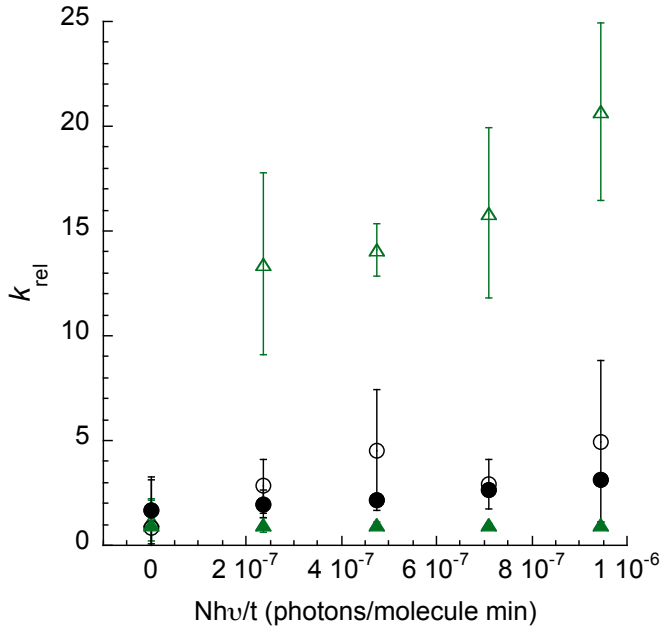

Figure 3.3. Dependence of rate constant values, relative to k_3, of k_1 (Δ), k_2 (°), k_3 (▲), and k_4 (•) on amount of irradiation at 360 nm. Initial concentrations of TCE were 2.3-2.7 mM, 3.2-3.5 mM for cDCE, 2.9-6.3 mM for tDCE, and 54 mM for **1**.

The effect of [**1**] on rates of CE decay was also examined. With maximum irradiation from the LED box, an increase in [**1**] led to a linear increase in the rate of TCE decay (k_{TCE}) (Figure 3.4). This indicates that the photochemical reaction between **1** and TCE is first-order with respect to **1** and that the reaction between **1** and CE substrates is stoichiometric with respect to **1**.

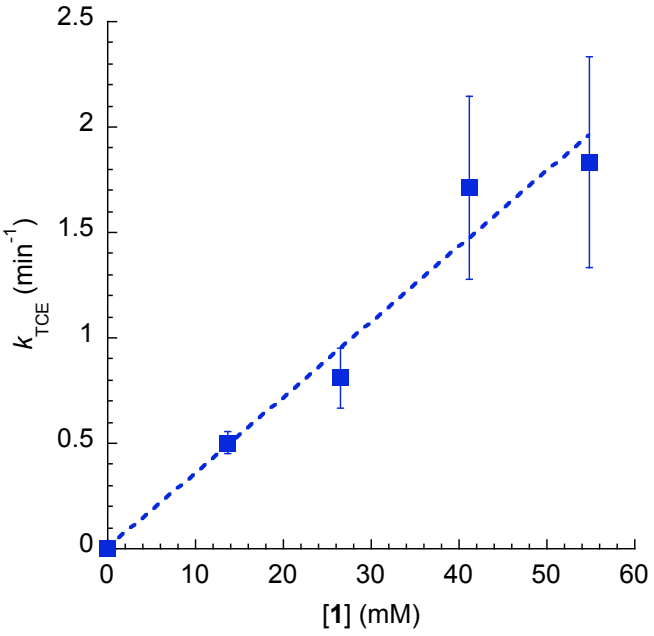

Figure 3.4. Dependence of TCE decay values (■, k_{TCE}, R^2=0.96) on [**1**]. Initial TCE concentrations were 2.3-2.7 mM for all trials.

The photochemical reaction between **1** and CE substrates was also found to be first-order with respect to CE (Figure 3.5, Figure 3.6, Figure 3.7, and Figure 3.8). The fastest phototransformation rate was observed for the degradation of TCE (k_{TCE}), followed by tDCE (k_{tDCE}), cDCE (k_{cDCE}), and VC (k_{VC}). The relative rates, determined using a combination of kinetic methods (monitoring by headspace GC-MS analysis and ^{1}H NMR spectroscopy), were found to be 220:30:9:1. The rate constants determined for each CE substrate is summarized in Table 3.5. These data clearly show that a decrease in the degree of chlorination of the CE substrate leads to a decrease in the rate of reaction between the CE and **2**. The observed rates of substrate decay are about 50% lower for ^{1}H NMR experiments due to the difference in the reaction vessels (glass of the sample tube and distance from the photoreactor) used for ^{1}H NMR and GC-MS experiments.

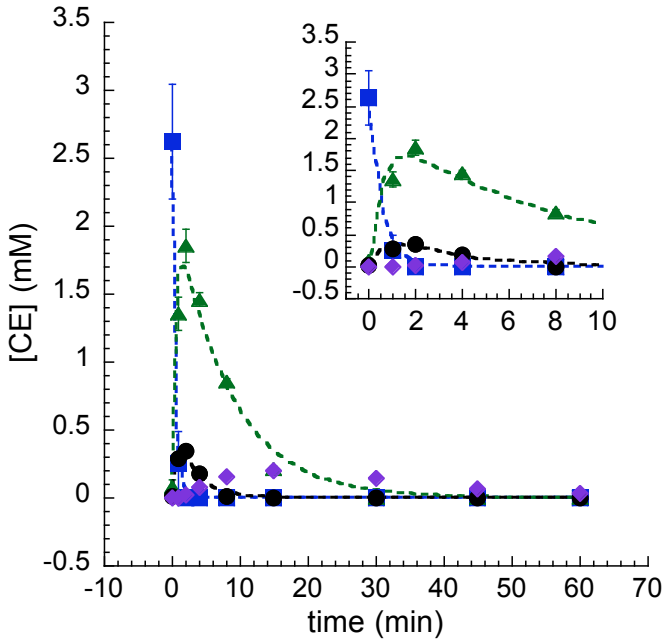

Figure 3.5. Decay of TCE (■, R^2=0.99) upon photolysis at 360 nm with **1** (52.3 mM). The photoproducts observed by GC-MS are cDCE (▲, R^2=0.97) and tDCE (•, R^2=0.96). cDCE and tDCE further react with **1** to generate VC (◆).

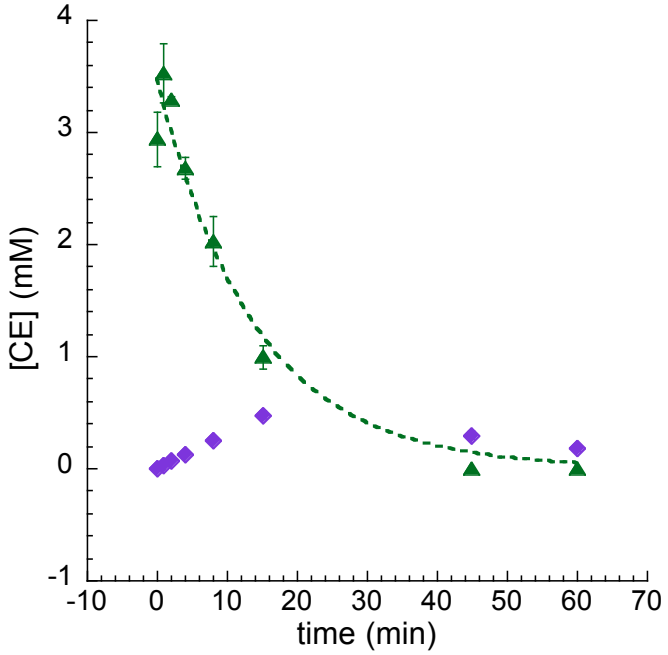

Figure 3.6. Decay of cDCE (▲, R^2=0.96) upon photolysis at 360 nm with **1** (52.3 mM). The only observed photoproduct by GC-MS is VC (◆).

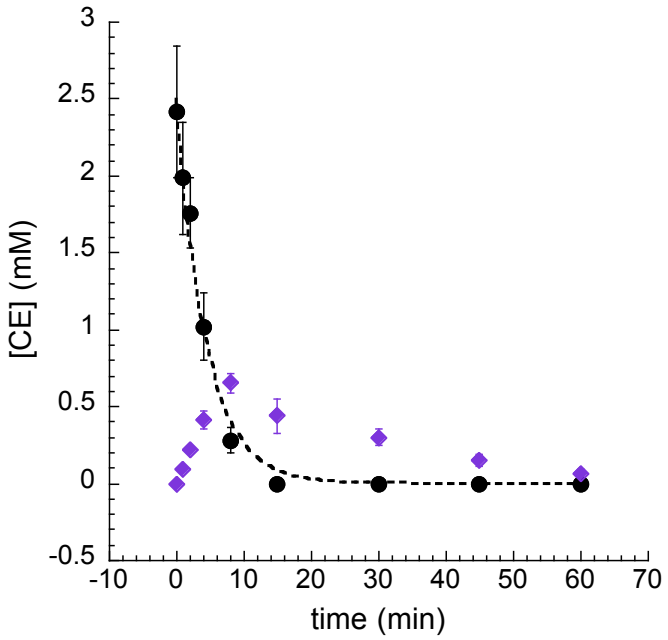

Figure 3.7. Decay of tDCE (•, R^2=0.99) upon photolysis at 360 nm with **1** (57.3 mM). The only observed photoproduct by GC-MS is VC (◆).

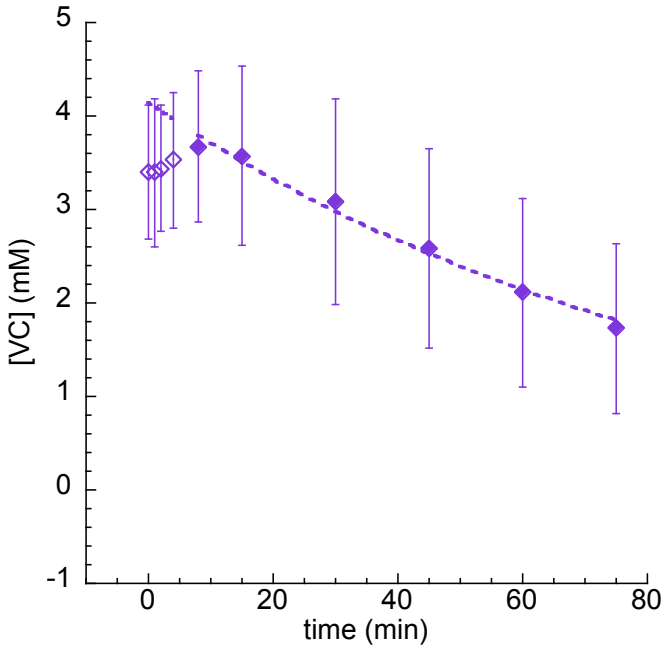

Figure 3.8. Decay of VC (◆, R^2=0.99) upon photolysis at 360 nm with **1** (52 mM), observed by ^{1}H NMR. These data were fit beginning with the 8 minute time point (solid) to allow for temperature equilibration between the sample and the NMR probe.

Table 3.5. Observed rate constant values (10^{-3} s^{-1}) for the reaction of CEs with **1** (56 mM). The measured irradiance in the GC-MS experiments was 9.44×10^{-7} photons/molecule min.

analysis method	rate constant (10^{-3} s^{-1})			
	TCE (k_{TCE})	tDCE (k_{tDCE})	cDCE (k_{cDCE})	VC (k_{VC})
GC-MS	30 ± 10	3.8 ± 0.2	1.2 ± 0.07	- [a]
^{1}H NMR	- [a]	1.7 ± 0.2	0.78 ± 0.1	0.18 ± 0.07

[a] Not measured

Because stepwise dechlorination is observed from the photochemical reaction between **1** and CE substrates, the origin of the H incorporated in volatile photoproducts was examined. To probe whether the H originated from the hydride ligands of **1**, $(dmpe)_2FeD_2$ (**1-D$_2$**) was synthesized (84% **1-D$_2$**, 16% **1** by ^{1}H NMR). Incorporation of deuterium into volatile photoproducts was clearly observed (Figure 3.9), and the amount of deuterium incorporation was calculated from the GC-MS chromatograms using a matrix method. The observed photoproducts are summarized in Table 3.6. The data were consistent with the major DCE product of the reaction being DCE-d_1 species. The presence of unlabelled **1** in the reaction mixture was likely the source of the unlabeled cDCE (12% cDCE-d_0) but cannot account for all of the unlabeled tDCE (35% tDCE-d_0). Currently, we do not yet understand why *cis*- and *trans*-DCE are formed with different levels of deuterium incorporation in these experiments, but it clearly points to a difference in the mechanism of formation of these two products.

For VC photoproducts, the major product observed (70%) is VC-d_2, presumably produced from the reaction between **1-D$_2$** and DCE-d_1. Minor product VC-d_1 (24%) was likely generated from either the reaction between **1** and DCE-d_1 or between **1-D$_2$** and DCE-d_0. VC-d_0 (6%) was also observed and presumed to form from the reaction

between **1** and DCE-d_0. No DCE-d_2 or VC-d_3 was observed, indicating that a maximum of only one chlorine was replaced with deuterium at each step of the reaction.

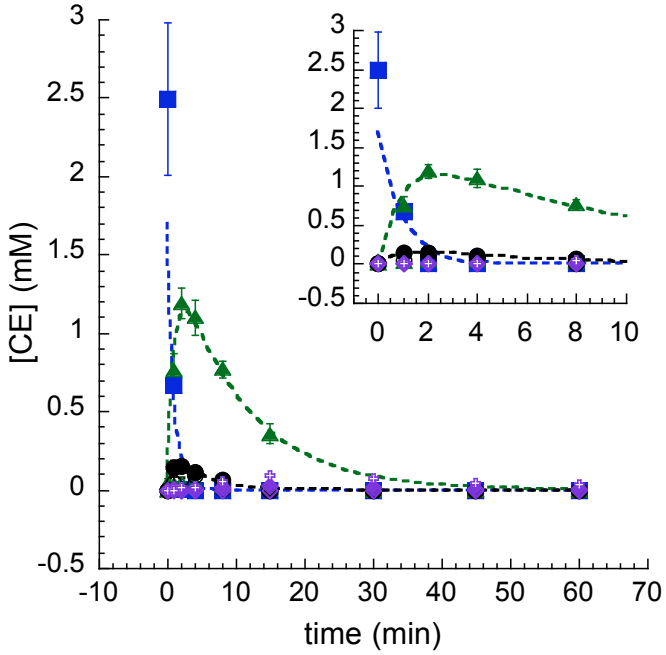

Figure 3.9. Decay of TCE (■, R^2=0.88) upon photolysis at 360 nm with **1-D$_2$** (52.3 mM). The observed photoproducts are cDCE (Δ), cDCE-d_1 (▲), tDCE (°), and tDCE-d_1 (•). These DCEs then decay to VC (purple), of which the major photoproduct is VC-d_2.

Table 3.6. Amount of deuterium incorporation (%) for the reaction of **1-D$_2$** and TCE over 60 minutes and an irradiation of 9.44×10^{-7} photons/molecule min.

CE	d_0	d_1	d_2	d_3
cDCE	12 ± 2	88 ± 2	0	
tDCE	35 ± 3	65 ± 3	0	
VC	5.7 ± 2	27 ± 4	70 ± 4	0

The incorporation of deuterium into volatile photoproducts indicated that the source of the incoming H atoms in the stepwise replacement of chlorine with hydrogen was the Fe-H moiety of **1**. Under the assumption that both hydrides of **1** are capable of being transferred to the olefin, the overall stoichiometry of **1** to CE substrate is 1.5:1.

While 1.5 equivalents of **1** are involved in the transformation of the CEs, the kinetic results, which show a first-order dependence in **1**, indicate that the reaction with a second equivalent of **1** occurs after the rate-determining step.

Replacing the hydride ligands of **1** with deuterium also caused the rate of TCE decay to decrease (Table 3.7), indicating the involvement of the Fe-H/D bond in the mechanism before or during the rate-determining step of the reaction between **1** and CE substrates. Whittlesey *et al*. found a weak isotope effect (k_H/k_D = 1.09 ± 0.07) for the reaction between H_2 and **2** (i.e. the k_r step in Scheme 3.4).[68] If this were the only isotope effect operating, it would predict a slightly *faster* reaction starting from **1-D$_2$**, as the reaction of **2** with D_2 would be less important than for the reaction of **2** with H_2. However, we observed the opposite, with an average 1.7-fold slower reaction starting with **1-D$_2$**. This seems to indicate that the observed isotope effect presented herein is related to different rates of release of H_2 and D_2 from the iron center (i.e. the k_f step of in Scheme 3.4). While the isotope effects associated with dihydrogen activation equilibria must be interpreted with care,[102] it is worth noting that D_2 has often been found to bind more tightly to metal centers than has H_2.[103-106]

Table 3.7. Observed rate constant values for reaction of TCE and either **1** (56 mM) or **1-D$_2$** (56 mM). The amount of irradiation was 9.44×10^{-7} photons/molecule min, and the initial TCE concentrations were 1.7-2.6 mM.

rate of decay (10^{-3} s^{-1})	k_1	k_2	k_3	k_4
[1]	24.7 ± 4.8	5.8 ± 4.5	2.07 ± 0.07	5.5 ± 4.8
[1-D$_2$]	15.0 ± 1.1	2.42 ± 0.1	1.6 ± 0.1	3.7 ± 0.8

In addition to the hydride of **1**, another potential source of hydrogen in the reaction between **1** and CE substrates is the solvent, cyclohexane. Because **1** has been shown to activate C-H bonds, including those of cyclohexane,[68] the reaction was

conducted in cyclohexane-d_{12} and analyzed via GC-MS for deuterium incorporation. Minimal deuterium incorporation was observed for the photoproducts of cDCE (96% cDCE-d_0), tDCE (81% tDCE-d_0), and VC (90% VC-d_0), indicating that cyclohexane does not contribute a significant amount of protons to the reaction between **1** and CE substrates.

Irradiation of **1** and CE substrates forms reactive intermediate **2** and releases H_2.[68] To probe the kinetic effect of this release, H_2 (or D_2) was bubbled into the system, and the effect on the rate of TCE decay was analyzed via GC-MS (Figure 3.10 and Figure 3.11). The results of these studies are summarized in Table 3.8. When H_2 is added, the degradation rate constant for TCE (k_{TCE}, sum of k_1 and k_2) decreased 7-fold and 5.9-fold upon addition of D_2. The decrease in k_{TCE} supports previous findings that H_2 is reversibly released in the photochemical reaction of **1**. This is also consistent with the observations of Whittlesey *et al*., who found that addition of H_2 and D_2 both increase the back reaction of **2** to **1**, which lowers the steady-state concentration of **2**.[68] They observed that adding H_2 to the system caused a decrease in the rate of formation of **2** and that adding D_2 instead of H_2 had little effect on the system.[68] No deuterium incorporation was observed in the reaction of **1** with D_2, indicating that the hydrogen atoms incorporated in the photoproducts are not from the released H_2.

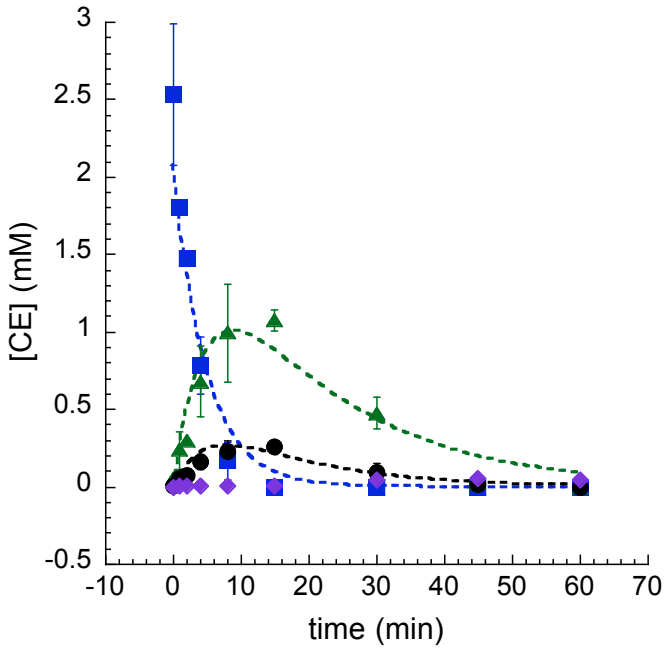

Figure 3.10. Decay of TCE (■) upon photolysis at 360 nm with **1** (52.3 mM) and 30 mL added H_2. The observed photoproducts are cDCE (▲) and tDCE (•), which both decay to VC (◆).

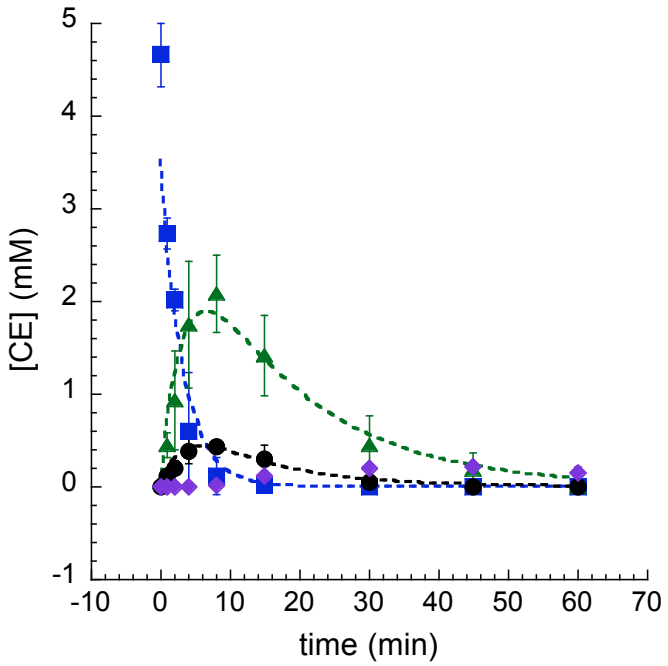

Figure 3.11. Decay of TCE (■) upon photolysis at 360 nm with **1** (52.3 mM) and 28 mL added D_2. The observed photoproducts are cDCE (▲) and tDCE (•), which both decay to VC (◆).

Table 3.8. Observed rate constant values for reaction of TCE and **1** (55 mM) with an addition of H_2 (30 mL) or D_2 (28 mL) gas. The amount of irradiation was 9.44×10^{-7} photons/molecule min, and initial TCE concentrations were 2.6-3.5 mM.

rate of decay (10^{-3} s^{-1})	k_{TCE}	k_{rel}
no gas	30 ± 10	1
H_2	4.3 ± 2.7	0.14
D_2	5.2 ± 2	0.17

Based on the kinetic data and isotope labeling studies, we propose the mechanism illustrated in Scheme 3.4. Upon introduction of light, complex **1** photodissociates, releasing H_2 and generating the reactive, 16 e^- intermediate **2**. This process proceeds with rate constant k_f, which is equal to the product of light flux at 360 nm (I_{360}, mmol photons/cm^2·s), molar extinction (ε_{360}, L/mol·cm), the quantum yield (Φ_{360}), and the natural logarithm of 10 to convert the decadic molar extinction to Naperian units. Intermediate **2** can one, react with H_2 to reform **1** (k_r); two, react with solvent (k_{solv}),[68] presumably forming an alkyl hydride complex analogous to those identified by Field *et al.*;[64] or three, react irreversibly with TCE (k_{TCE}). Upon reaction with TCE, we propose that the intermediate generated is the (dichlorovinyl)(chloro)iron complex **4**. Complex **4** is proposed to be in equilibrium with complex **5**, undergoing hydride/chloride exchange with an additional equivalent of **1** to form the (dichlorovinyl)(hydrido)iron complex **5** and the (hydrido)(chloro)iron complex **3**. Support for this comes from the observation of **3** by NMR spectroscopy, as well as the observation of the non-chlorinated analogues of **4** and **5** when VC is employed as the CE substrate. Such an exchange accounts for how complex **1** is the source of hydrogen atoms in the dechlorinated product. Complex **5** can undergo reductive elimination to form DCE products and reform **2**. The fact that

$(dmpe)_2Fe(vinyl)H$ was observed, while its chlorovinyl analogues were not, may indicate that the reductive elimination step is faster for the chlorovinyl complexes.

This mechanism correctly predicts the order in [**1**], [TCE], and the inhibition by added H_2. Upon initial consideration, this mechanism would seem to predict autocatalytic behavior, where the reaction would accelerate with time due to the reformation of active intermediate **2**. However, this is not observed because the majority of **2** goes on to react with solvent,[68] making the turnover number much less than 1.

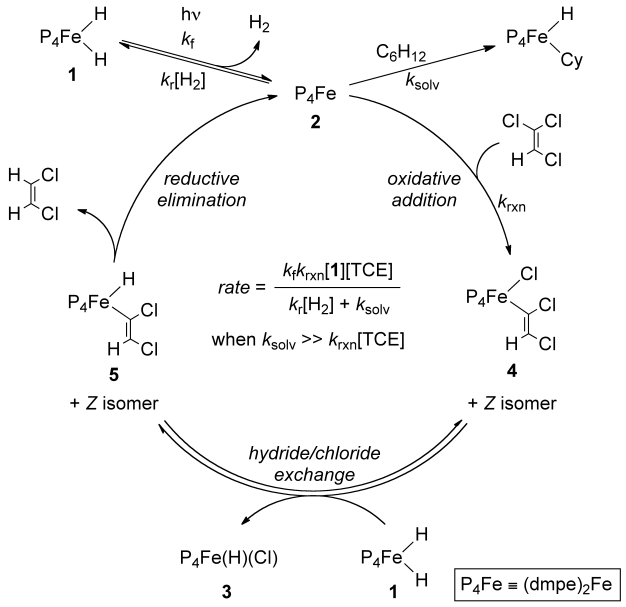

Scheme 3.4. Proposed mechanism and corresponding rate law for the photochemical conversion of TCE to cDCE mediated by **1**.

Considering the reaction between **2** and TCE, an alternative to the proposed C-Cl oxidative addition is an outer-sphere electron transfer to produce $(dmpe)_2Fe^+$ and a dichlorovinyl radical. These reactions typically produce low *cis*- to *trans*-DCE ratios (<5:1),[107] and the intermediate radicals can typically be trapped by D-atom donors such as THF-d_8.[108] When investigating the radical-based dechlorination of TCE by cobalamin, deuterium incorporation was found to occur in the majority of the products when high

(650 mM) trap concentrations were employed.[108] In the present work, while a low *cis*- to *trans*-DCE ratio (~4:1) was found, no deuterium incorporation was observed when the photoreaction of **1** and TCE was conducted in the presence of THF-d_8 (1 M), arguing strongly against the presence of chlorovinyl radical intermediates. We therefore favor the oxidative addition pathway presented in Scheme 3.4.

3.5 Conclusions

The reaction between photochemically generated **2** and CE substrates was found to proceed via a stepwise dechlorination mechanism, and increased substrate chlorination led to faster rates of CE substrate decay. A proposed mechanism accounts for the role of **1** as the source of hydrogen observed in photoproducts, as determined by deuterium labeling experiments. Opportunities for future study include evaluating **1** and its reaction with other chlorinated ground and drinking water contaminants, especially with a well defined model system that allows for increased control of reaction conditions and controlled generation of the reactive Fe^0 species.*

* This work was funded by the National Science Foundation (CHE-0809575). We thank Matt Hauwiller for his work developing the actinometry system and photolysis conditions, Dr. Alicia A. Peterson for initial studies, and Dr. Letitia Yao for helpful NMR discussions. Special thanks also to Tom Pundsack for his assistance in constructing the LED photoreactor.

Chapter 4

C-F and C-H activation of fluorinated benzenes by $(dmpe)_2FeH_2$ and $(dmpe)_2Fe$ (dmpe = 1,2-bis(dimethylphosphino)ethane)

4.1 Overview

The reaction of $(dmpe)_2FeH_2$ and hexa-, penta-, tetra-, and fluorobenzene substrates was found to proceed via two different pathways, C-F activation and photochemically induced C-H activation. Activation of C-F bonds was found to occur in reactions with hexa- and pentafluorobenzene. Introduction of light into the reaction system led to C-H activation for reactions with penta-, tetra-, and fluorobenzene substrates. The final products for all reactions were $(dmpe)_2Fe(aryl)H$ complexes as observed by ^{19}F and ^{31}P NMR studies, as well as trace amounts of singly defluorinated fluorobenzene substrates for reactions with hexa- and pentafluorobenzene observed by GC-MS studies. While C-H activation is the only pathway observed for tetrafluorobenzene and fluorobenzene substrates, competitive C-F and C-H activation occurs with pentafluorobenzene when 360 nm light is introduced into the system. A mechanism for both C-H and C-F activation pathways is proposed.

4.2 Introduction

C-F bonds are among the strongest bonds in organic chemistry. For instance, aromatic C-H bonds have a bond dissociation energy of 110 kcal/mol but aromatic C-F bonds require 127 kcal/mol of energy to break the bond.[65] Because of its strength and associated inertness, C-F bonds have been employed in a variety of sectors to impart specific functionality to a variety of substances.[109] The incorporation of C-F bonds into materials including Teflon® and perfluorooctanoic acid,[110] pharmaceuticals such as Lipitor®[111] and Paxil®,[112] and agrochemicals[113] (Figure 4.1) has led to myriad advances in their respective fields. However, the increase in use of these fluorinated compounds has led to their introduction into environmental systems, and the environmental fate of these compounds is important to understand.[19]

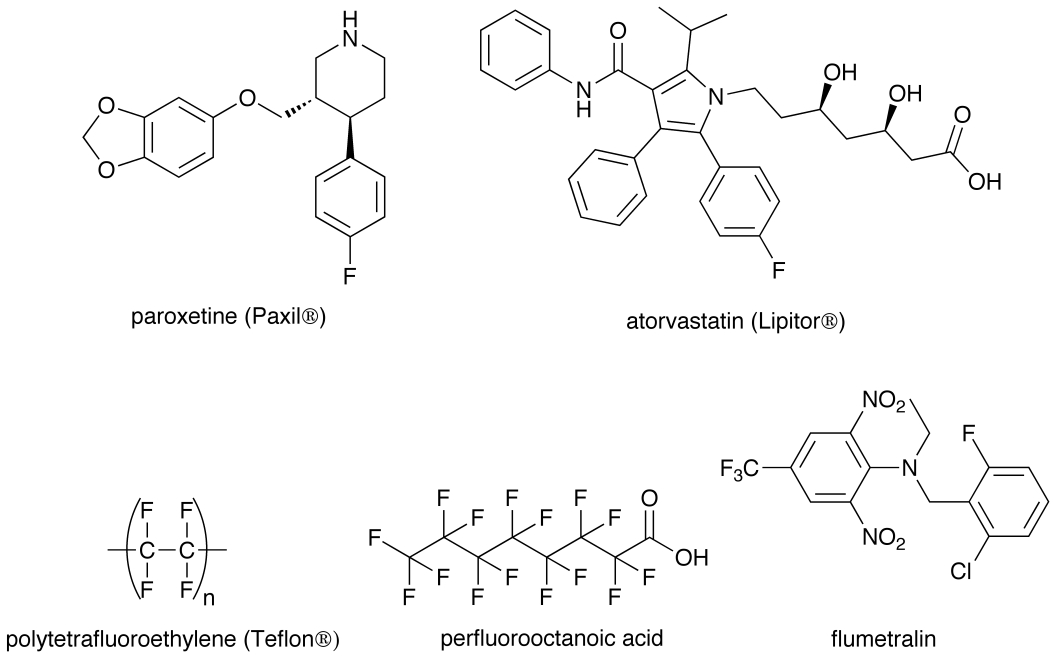

Figure 4.1. Representative organofluorine compounds. Paroxetine and atorvastatin are oft-prescribed pharmaceuticals, commonly known by their brand names. Polytetrafluoroethylene (Teflon®) and perfluorooctanoic acid (PFOA) are widely used for their unique non-stick material properties. Flumetralin is a pesticide used on tobacco plants.

Fluoroaromatic compounds are a specific subclass of fluorinated compounds, characterized by one or more fluorine substituents on an aromatic ring. In 2000, the capacity to generate over 35,000 tons of fluoroaromatic compounds was realized.[114] Past trends in fluoroaromatic production,[19] coupled with the use of fluoroaromatics as a popular pharmaceutical motif,[115] indicates that the production of these compounds has increased since 2000. Due to their widespread use and employment, fluoroaromatics are considered emerging environmental contaminants and have entered groundwater systems due to improper industrial disposal.[116] It is thus important to understand the environmental fate of these compounds and possible pathways for remediation from contaminated systems.

Several approaches have been employed to activate the C-F bond of fluoroaromatic compounds. One of the most common methods for remediation is hydrodehalogenation, or the replacement of the C-F bond with a C-H bond.[27] Biological,[117] photochemical,[118] and catalytic[119] methods have all shown an ability to activate the C-F bond, and transition metal-mediated activation is an especially robust area of research.[27]

Transition metal-mediated aromatic hydrodefluorination has been achieved with the use of expensive, relatively rare metal catalysts, including rhodium,[116, 120] platinum,[121] and ruthenium.[122, 123] These systems, while effective, are limited in their applicability by their rarity and expense. Thus, efforts to achieve hydrodefluorination of aromatic C-F bonds by more earth abundant, cheaper transition metals are a favorable endeavor.

One such transition metal that could be employed is iron, a transition metal that is much cheaper and more abundant. Zero-valent iron (Fe^0) has been employed in

permeable reactive barriers to remediate groundwater from a variety of contaminants[42] and has been shown to defluorinate aromatic C-F bonds.[66] Much of the research into defluorination by iron has focused on bulk iron systems, but these studies introduce bulk effects that can hinder understanding of hydrodefluorination events on a molecular level. Relatively few studies have examined the role of molecular iron complexes in aromatic hydrodefluorination,[124-126] and increased research into these types of systems is important to further understand the role of iron in defluorination processes.

To this end, a well defined iron complex, $(dmpe)_2FeH_2$ (**1**; dmpe = 1,2-bis(dimethylphosphino)ethane), is known to photochemically activate a variety of C-H and C-Cl bonds,[68, 87] but C-F bond activation has not been explored with this system. In this study, $(dmpe)_2FeH_2$ was photochemically activated and allowed to react with hexafluorobenzene (C_6F_6), pentafluorobenzene (C_6F_5H), tetrafluorobenzenes ($C_6F_4H_2$), and fluorobenzene (C_6FH_5) to evaluate its propensity toward C-F activation. C-F activation was observed to occur independent of photochemical activation with hexa- and pentafluorobenzene, while light-mediated C-H activation was observed for pentafluorobenzene, the tetrafluorobenzenes, and fluorobenzene. A proposed mechanism for both pathways was developed to account for experimental observations and the competition between both pathways for pentafluorobenzene substrates.

4.3 Experimental

4.3.1 General considerations

All experiments were conducted under anhydrous and anaerobic conditions using glovebox and Schlenk line techniques. All chemicals were purchased from Aldrich and used as received, unless otherwise noted. Solvents were dried prior to use.[99] All fluorobenzene substrates (Figure 4.2) were prepared by vacuum transferring the substrate after drying over P_2O_5. NMR spectra were collected on a Varian VXR-300 instrument. GC-MS data were collected on an Agilent 6890 GC system (Phenomenex ZB-624, 60 m x 0.32 mm i.d., 1.8 μm film thickness) with a 5973 mass selection detector, and data were analyzed with the accompanying software. The complexes $(dmpe)_2FeCl_2$, **1**, and **1-D$_2$** were synthesized and characterized following the methods described in Chapter 3.

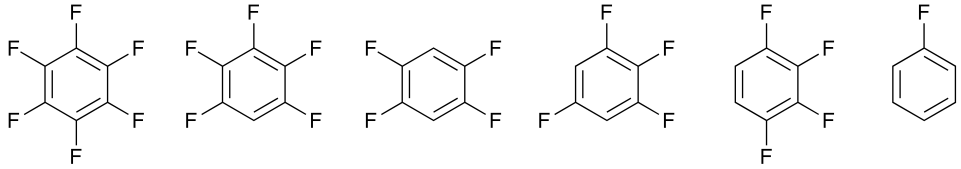

Figure 4.2. Fluorobenzene substrates investigated for reaction with **1**.

The 360 nm LED photoreactor used in these experiments was the same described and employed in Chapter 3. All photolysis experiments were conducted in the dark using the LED light source. The source was allowed to warm up for at least 30 minutes prior to photolysis.

4.3.2 GC-MS photolysis experiments

General. In the glovebox, a solution of **1** in cyclohexane (250 μL, 15.7 μmol) was placed in a glass crimp-cap vial fitted with a small stir bar. An aliquot of

fluorobenzene solution in cyclohexane (50 μL, 1.0 μmol) was added, and the vial was sealed. The final concentrations of **1** and the fluorinated substrate were 50 mM and 5.0 mM, respectively. The vial was allowed to stand for five minutes in the dark. A headspace sample (200 μL) was removed from the vial (t = 0 min), and then the vial was placed into the light source (36 LEDs) for one minute. At the t = 1 min time point, the vial was removed from the light source, another headspace sample was removed, and then the vial was placed again into the light source. The process was repeated for time points t = 0, 1, 2, 4, 8, 15, 30, 45, and 60 min. Headspace samples were analyzed using GC-MS. Control experiments were conducted in the same way, but samples were not exposed to the light source. Experiments were conducted in triplicate.

GC-MS analysis. All studies were conducted using headspace injections (200 μL) of crimp-capped vials containing the reaction mixture. All spectra were collected in scan mode, and peaks of interest were detected using extracted ion chromatograms set to detect m/z values of the molecular ions. Detected m/z values were 186 for C_6F_6, 168 for C_6F_5H, 150 for $C_6F_4H_2$ congeners, 132 for $C_6F_3H_3$ congeners, 96 for C_6FH_5, and 78 for C_6H_6. GC retention times were used to identify the products and were compared to the retention times of known standards.

Hexafluorobenzene. The volume was injected into the column at 140°C, and the sample ran for 11.5 minutes. The substrates C_6F_6 and C_6F_5H were able to be separated using this method.

Pentafluorobenzene. The volume was injected into the column at 40°C. The temperature of the column was held at 40°C for 5 min, ramped at 1°C/min until 60°C, and then ramped at 10°C/min until 70°C. The column was held at 70°C for 4

minutes. The substrates C_6F_5H, 1,2,3,4-$C_6F_4H_2$, 1,2,3,5-$C_6F_4H_2$, and 1,2,4,5-$C_6F_4H_2$ were all able to be separated using this method.

Tetrafluorobenzenes. The volume was injected into the column at 110°C, and the sample ran for 12.5 minutes. The substrates 1,2,3,4-$C_6F_4H_2$, 1,2,3,5-$C_6F_4H_2$, 1,2,4,5-$C_6F_4H_2$, 1,2,3-$C_6F_3H_3$, 1,2,4-$C_6F_3H_3$, and 1,3,5-$C_6F_3H_3$ were all able to be separated using this method.

Fluorobenzene. The volume was injected into the column at 40°C where it was held for 7 minutes. The temperature of the column was ramped at 40°C/min until 140°C. The column was held at 140°C for 5.5 minutes. The substrates C_6FH_5 and C_6H_6 were able to be separated using this method.

4.3.3 NMR photolysis experiments

In the glovebox, a solution of **1** in cyclohexane (500 μL, 31.4 μmol) was placed in a sealable NMR tube. An aliquot of fluorinated benzene solution in cyclohexane (100 μL, 2.0 μmol) was added, and the vial was sealed. The final concentrations of **1** and the fluorinated substrate were 50 mM and 5.0 mM, respectively. The sample tubes were protected from light outside of photolysis.

After sample preparation, ^{19}F and ^{31}P NMR spectra were collected (t = 0 min), and then the tube was placed into the photoreactor. After 5 minutes, the tube was removed from light and spectra collected. This process was repeated at all time points (t = 0, 5, 10, 20, 30, and 60 minutes). The non-photochemical (thermal) reaction for C_6F_5H was conducted in the same way, but the tube was not exposed to light. ^{19}F NMR shifts of complexes **3**-**9** were determined using comparisons to previously known compounds.

4.4 Results and Discussion

4.4.1 Reaction of 1 with C_6F_6

Reaction of **1** with C_6F_6 was observed to occur under ambient conditions and was unaffected by the presence of 360 nm light (Figure 4.3). GC-MS experiments showed that C_6F_6 reacted over one hour, and this decay was fit to a first-order function giving rate constant k_{C6F6}. The only product observed by GC-MS was C_6F_5H (Scheme 4.1) in ~10% conversion. The reaction was found to be independent of the presence of light because the rate of C_6F_6 substrate decay in the presence of **1** was the same with and without light (Table 4.1), and the same amount of C_6F_5H photoproducts was observed in both reactions. In the absence of **1**, no decay of C_6F_6 was observed to occur over 1 hour by GC-MS, and no C_6F_5H was detected, indicating that leaks or other loss processes were unimportant.

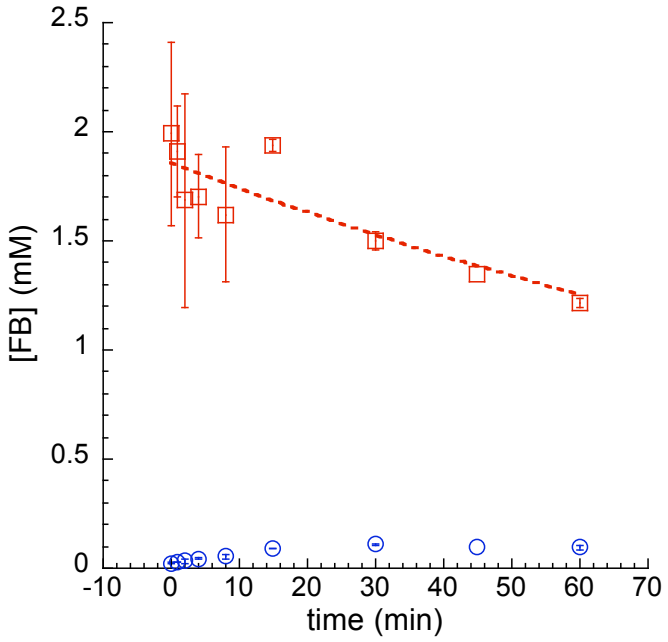

Figure 4.3. Decay of C_6F_6 (□, 5.0 mM) upon irradiation at 360 nm with **1** (58.5 mM). The only product observed by GC-MS was C_6F_5H (○).

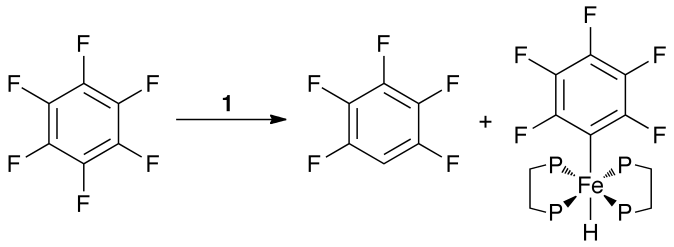

C_6F_6 C_6F_5H **3**

Scheme 4.1. Reaction of C_6F_6 and **1**. C_6F_5H was the only observed product by GC-MS, and complex **3** was the product observed by ^{19}F and ^{31}P NMR (**Figure 4.4**).

Table 4.1. Observed rate constant values (10^{-3} s^{-1}) for the reaction of C_6F_6 with **1** (50-56 mM) without and with light. The measured irradiance in the GC-MS experiments was 9.44×10^{-7} photons/molecule min.

	k_{C6F6}
1 + C_6F_6	1.14 ± 0.56
1 + C_6F_6 + hν	1.10 ± 0.91

The replacement of only one fluorine with a hydrogen is consistent with a hydrogenolysis pathway**.** In order to determine the source of the hydrogen in C_6F_5H products, the photolysis of C_6F_6 in the presence of **1-D₂** was conducted. Deuterium incorporation was observed to occur, as C_6F_5D was the observed product. Because no difference was observed in the rates of C_6F_6 decay with or without light in these studies (Table 4.1), **2** is likely not involved in the reaction between **1** and C_6F_6. However, the incorporation of deuterium from the iron starting material into photoproducts is consistent with a hydrogen/aryl exchange mechanism, similar to that observed in Chapter 3.

Previous studies of **1** with CE substrates showed that low mass balance in GC-MS experiments was often due to the generation of $(dmpe)_2Fe$-based photoproducts, and the

same is true of the reaction of **1** with C_6F_6. In the photoreaction, the $(dmpe)_2Fe(C_6F_5)(H)$ complex **3** was observed by ^{19}F and ^{31}P NMR spectroscopy (Figure 4.4). Because **2** is not the active species in this reaction, it is unlikely that C-F activation occurs via oxidative insertion of **2** into a C-F bond of C_6F_6.

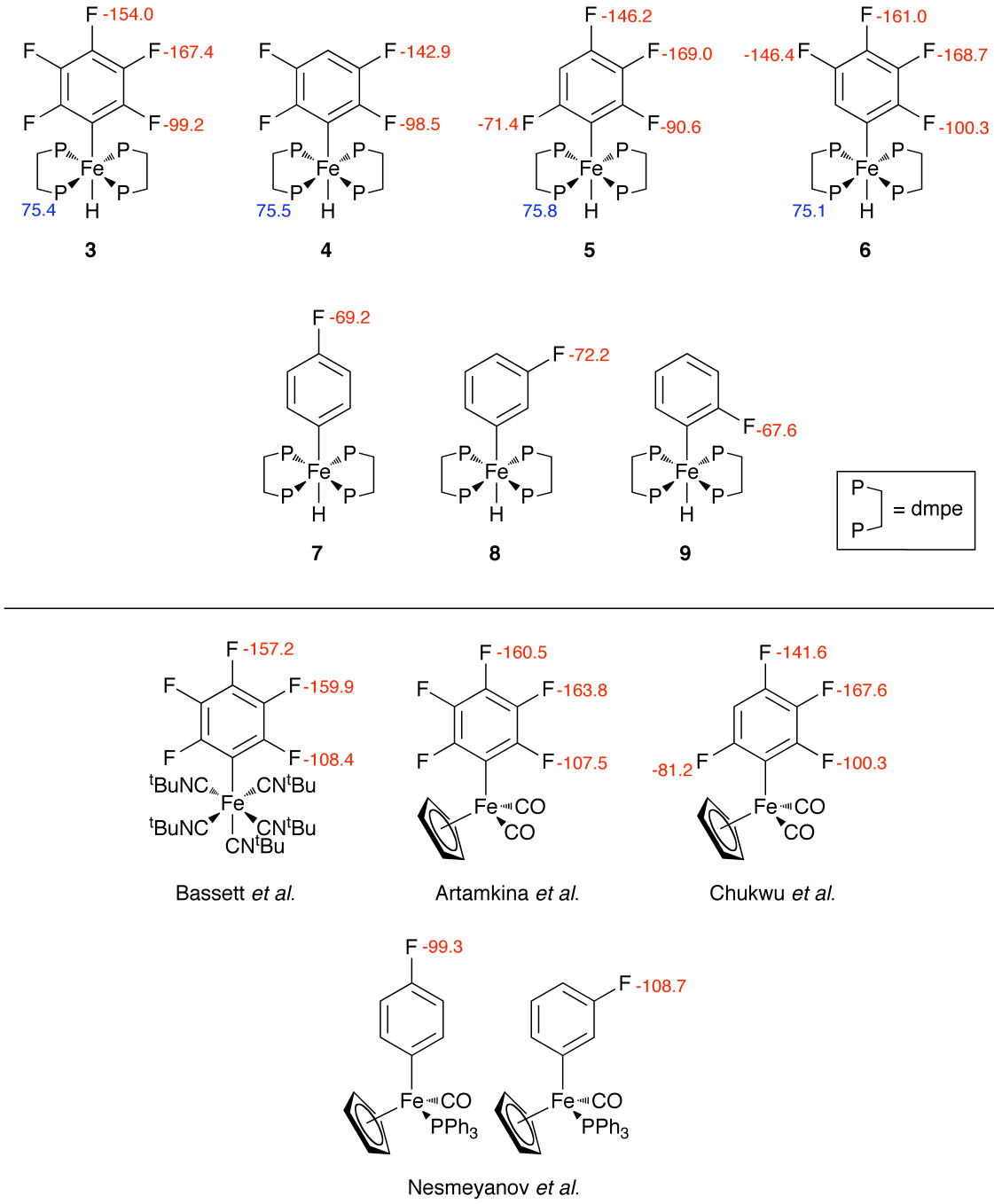

Figure 4.4. ^{19}F and ^{31}P NMR shifts for complexes **3-9**. ^{19}F NMR shifts are indicated in red, and ^{31}P NMR shifts are in blue. Complexes **3-6** were referenced to hexafluorobenzene. Complexes **7-9** have ^{31}P NMR shifts of ~75 ppm and were referenced to fluorobenzene. ^{19}F NMR shifts of complexes **3-9** were compared to reported iron complexes.[127-130]

Because strict oxidative addition similar to that observed in CE dechlorination with **1** is not predicted to play a role in the defluorination studied in the reaction with C_6F_6, the role of an outer-sphere mechanism was investigated. In order to evaluate the potential role of an outer-sphere electron transfer mechanism between **1** and C_6F_6, the reaction was conducted in the presence of THF-d_8 (a known radical trap). If pentafluorophenyl radicals were formed, they would be expected to abstract a D atom from THF-d_8. No deuterium incorporation was observed in the C_6F_5H photoproducts, arguing strongly against an outer-sphere mechanism for this reaction or any mechanism involving pentafluorophenyl radicals.

4.4.2 Reaction of 1 with C_6F_5H

Reaction of **1** with C_6F_5H was observed to occur with and without the presence of 360 nm light over 60 minutes (Figure 4.5). The only observed products by GC-MS were trace amounts of 1,2,4,5-$C_6F_4H_2$ and C_6F_6 (Scheme 4.2). No 1,2,3,5-$C_6F_4H_2$ or 1,2,3,4-$C_6F_4H_2$ photoproducts were observed in any trial.

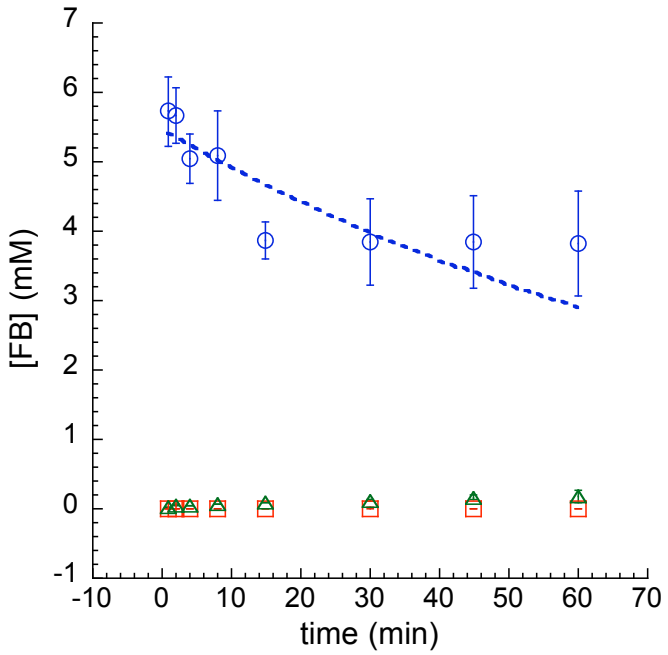

Figure 4.5. Decay of C_6F_5H (○, 5.0 mM) upon photolysis at 360 nm with **1** (54.9 mM). The only products observed by GC-MS were 1,2,4,5-$C_6F_4H_2$ (Δ) and C_6F_6 (□).

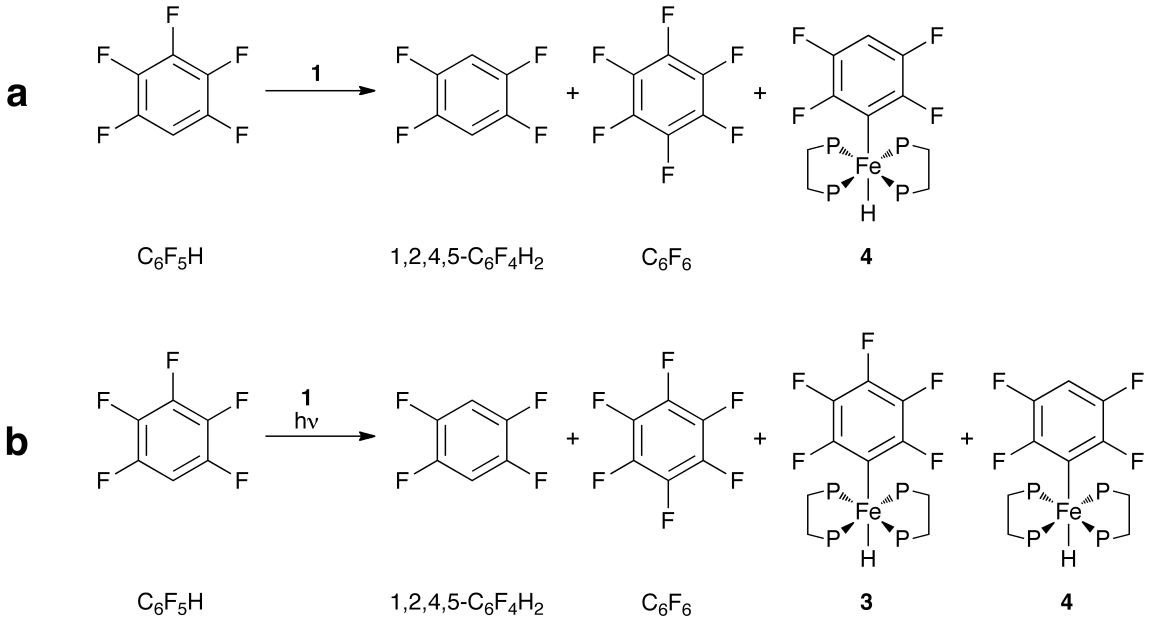

Scheme 4.2. Reactions of C_6F_5H and **1**. (a) The reaction without 360 nm light. (b) The reaction with 360 nm light. Both 1,2,4,5-$C_6F_4H_2$ and C_6F_6 were observed via GC-MS experiments, and complexes **3** and **4** were observed via ^{19}F and ^{31}P NMR (**Figure 4.4**).

Similar to the reaction of **1** with C_6F_6, the mass balance of the reaction by GC-MS was low (~10%), but ^{19}F and ^{31}P NMR studies showed a considerable generation of fluorine-containing $(dmpe)_2Fe$-based photoproducts. Specifically, complexes **3** and **4** were observed from the photochemical reaction of **1** and C_6F_5H (Scheme 4.2b). Complex **3**, also observed in the reaction of **1** and C_6F_6, is the C-H activation product of C_6F_5H. Because it is observed in photochemical experiments of **1** and C_6F_5H, the generation of **3** is likely the result of the reaction between 16-e^- intermediate **2** and C_6F_5H. Additionally, the reaction of **1** and C_6F_5H without light (and thus no production of **2**) shows no generation of **3** by NMR (Scheme 4.2a). Previous studies have shown that aryl C-H activation is readily observed with UV irradiation of **1**,[61, 64, 68] and generation of **3** from the photolysis of **1** and C_6F_5H is consistent with those findings.

The other $(dmpe)_2Fe$-based species observed in these photochemical reactions was complex **4**, which is also observed from the photolysis of **1** and 1,2,4,5-$C_6F_4H_2$ (*vide infra*). One can envision two pathways for the formation of this complex. The first is C-H activation of 1,2,4,5-$C_6F_4H_2$ by **2**. As evidenced by GC-MS experiments, 1,2,4,5-$C_6F_4H_2$ is generated in low concentrations upon photolysis, and the activation of the C-H bonds of 1,2,4,5-$C_6F_4H_2$ can occur readily in the experimental conditions employed to generate complex **4**. However, NMR experiments of **1** and C_6F_5H without light show only generation of complex **4** (Scheme 4.2a). Thus, because **2** is not formed, **4** is not likely to be generated via C-H activation in this reaction.

A second possible pathway is hydrogen/aryl exchange, similar to the process envisioned in the generation of **3** from the reaction of **1** and C_6F_6, where the Fe-H moiety of **1** is replaced with an aryl ligand (see Scheme 3.4 for an example of hydrogen/ligand

exchange). In this pathway, **1** reacts with C_6F_5H at the *para*-C-F bond to form complex **4**. Under photochemical conditions, both pathways could contribute to the formation of **4** in NMR experiments, but only this second pathway is likely to occur to generate **4** without the presence of light.

In dark control studies of C_6F_5H and **1** monitored by GC-MS, C_6F_5H decays at a rate (k_{C6F5H}) similar to that of C_6F_6 with and without light (Table 4.2). It is interesting to note that these three reactions are all predicted to proceed via **1** and the fluorobenzene substrate without **2**.

Table 4.2. Observed rate constant values (10^{-3} s^{-1}) for the reaction of C_6F_5H with **1** (50-56 mM) without and with light. The measured irradiance in the GC-MS experiments was 9.44×10^{-7} photons/molecule min.

	k_{C6F5H}
1 + C_6F_5H	1.77 ± 0.86
1 + C_6F_5H + hν	5.13 ± 1.7

When light was introduced into the reaction of **1** and C_6F_5H, the rate of C_6F_5H decay increased three-fold (Table 4.2). While k_{C6F5H} increases upon introduction of light, the amount of 1,2,4,5-$C_6F_4H_2$ and C_6F_6 generated (as detected by GC-MS) does not increase when light is added into the system. This suggests that volatile photoproducts 1,2,4,5-$C_6F_4H_2$ and C_6F_6 are generated by the "dark" reaction of **1** and C_6F_5H. The major change in the reaction when light is introduced is the generation of **2**, capable of C-H activation. Because this is the key difference between dark control and photochemical experiments, it is predicted that introducing light into the reaction promotes C-H activation to generate complex **3**. Thus, the observed k_{C6F5H} for the reaction with light is

the sum of the dark reaction (1.77×10^{-3} s^{-1}) and the C-H activation of C_6F_5H (3.36×10^{-3} s^{-1}). No decay of C_6F_5H is observed by GC-MS in the absence of **1**.

4.4.3 Reactions of 1 with $C_6F_4H_2$

Upon reaction with **1** and 360 nm light, all $C_6F_4H_2$ substrates decayed over 1 hour (Figure 4.6, Figure 4.7, and Figure 4.8). By GC-MS, no trifluorobenzene ($C_6F_3H_3$) photoproducts were observed in any trial. This indicates that the replacement of C-F bonds with C-H bonds (as observed in reactions of **1** with C_6F_6 and C_6F_5H) is not occurring in the reactions of **1** and any $C_6F_4H_2$ substrates but that the substrates *are* reacting and decaying with time. Because no $C_6F_3H_3$ photoproducts were observed, NMR experiments were conducted to determine the fate of the $C_6F_4H_2$ substrates. ^{19}F and ^{31}P NMR experiments confirm that C-H activation is occurring.

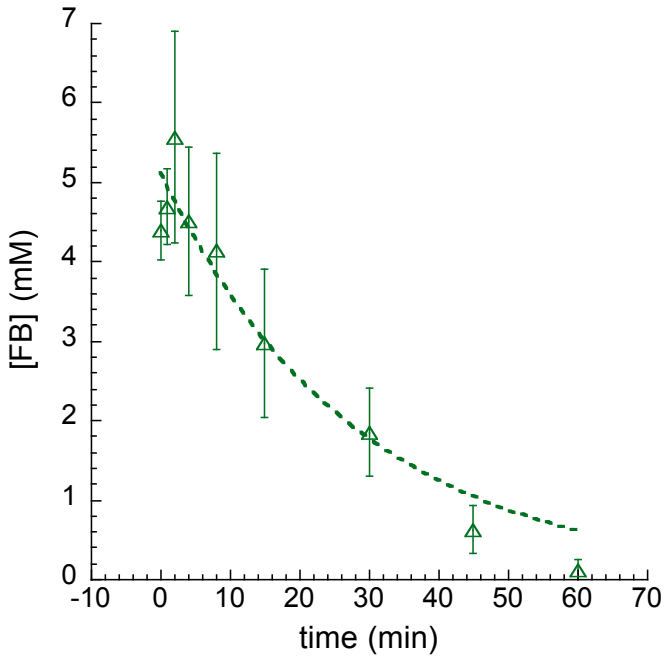

Figure 4.6. Decay of 1,2,4,5-$C_6F_4H_2$ (Δ, 5.0 mM) upon photolysis at 360 nm with **1** (50.7 mM). No $C_6F_3H_3$ photoproducts were observed by GC-MS.

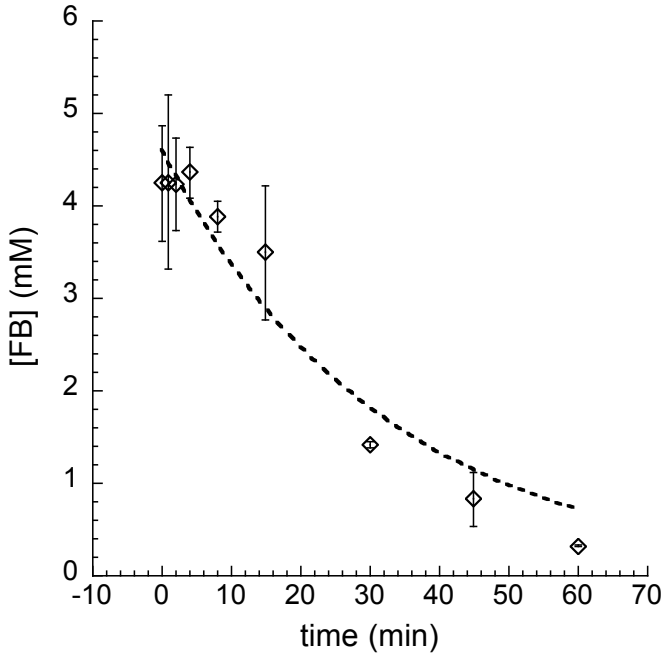

Figure 4.7. Decay of 1,2,3,5-$C_6F_4H_2$ (◇, 5.0 mM) upon photolysis at 360 nm with **1** (50.7 mM). No $C_6F_3H_3$ photoproducts were observed by GC-MS.

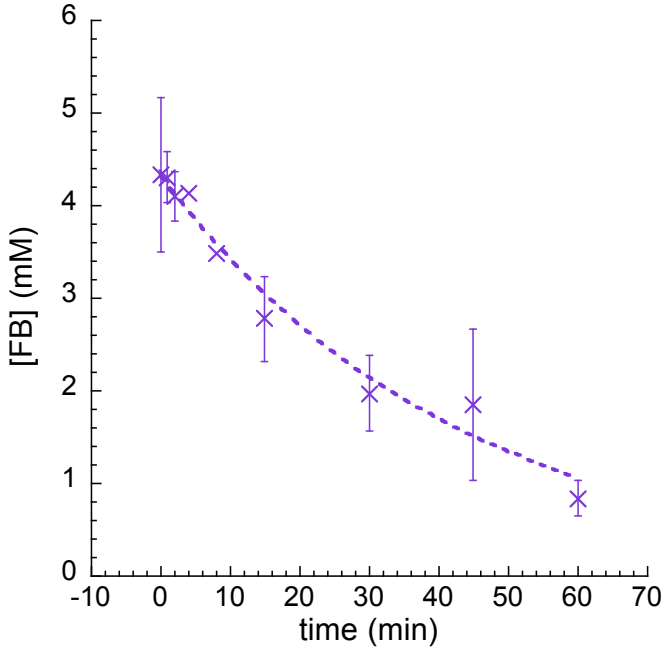

Figure 4.8. Decay of 1,2,3,4-$C_6F_4H_2$ (×, 5.0 mM) upon photolysis at 360 nm with **1** (50.7 mM). No $C_6F_3H_3$ photoproducts were observed by GC-MS.

In reactions of **1** and 1,2,4,5-$C_6F_4H_2$, only one photoproduct, complex **4**, is observed (Scheme 4.3) by NMR. Complex **4** is generated from the C-H activation of

1,2,4,5-$C_6F_4H_2$ by **2**, a process that has been well documented.[68] Because no reaction occurs between **1** and 1,2,4,5-$C_6F_4H_2$ without the presence of light (Table 4.3), reactive intermediate **2** is understood to be the active species in the system, inserting into the C-H bond of 1,2,4,5-$C_6F_4H_2$ to generate complex **4**.

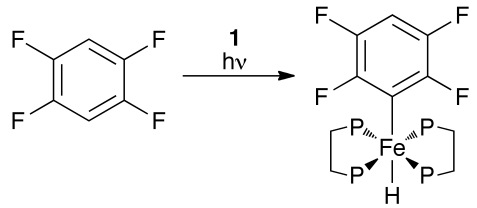

1,2,4,5-$C_6F_4H_2$ **4**

Scheme 4.3. Reaction of 1,2,4,5-$C_6F_4H_2$ and **1** with 360 nm light. Complex **4** was observed via ^{19}F and ^{31}P NMR (**Figure 4.4**).

Table 4.3. Observed rate constant values (10^{-3} s^{-1}) for the reaction of $C_6F_4H_2$ substrates with **1** (50.7 mM) without and with light. The measured irradiance in the GC-MS experiments was 9.44×10^{-7} photons/molecule min.

	1,2,4,5-$C_6F_4H_2$ ($k_{1,2,4,5\text{-}C6F4H2}$)	1,2,3,5-$C_6F_4H_2$ ($k_{1,2,3,5\text{-}C6F4H2}$)	1,2,3,4-$C_6F_4H_2$ ($k_{1,2,3,4\text{-}C6F4H2}$)
1 + $C_6F_4H_2$	0.345 ± 0.60	0.105 ± 0.13	0.0048 ± 0.24
1 + $C_6F_4H_2$ + hν	5.88 ± 2.08	5.17 ± 0.67	3.9 ± 1.95

The photochemical reactions of **1** with substrates 1,2,3,5-$C_6F_4H_2$ and 1,2,3,4-$C_6F_4H_2$ also proceed via C-H activation (Scheme 4.4 and Scheme 4.5). Complex **5** is the sole product observed by NMR for the reaction of **1** with 1,2,3,5-$C_6F_4H_2$, and complex **6** is the sole product for the identical reaction with 1,2,3,4-$C_6F_4H_2$. As with 1,2,4,5-$C_6F_4H_2$, no decay of 1,2,3,5-$C_6F_4H_2$ or 1,2,3,4-$C_6F_4H_2$ occurs in the absence of **1** or in the absence of light (Table 4.3).

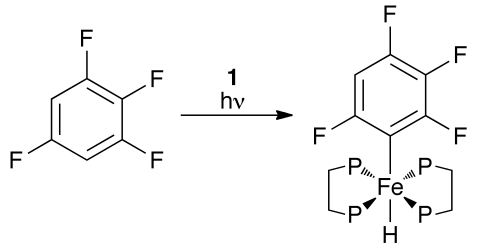

1,2,3,5-$C_6F_4H_2$ **5**

Scheme 4.4. Reaction of 1,2,3,5-$C_6F_4H_2$ and **1** with 360 nm light. Complex **5** was observed via ^{19}F and ^{31}P NMR (**Figure 4.4**).

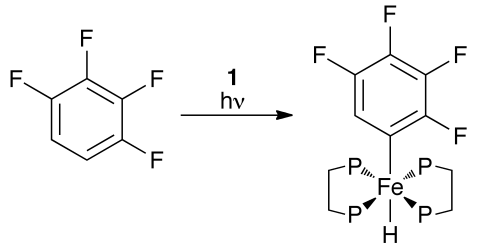

1,2,3,4-$C_6F_4H_2$ **6**

Scheme 4.5. Reaction of 1,2,3,4-$C_6F_4H_2$ and **1** with 360 nm light. Complex **6** was observed via ^{19}F and ^{31}P NMR (**Figure 4.4**).

4.4.4 Reactions of 1 with C_6FH_5

Upon irradiation with 360 nm light, **1** reacted with C_6FH_5 and decayed fully over one hour (Figure 4.9). Light was required for fluorobenzene decay, as C_6FH_5 did not decay in the absence of light (Table 4.4). Trace amounts of the defluorinated product, benzene, were observed via GC-MS, but the mass balance was quite low, similar to the observations of **1** and $C_6F_4H_2$. No decay of C_6FH_5 was observed without light.

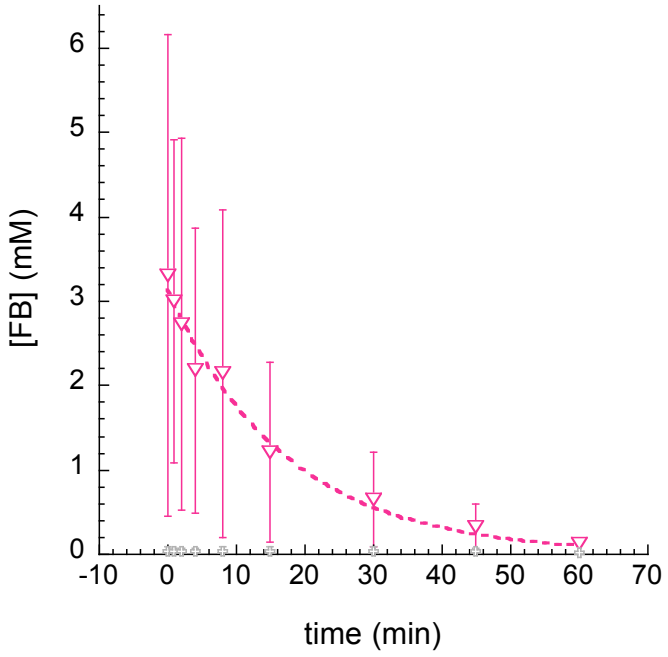

Figure 4.9. Decay of C_6FH_5 (▽, 3.0 mM) upon photolysis at 360 nm with **1** (50.7 mM). Trace amounts of benzene (✢) were observed by GC-MS.

Table 4.4. Observed rate constant values (10^{-3} s^{-1}) for the reaction of C_6FH_5 with **1** (50-56 mM) without and with light. The measured irradiance in the GC-MS experiments was 9.44×10^{-7} photons/molecule min.

	k_{C6FH5}
1 + C_6FH_5	$1.94 \times 10^{-15} \pm 0.0049$
1 + C_6FH_5 + hν	0.964 ± 0.18

^{19}F and ^{31}P NMR experiments were conducted to determine if $(dmpe)_2Fe$-based photoproducts accounted for the missing mass balance. Three signals were observed in the ^{19}F NMR spectrum, corresponding to three products, **7**, **8**, and **9** (Scheme 4.6). The production of three products is consistent with C-H activation of C_6FH_5 by **2**, as three unique C-H bonds are available for activation, the *para*-C-H bond (**7**), the *meta*-C-H (**8**), and the *ortho*-C-H bond (**9**). It is interesting to note that all three were generated,

suggesting that the fluorine on the aryl ring does not specifically direct photochemically induced C-H activation in this system.

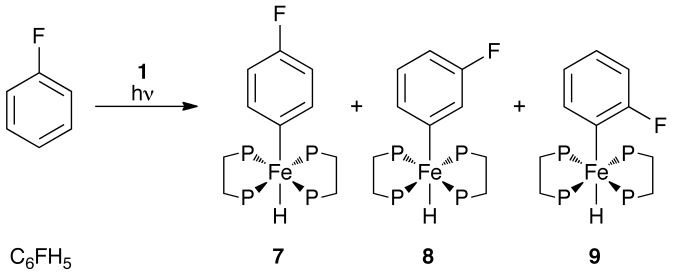

Scheme 4.6. Reaction of C_6FH_5 and **1** with 360 nm light. Complexes **7**, **8**, and **9** were observed via ^{19}F and ^{31}P NMR (**Figure 4.4**).

4.4.5 Mechanistic considerations

In comparing the reactions of **1** with the fluorinated substrates selected for these studies, it is apparent that two reactions are occurring (Scheme 4.7): C-F activation occurs for C_6F_6 and C_6F_5H, and C-H activation occurs for C_6F_5H, $C_6F_4H_2$, and C_6FH_5 substrates.

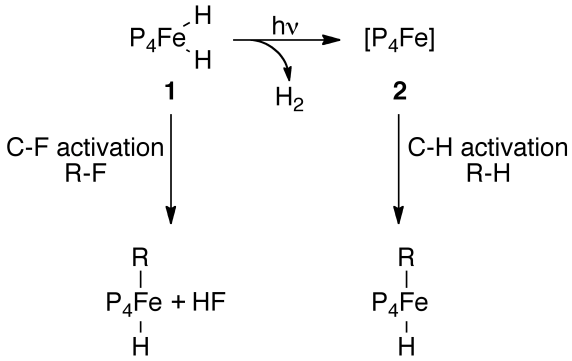

Scheme 4.7. Proposed C-F and C-H activation pathways for **1** and fluorobenzene substrates.

C-H activation of aryl substrates has been well studied in other systems[68] and is mediated by **2**, the 16-e$^-$ intermediate generated from **1**. In the photochemical reactions of C_6F_5H, $C_6F_4H_2$, and C_6FH_5 substrates, **2** preferentially inserts into the C-H bond of the

fluorobenzene substrate, generating *trans*-$(dmpe)_2Fe(aryl)(H)$ complexes **4-9**. The complexes are the final product of the C-H activation pathway and do not react further over 60 minutes. Because no volatile photoproducts are generated from this C-H activation pathway, the parent fluorobenzene substrate decays fully but no photoproduct is observed via GC-MS.

Unlike the C-H activation pathway mediated by light-induced **2**, light does not play a role in the second pathway, the C-F activation of C_6F_6 and C_6F_5H mediated by **1**. In this pathway, dihydride **1** reacts with fluorobenzene substrates to generate $(dmpe)_2Fe(aryl)H$ complexes **3** (for C_6F_6) and **4** (for C_6F_5H). This process also generates trace amounts of C_6F_5H from C_6F_6 and 1,2,4,5-$C_6F_4H_2$ from C_6F_5H.

Based on the collected NMR and GC-MS data, we propose the C-F activation mechanism illustrated in Scheme 4.8. Complex **1** and C_6F_6 react within the solvent cage to generate radical cation $(dmpe)_2FeH_2^{\cdot+}$ and radical anion $C_6F_6^{\cdot-}$. HF is lost from the cage, functioning as the thermodynamic sink for the system,[123] and the resulting $(dmpe)_2FeH^{\cdot}$ and $C_6F_5^{\cdot}$ radical species are formed. The two radical species recombine within the solvent cage, resulting in the generation of *trans*-$(dmpe)_2Fe(C_6F_5)H$ (**3**).

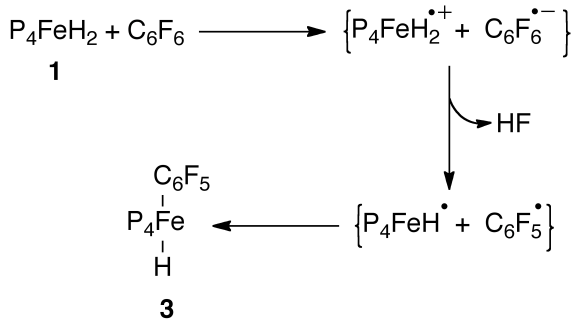

Scheme 4.8. Proposed mechanism for C-F activation pathway of **1** and C_6F_6 (adapted from ref. 123).

This mechanism accounts for the light independence of the C-F activation pathway, as light and **2** are not involved in the process, and the generation of **3** (or **4** for C_6F_5H). Additionally, only one C-F bond is activated in this mechanism, consistent with the observation that only one C-F bond is activated in C_6F_6 and only the *para*-C-F bond is activated in C_6F_5H. The preferential activation of the *para*-C-F bond in C_6F_5H has been observed in studies with analogous compound $(dmpe)_2RuH_2$ and was attributed to increased electron density of the *para*-C-F bond in the C_6F_5H radical anion.[123, 131]

One of the key components of the proposed mechanism is electron transfer that occurs exclusively within a solvent cage. As previously discussed, the reaction of **1** and C_6F_6 in the presence of THF-d_8 (a known radical trap) shows no deuterium incorporation into pentafluorobenzene photoproducts by GC-MS, indicating that outer-sphere electron transfer is not occurring. The proposed mechanism accounts for this observation since all electron transfer occurs within a solvent cage. Because no radical species escapes the solvent cage, there is no reaction between either the iron-based or fluorobenzene-based radicals and THF-d_8.

Whittlesey *et al*. reached similar conclusions for the reaction of $(dmpe)_2RuH_2$ and C_6F_6.[123] In their studies, conducting the reaction in the presence of 9,10-dihydroanthracene (another known radical trap) generated very little anthracene, supporting an electron-transfer mechanism that occurs exclusively within a solvent cage. Their studies also found small amounts of hydrodehalogenation products (C_6F_5H from C_6F_6, 1,2,4,5-$C_6F_4H_2$ from C_6F_5H, etc.). Additionally, the reaction of $(dmpe)_2RuD_2$ (analogous to **1-D$_2$**) with C_6F_6 showed generation of C_6F_5D, the same observations made in these studies, lending credence to the proposed mechanism.

Oxidative addition is unlikely to play a significant role in the reaction of **1** and C_6F_6 or the dark reaction with C_6F_5H. Oxidative addition would require either generation of reactive intermediate **2**, with a *cis*-divalent site available for oxidative insertion into the C-F bond, or generation of an iron(IV) intermediate. Because the reaction is not affected by light, and thus presence of **2**, oxidative addition via **2** is not a viable mechanistic pathway for this reaction. Generation of an iron(IV) intermediate is also unlikely, due to not only the dissimilar interactions of the hard Fe^{IV} center and the soft dmpe ligands but also the steric hindrance of coordinating the substrate to the six-coordinate Fe center. NMR experiments do not show any dissociation of the dmpe ligand, making dmpe dissociation to expose the iron center for oxidative addition unlikely. Thus, oxidative addition is not expected to contribute significantly to the C-F activation pathway observed in these studies.

4.5 Conclusions

The reaction between **1** and fluorobenzene substrates was found to proceed via two different pathways, C-F activation and photochemically induced C-H activation. C-F activation was found to occur in reactions of **1** and C_6F_6 and C_6F_5H, and an in-cage electron transfer mechanism for this process was proposed. C-H activation was observed for reactions of **1** with C_6F_5H, $C_6F_4H_2$, and C_6FH_5 substrates and proceeds via oxidative addition of the C-H bond to photochemically generated intermediate **2**. The final products for all reactions were $(dmpe)_2Fe(aryl)H$ complexes as observed by ^{19}F and ^{31}P NMR studies, as well as trace amounts of singly defluorinated fluorobenzene substrates for reactions of **1** with C_6F_6 and C_6F_5H observed by GC-MS studies. C-F activation is the exclusive pathway for C_6F_6, and C-H activation is the exclusive pathway for $C_6F_4H_2$ substrates. C-F activation is observed for C_6F_5H substrates, but C-H activation of C_6F_5H becomes a competitive pathway when 360 nm light is introduced into the system, generating $(dmpe)_2Fe$-based photoproducts from both pathways. Opportunities for future studies include expanding dark reactions of **1** with $C_6F_4H_2$ and other lower fluorinated substrates to see if C-F activation will occur. Studies with $(dmpe)_2RuH_2$ show that C-F activation of lower fluorinated substrates required longer reaction times,[123] so omitting light and extending reaction times or heating would be an important avenue for investigation.

References

1. R. E. Doherty. A history of the production and use of carbon tetrachloride, tetrachloroethylene, trichloroethylene and 1,1,1-trichloroethane in the United States: Part 1 - historical background; carbon tetrachloride and tetrachloroethylene. *Environ. Forensics*, 2000, **1**, 69-81.

2. R. E. Doherty. A history of the production and use of carbon tetrachloride, tetrachloroethylene, trichloroethylene and 1,1,1-trichloroethane in the United States: Part 2 - trichloroethylene and 1,1,1-trichloroethane. *Environ. Forensics*, 2000, **1**, 83-93.

3. M. J. Moran, J. S. Zogorski and P. J. Squillace. Chlorinated solvents in groundwater of the United States. *Environ. Sci. Technol.*, 2007, **41**, 74-81.

4. B. Sherwood Lollar, G. F. Slater, B. Sleep, M. Witt, G. M. Klecka, M. Harkness and J. Spivack. Stable Carbon Isotope Evidence for Intrinsic Bioremediation of Tetrachloroethene and Trichloroethene at Area 6, Dover Air Force Base. *Environ. Sci. Technol.*, 2000, **35**, 261-269.

5. P. L. Morrill, G. Lacrampe-Couloume, G. F. Slater, B. E. Sleep, E. A. Edwards, M. L. McMaster, D. W. Major and B. Sherwood Lollar. Quantifying chlorinated ethene degradation during reductive dechlorination at Kelly AFB using stable carbon isotopes. *J. Contam. Hydrol.*, 2005, **76**, 279-293.

6. R. D. Norris, *In-Situ Bioremediation of Ground Water and Geological Material: A Review of Technologies*, DIANE Publishing Company, Derby, PA, 1995.

7. US Environmental Protection Agency, CERCLA Priority List of Hazardous Substances, http://www.atsdr.cdc.gov/cercla/07list.html, Accessed 09/01/2009.

8. C.-L. Du and J.-D. Wang. Increased morbidity odds ratio of primary liver cancer and cirrhosis of the liver among vinyl chloride monomer workers. *Occup. Environ. Med.*, 1998, **55**, 528-532.

9. G. G. Bond, E. A. McLaren, F. L. Sabel, K. M. Bodner, T. E. Lipps and R. R. Cook. Liver and Biliary-Tract Cancer among Chemical Workers. *American Journal of Industrial Medicine*, 1990, **18**, 19-24.

10. P. Doyle, E. Roman, V. Beral and M. Brookes. Spontaneous abortion in dry cleaning workers potentially exposed to perchloroethylene. *Occup. Environ. Med.*, 1997, **54**, 848-853.

11. M. L. Lindbohm, H. Taskinen, M. Sallmen and K. Hemminki. Spontaneous-Abortions among Women Exposed to Organic-Solvents. *American Journal of Industrial Medicine*, 1990, **17**, 449-463.

12. U. F. Haustein and V. Ziegler. Environmentally induced systemic sclerosis-like disorders. *Int J Dermatol*, 1985, **24**, 147-151.

13. D. H. Garabrant, J. V. Lacey, Jr., T. J. Laing, B. W. Gillespie, M. D. Mayes, B. C. Cooper and D. Schottenfeld. Scleroderma and solvent exposure among women. *Am J Epidemiol*, 2003, **157**, 493-500.

14. A. M. Ruder. Potential health effects of occupational chlorinated solvent exposure. *Ann. N. Y. Acad. Sci.*, 2006, **1076**, 207-227.

15. F. D. Gilliland and J. S. Mandel. Serum perfluorooctanoic acid and hepatic enzymes, lipoproteins, and cholesterol: A study of occupationally exposed men. *American Journal of Industrial Medicine*, 1996, **29**, 560-568.

16. J. Belisle. Organic fluorine in human serum: natural versus industrial sources. *Science (Washington, D. C., 1883-)*, 1981, **212**, 1509-1510.

17. R. Renner. Growing Concern Over Perfluorinated Chemicals. *Environ. Sci. Technol.*, 2001, **35**, 154A-160A.

18. K. J. Hansen, L. A. Clemen, M. E. Ellefson and H. O. Johnson. Compound-Specific, Quantitative Characterization of Organic Fluorochemicals in Biological Matrices. *Environ. Sci. Technol.*, 2001, **35**, 766-770.

19. B. D. Key, R. D. Howell and C. S. Criddle. Fluorinated Organics in the Biosphere. *Environ. Sci. Technol.*, 1997, **31**, 2445-2454.

20. P. H. Howard and D. C. G. Muir. Identifying New Persistent and Bioaccumulative Organics Among Chemicals in Commerce. *Environ. Sci. Technol.*, 2010, **44**, 2277-2285.

21. G. Glod, U. Brodmann, W. Angst, C. Holliger and R. P. Schwarzenbach. Cobalamin-Mediated Reduction of cis- and trans-Dichloroethene, 1,1-Dichloroethene, and Vinyl Chloride in Homogeneous Aqueous Solution: Reaction Kinetics and Mechanistic Considerations. *Environ. Sci. Technol.*, 1997, **31**, 3154-3160.

22. S. Kliegman and K. McNeill. Dechlorination of chloroethylenes by cob(I) alamin and cobalamin model complexes. *Dalton Trans.*, 2008, 4191-4201.

23. V. Ochoa-Herrera, R. Sierra-Alvarez, A. Somogyi, N. E. Jacobsen, V. H. Wysocki and J. A. Field. Reductive Defluorination of Perfluorooctane Sulfonate. *Environ. Sci. Technol.*, 2008, **42**, 3260-3264.

24. C. J. Gantzer and L. P. Wackett. Reductive dechlorination catalyzed by bacterial transition-metal coenzymes. *Environ. Sci. Technol.*, 1991, **25**, 715-722.

25. S. Li and L. P. Wackett. Reductive dehalogenation by cytochrome P450CAM: Substrate binding and catalysis. *Biochemistry*, 1993, **32**, 9355-9361.

26. E. D. Kharasch and K. E. Thummel. Identification of Cytochrome P450 2E1 as the Predominant Enzyme Catalyzing Human Liver Microsomal Defluorination of Sevoflurane, Isoflurane, and Methoxyflurane. *Anesthesiology*, 1993, **79**, 795-807.

27. F. Alonso, I. P. Beletskaya and M. Yus. Metal-Mediated Reductive Hydrodehalogenation of Organic Halides. *Chem. Rev. (Washington, DC, U. S.)*, 2002, **102**, 4009-4091.

28. J. C. Hackett, T. T. Sanan and C. M. Hadad. Oxidative dehalogenation of perhalogenated benzenes by cytochrome P450 Compound I. *Biochemistry*, 2007, **46**, 5924-5940.

29. NRC, *Alternatives for Groundwater Cleanup*, National Academy Press, Washington, D.C., 1994.

30. C. G. Schreier and M. Reinhard. Catalytic hydrodehalogenation of chlorinated ethylenes using palladium and hydrogen for the treatment of contaminated water. *Chemosphere*, 1995, **31**, 3475-3487.

31. G. M. Masters, *Introduction to Environmental Engineering and Science*, Prentice Hall, Upper Saddle River, NJ, 1998.

32. D. M. Mackay and J. A. Cherry. Groundwater contamination: pump-and-treat remediation. *Environ. Sci. Technol.*, 1989, **23**, 630-636.

33. T. Gingrich, S. Suthersan, K. Houston and E. Panhorst. Groundwater remediation: The evolution of technology. *Pollution Engineering*, 2007, **39**, 24-29.

34. US Environmental Protection Agency, *Elements for Effective Management of Operating Pump and Treat Systems*, 2002.

35. J. Striegel, D. A. Sanders and J. N. Veenstra. Treatment of contaminated groundwater using permeable reactive barriers. *Environ. Geosci.*, 2001, **8**, 258-265.

36. A. D. Henderson and A. H. Demond. Long-term performance of zero-valent iron permeable reactive barriers: A critical review. *Environmental Engineering Science*, 2007, **24**, 401-423.

37. R. W. Puls, D. W. Blowes and R. W. Gillham. Long-term performance monitoring for a permeable reactive barrier at the US Coast Guard Support Center, Elizabeth City, North Carolina. *Journal of Hazardous Materials*, 1999, **68**, 109-124.

38. C. Vecitis, H. Park, J. Cheng, B. Mader and M. Hoffmann. Treatment technologies for aqueous perfluorooctanesulfonate (PFOS) and perfluorooctanoate (PFOA). *Frontiers of Environmental Science & Engineering in China*, 2009, **3**, 129-151.

39. M. Yang, Y. Zhang, B. Shao, R. Qi and H. Myoga. Precipitative Removal of Fluoride from Electronics Wastewater. *Journal of Environmental Engineering*, 2001, **127**, 902-907.

40. H. Hori, Y. Nagaoka, A. Yamamoto, T. Sano, N. Yamashita, S. Taniyasu, S. Kutsuna, I. Osaka and R. Arakawa. Efficient Decomposition of Environmentally Persistent Perfluorooctanesulfonate and Related Fluorochemicals Using Zerovalent Iron in Subcritical Water. *Environ. Sci. Technol.*, 2006, **40**, 1049-1054.

41. H. Hori, Y. Nagaoka, T. Sano and S. Kutsuna. Iron-induced decomposition of perfluorohexanesulfonate in sub- and supercritical water. *Chemosphere*, 2008, **70**, 800-806.

42. R. W. Gillham and S. F. O'Hannesin. Enhanced degradation of halogenated aliphatics by zero-valent iron. *Ground Water*, 1994, **32**, 958-967.

43. S. F. Cheng and S. C. Wu. The enhancement methods for the degradation of TCE by zero-valent metals. *Chemosphere*, 2000, **41**, 1263-1270.

44. J. W. Moon, H. S. Moon, H. Kim and Y. Roh. Remediation of TCE-contaminated groundwater using zero valent iron and direct current: experimental results and electron competition model. *Environmental Geology*, 2005, **48**, 805-817.

45. S. F. O'Hannesin and R. W. Gillham. Long-term performance of an in situ "iron wall" for remediation of VOCs. *Ground Water*, 1998, **36**, 164-170.

46. W. A. Arnold and A. L. Roberts. Pathways and kinetics of chlorinated ethylene and chlorinated acetylene reaction with Fe(O) particles. *Environ. Sci. Technol.*, 2000, **34**, 1794-1805.

47. T. J. Campbell, D. R. Burris, A. L. Roberts and J. R. Wells. Trichloroethylene and tetrachloroethylene reduction in a metallic iron-water-vapor batch system. *Environ. Toxicol. Chem.*, 1997, **16**, 625-630.

48. A. L. Roberts, L. A. Totten, W. A. Arnold, D. R. Burris and T. J. Campbell. Reductive Elimination of Chlorinated Ethylenes by Zero-Valent Metals. *Environ. Sci. Technol.*, 1996, **30**, 2654-2659.

49. R. Kober, O. Schlicker, M. Ebert and A. Dahmke. Degradation of chlorinated ethylenes by Fe0: inhibition processes and mineral precipitation. *Environ. Geol. (Berlin, Ger.)*, 2002, **41**, 644-652.

50. N. A. VanStone, R. M. Focht, S. A. Mabury and B. S. Lollar. Effect of iron type on kinetics and carbon isotopic enrichment of chlorinated ethylenes during abiotic reduction on Fe(0). *Ground Water*, 2004, **42**, 268-276.

51. L. A. Totten and A. L. Roberts. Calculated one- and two-electron reduction potentials and related molecular descriptors for reduction of alkyl and vinyl halides in water. *Crit. Rev. Environ. Sci. Technol.*, 2001, **31**, 175-221.

52. D. R. Burris, T. J. Campbell and V. S. Manoranjan. Sorption of Trichloroethylene and Tetrachloroethylene in a Batch Reactive Metallic Iron-Water System. *Environ. Sci. Technol.*, 1995, **29**, 2850-2855.

53. R. M. Allen-King, R. M. Halket and D. R. Burris. Reductive transformation and sorption of cis- and trans-1,2-dichloroethene in a metallic iron-water system. *Environmental Toxicology and Chemistry*, 1997, **16**, 424-429.

54. S. M. Nelson, C. M. Regan and M. Sloan. Activation of carbon-chlorine bonds in iron carbonyl complexes of chlorobutadienes. *J. Organomet. Chem.*, 1975, **96**, 383-389.

55. Y. Shi, M. Li, Q. Hu, X. Li and H. Sun. C-Cl Bond Activation of ortho-Chlorinated Imine with Iron Complexes in Low Oxidation States. *Organometallics*, 2009, **28**, 2206-2210.

56. S. D. Ittel, C. A. Tolman, A. D. English and J. P. Jesson. Novel carbon-hydrogen bond cleavage by bis(dimethylphosphino)ethane complexes of iron, ruthenium, and osmium. *J. Am. Chem. Soc.*, 1976, **98**, 6073-6075.

57. C. A. Tolman, S. D. Ittel, A. D. English and J. P. Jesson. The chemistry of 2-naphthyl bis[bis(dimethylphosphino)ethane] hydride complexes of iron, ruthenium, and osmium. 1. Characterization and reactions with hydrogen and Lewis base ligands. *J. Am. Chem. Soc.*, 1978, **100**, 4080-4089.

58. H. H. Karsch, H. F. Klein and H. Schmidbaur. Dimethylphosphinomethanide ion, (CH3)2P CH2-, a new ligand for transition metals. *Angew. Chem.*, 1975, **87**, 630-631.

59. J. Gotzig, A. L. Rheingold and H. Werner. (PMe3)3MS7 (M = Ru,Os): first sulfidometal complexes with a tridentate Sn2- ligand. *Angew. Chem.*, 1984, **96**, 813-814.

60. S. D. Ittel, C. A. Tolman, A. D. English and J. P. Jesson. The chemistry of 2-naphthyl bis[bis(dimethylphosphino)ethane] hydride complexes of iron, ruthenium, and osmium. 2. Cleavage of sp and sp3 carbon-hydrogen, carbon-oxygen, and carbon-halogen bonds. Coupling of carbon dioxide and acetonitrile. *J. Am. Chem. Soc.*, 1978, **100**, 7577-7585.

61. C. A. Tolman, S. D. Ittel, A. D. English and J. P. Jesson. Chemistry of 2-naphthyl bis[bis(dimethylphosphino)ethane] hydride complexes of iron, ruthenium, and osmium. 3. Cleavage of sp2 carbon-hydrogen bonds. *J. Am. Chem. Soc.*, 1979, **101**, 1742-1751.

62. A. D. Follett, Ph.D., University of Minnesota, 2006.

63. K. A. Thoreson, A. D. Follett and K. McNeill. Synthesis and characterization of pentaphosphino zero valent iron complexes and their corresponding iron(II)-chloride and hydride complexes. *Inorg. Chem.*, 2010, **49**, 3942-3949.

64. M. V. Baker and L. D. Field. Reaction of sp2 carbon-hydrogen bonds in unactivated alkenes with bis(diphosphine) complexes of iron. *J. Am. Chem. Soc.*, 1986, **108**, 7433-7434.

65. S. J. Blanksby and G. B. Ellison. Bond dissociation energies of organic molecules. *Accounts of Chemical Research*, 2003, **36**, 255-263.

66. A. Ghauch. Rapid removal of flutriafol in water by zero-valent iron powder. *Chemosphere*, 2008, **71**, 816-826.

67. M. V. Baker and L. D. Field. Reaction of carbon-hydrogen bonds in alkanes with bis(diphosphine) complexes of iron. *J. Am. Chem. Soc.*, 1987, **109**, 2825-2826.

68. M. K. Whittlesey, R. J. Mawby, R. Osman, R. N. Perutz, L. D. Field, M. P. Wilkinson and M. W. George. Transient and matrix photochemistry of Fe(dmpe)2H2 (dmpe = Me2PCH2CH2Me2): dynamics of C-H and H-H activation. *J. Am. Chem. Soc.*, 1993, **115**, 8627-8637.

69. E. V. Anslyn and D. A. Dougherty, *Modern Physical Organic Chemistry*, University Science Books, Sausalito, CA, 2006.

70. S. T. Belt, F. W. Grevels, W. E. Klotzbuecher, A. McCamley and R. N. Perutz. Intermediates in the time-resolved and matrix photochemistry of (h5-cyclopentadienyl)rhodium complexes. Roles of alkane activation and rhodium-rhodium bond formation. *J. Am. Chem. Soc.*, 1989, **111**, 8373-8382.

71. E. Rabinowitch and W. C. Wood. Collision mechanism and the primary photochemical process in solutions. *Trans. Faraday Soc.*, 1936, **32**, 1381-1387.

72. E. Rabinowitch and W. C. Wood. Properties of illuminated iodine solutions. I. Photochemical dissociation of iodine molecules in solution. *Trans. Faraday Soc.*, 1936, **32**, 547-556.

73. J. Franck and E. Rabinowitsch. Free radicals and the photochemistry of solutions. *Trans. Faraday Soc.*, 1934, **30**, 120-131.

74. A. B. Oelkers, E. J. Schutte and D. R. Tyler. Solvent cage effects: the influence of radical mass and volume on the recombination dynamics of radical cage pairs generated by photolysis of [CpCH2CH2N(CH3)C(O)(CH2)(n)CH3Mo(CO)(3)](2) (n=3, 8, 13, 18) (Cp = eta(5)-C5H4) complexes. *Photochemical & Photobiological Sciences*, 2008, **7**, 228-234.

75. D. E. Smith and C. B. Harris. Studies of Chemical-Reactivity in the Condensed Phase .3. Direct Measurement of Predissociation and Geminate Recombination Times for Iodine in Solution. *Journal of Chemical Physics*, 1987, **87**, 2709-2715.

76. A. B. Oelkers, L. F. Scatena and D. R. Tyler. Femtosecond pump-probe transient absorption study of the photolysis of [Cp ' Mo(CO)(3)](2) (Cp ' = eta(5)-C5H4CH3): Role of translational and rotational diffusion in the radical cage effect. *Journal of Physical Chemistry A*, 2007, **111**, 5353-5360.

77. B. J. Schwartz, J. C. King, J. Z. Zhang and C. B. Harris. Direct Femtosecond Measurements of Single Collision Dominated Geminate Recombination Times of Small Molecules in Liquids. *Chem. Phys. Lett.*, 1993, **203**, 503-508.

78. D. Raftery, E. Gooding, A. Romanovsky and R. M. Hochstrasser. Vibrational Product State Dynamics in Solution-Phase Bimolecular Reactions - Transient Infrared Study of Cn Radical Reactions. *Journal of Chemical Physics*, 1994, **101**, 8572-8579.

79. D. Booth and R. M. Noyes. Effect of viscosity on the quantum yield for iodine dissociation. *J. Am. Chem. Soc.*, 1960, **82**, 1868-1872.

80. A. G. Joly and K. A. Nelson. Metal carbonyl photochemistry in organic solvents: Femtosecond transient absorption and preliminary resonance Raman spectroscopy. *Chemical Physics*, 1991, **152**, 69-82.

81. T. Lian, S. E. Bromberg, M. C. Asplund, H. Yang and C. B. Harris. Femtosecond Infrared Studies of the Dissociation and Dynamics of Transition Metal Carbonyls in Solution. *The Journal of Physical Chemistry*, 1996, **100**, 11994-12001.

82. A. G. Joly and K. A. Nelson. Femtosecond transient absorption spectroscopy of chromium hexacarbonyl in methanol: observation of initial excited states and carbon monoxide dissociation. *The Journal of Physical Chemistry*, 1989, **93**, 2876-2878.

83. J. N. Bechara, S. E. J. Bell, J. J. McGarvey and J. J. Rooney. Ligand-field photolysis of the fischer complex, (OC)5W[double bond, length half m-dash]C(OMe)Ph: time-resolved resonance Raman spectroscopic evidence for alkyl-metal interaction following co photodissociation. *J. Chem. Soc., Chem. Commun.*, 1986, 1785-1787.

84. G. L. Geoffroy and R. Pierantozzi. Photochemistry of Transition-Metal Hydride Complexes .1. Photoinduced Elimination of Molecular-Hydrogen from [Irclh2(Pph3)3] and [Irh3(Pph3)3]. *J. Am. Chem. Soc.*, 1976, **98**, 8054-8059.

85. H. Itagaki, H. Murayama and Y. Saito. Photocatalysis of Rhcl(Pcy3)2 for Cyclohexane Dehydrogenation - Thermal-Dissociation of C-H Bond and Photoelimination of H2. *Bulletin of the Chemical Society of Japan*, 1994, **67**, 1254-1257.

86. C. Hall, W. D. Jones, R. J. Mawby, R. Osman, R. N. Perutz and M. K. Whittlesey. Matrix-Isolation and Transient Photochemistry of Ru(Dmpe)2h2 - Characterization and Reactivity of Ru(Dmpe)2 (Dmpe = Me2pch2ch2pme2). *J. Am. Chem. Soc.*, 1992, **114**, 7425-7435.

87. E. J. Pelton, D. A. Blank and K. McNeill. *Dalton Trans.*, 2013, **42**, 10121-10128.

88. N. P. Wells, B. W. Boudouris, M. A. Hillmyer and D. A. Blank. Intramolecular exciton relaxation and migration dynamics in poly(3-hexylthiophene). *Journal of Physical Chemistry C*, 2007, **111**, 15404-15414.

89. CRC Handbook of Chemistry and Physics, 84th Edition, Edited by David R. Lide. *J. Am. Chem. Soc.*, 2004, **126**, 1586.

90. D. Kowalska, X. Liu, U. Tripathy, A. Mahammed, Z. Gross, S. Hirayama and R. P. Steer. Ground- and Excited-State Dynamics of Aluminum and Gallium Corroles. *Inorg. Chem.*, 2009, **48**, 2670-2676.

91. S. E. Bromberg, T. Lian, R. G. Bergman and C. B. Harris. Ultrafast Dynamics of Cp*M(CO)2 (M = Ir, Rh) in Solution: The Origin of the Low Quantum Yields for C-H Bond Activation. *J. Am. Chem. Soc.*, 1996, **118**, 2069-2072.

92. B. L. Rowe, P. L. Toccalino, M. J. Moran, J. S. Zogorski and C. V. Price. Occurrence and potential human-health relevance of volatile organic compounds in drinking water from domestic wells in the United States. *Environmental Health Perspectives*, 2007, **115**, 1539-1546.

93. C. G. Schreier and M. Reinhard. Transformation of Chlorinated Organic-Compounds by Iron and Manganese Powders in Buffered Water and in Landfill Leachate. *Chemosphere*, 1994, **29**, 1743-1753.

94. J. Gotpagar, E. Grulke, T. Tsang and D. Bhattacharyya. Reductive dehalogenation of trichloroethylene using zero-valent iron. *Environmental Progress*, 1997, **16**, 137-143.

95. J. Hara, H. Ito, K. Suto, C. Inoue and T. Chida. Kinetics of trichloroethene dechlorination with iron powder. *Water Research*, 2005, **39**, 1165-1173.

96. D. H. Lim and C. M. Lastoskie. Density Functional Theory Studies on the Relative Reactivity of Chloroethenes on Zerovalent Iron. *Environ. Sci. Technol.*, 2009, **43**, 5443-5448.

97. M. Elsner, M. Chartrand, N. VanStone, G. Lacrampe Couloume and B. Sherwood Lollar. Identifying Abiotic Chlorinated Ethene Degradation: Characteristic Isotope Patterns in Reaction Products with Nanoscale Zero-Valent Iron. *Environ. Sci. Technol.*, 2008, **42**, 5963-5970.

98. K. A. Thoreson and K. McNeill. Vicinal dichlorine elimination at dichloroalkenes promoted by a well-defined iron(0) complex. *Dalton Trans.*, 2011, **40**, 1646-1648.

99. D. D. Perrin and W. L. F. Armarego, *Purification of Laboratory Chemicals*, 1997.

100. J. Chatt and R. G. Hayter. Some hydrido-complexes of Fe(II). *J. Chem. Soc.*, 1961, 5507-5511.

101. M. Montalti, *Handbook of Photochemistry*, CRC, Boca Raton, 2006.

102. G. Parkin. Applications of deuterium isotope effects for probing aspects of reactions involving oxidative addition and reductive elimination of H-H and C-H bonds. *Journal of Labelled Compounds & Radiopharmaceuticals*, 2007, **50**, 1088-1114.

103. B. R. Bender, G. J. Kubas, L. H. Jones, B. I. Swanson, J. Eckert, K. B. Capps and C. D. Hoff. Why does D-2 bind better than H-2? A theoretical and experimental study of the equilibrium isotope effect on H-2 binding in a M(eta(2)-H-2) complex. Normal coordinate analysis of W(CO)(3)(PCy3)(2)(eta(2)-H-2). *J. Am. Chem. Soc.*, 1997, **119**, 9179-9190.

104. B. E. Hauger, D. Gusev and K. G. Caulton. H-2 Binding to and Fluxional Behavior of Ir(H)2x(Ptbu2r)2 (X=Cl, Br, I R=Me, Ph). *J. Am. Chem. Soc.*, 1994, **116**, 208-214.

105. V. I. Bakhmutov, J. Bertran, M. A. Esteruelas, A. Lledos, F. Maseras, J. Modrego, L. A. Oro and E. Sola. Dynamic behavior in solution of the trans-hydridodihydrogen complex [OsHCl(eta(2)-H-2)(Co)(PiPr(3))(2)]: Ab initio and NMR studies. *Chemistry-a European Journal*, 1996, **2**, 815-825.

106. D. M. Heinekey. Transition metal dihydrogen complexes: isotope effects on reactivity and structure. *J. Labelled Compd. Radiopharm.*, 2007, **50**, 1063-1071.

107. A. D. Follett and K. McNeill. Reduction of trichloroethylene by outer-sphere electron-transfer agents. *J. Am. Chem. Soc.*, 2005, **127**, 844-845.

108. S. Kliegman and K. McNeill. Reconciling Disparate Models of the Involvement of Vinyl Radicals in Cobalamin-Mediated Dechlorination Reactions. *Environ. Sci. Technol.*, 2009, **43**, 8961-8967.

109. J. L. Kiplinger, T. G. Richmond and C. E. Osterberg. Activation of Carbon Fluorine Bonds by Metal-Complexes. *Chemical Reviews*, 1994, **94**, 373-431.

110. C. Lau, K. Anitole, C. Hodes, D. Lai, A. Pfahles-Hutchens and J. Seed. Perfluoroalkyl acids: A review of monitoring and toxicological findings. *Toxicological Sciences*, 2007, **99**, 366-394.

111. Y. Kawato, S. Chaudhary, N. Kumagai and M. Shibasaki. Streamlined Catalytic Asymmetric Synthesis of Atorvastatin. *Chemistry-a European Journal*, 2013, **19**, 3802-3806.

112. L. Czibula, A. Nemes, F. Sebok, C. Szantay and M. Mak. A convenient synthesis of (-)-paroxetine. *European Journal of Organic Chemistry*, 2004, 3336-3339.

113. G. Theodoridis, in *Advances in Fluorine Science*, ed. T. Alain, Elsevier, 2006, vol. Volume 2, pp. 121-175.

114. R. Bryant, *Pharmaceutical Fine Chemicals Global Perspectives 2000*, Informa Publishing Group Ltd., Kent, U.K., 2000.

115. D. O'Hagan. Fluorine in health care: Organofluorine containing blockbuster drugs. *Journal of Fluorine Chemistry*, 2010, **131**, 1071-1081.

116. R. Baumgartner, G. K. Stieger and K. McNeill. Complete Hydrodehalogenation of Polyfluorinated and Other Polyhalogenated Benzenes under Mild Catalytic Conditions. *Environ. Sci. Technol.*, 2013, **47**, 6545-6553.

117. P. W. Y. Chan, A. F. Yakunin, E. A. Edwards and E. F. Pai. Mapping the Reaction Coordinates of Enzymatic Defluorination. *J. Am. Chem. Soc.*, 2011, **133**, 7461-7468.

118. H. Hidaka, T. Tsukamoto, T. Oyama, Y. Mitsutsuka, T. Takamura and N. Serpone. Photoassisted defluorination of fluorinated substrates and pharmaceuticals by a wide bandgap metal oxide in aqueous media. *Photochemical & Photobiological Sciences*, 2013.

119. U. Jager-Fiedler, M. Klahn, P. Arndt, W. Baumann, A. Spannenberg, V. V. Burlakov and U. Rosenthal. Room-temperature catalytic hydrodefluorination of pentafluoro-pyridine by zirconocene fluoro complexes and diisobutylaluminumhydride. *Journal of Molecular Catalysis a-Chemical*, 2007, **261**, 184-189.

120. R. Baumgartner and K. McNeill. Hydrodefluorination and Hydrogenation of Fluorobenzene under Mild Aqueous Conditions. *Environ. Sci. Technol.*, 2012, **46**, 10199-10205.

121. Y. Sawama, Y. Yabe, M. Shigetsura, T. Yamada, S. Nagata, Y. Fujiwara, T. Maegawa, Y. Monguchi and H. Sajiki. Platinum on Carbon-Catalyzed Hydrodefluorination of Fluoroarenes using Isopropyl Alcohol-Water-Sodium Carbonate Combination. *Advanced Synthesis & Catalysis*, 2012, **354**, 777-782.

122. S. P. Reade, M. F. Mahon and M. K. Whittlesey. Catalytic Hydrodefluorination of Aromatic Fluorocarbons by Ruthenium N-Heterocyclic Carbene Complexes. *J. Am. Chem. Soc.*, 2009, **131**, 1847-1861.

123. M. K. Whittlesey, R. N. Perutz and M. H. Moore. Facile intermolecular aromatic C-F bond activation reactions of [Ru(dmpe)(2)H-2] (dmpe=Me(2)PCH(2)CH(2)PMe(2)). *Chemical Communications*, 1996, 787-788.

124. R. Rumin, K. Guennou, R. Pichon, F. Y. Petillon, K. W. Muir and D. S. Yufit. Carbon-fluorine bond activation by iron(I). C-F bond cleavage induced by addition of phosphines or thiols to a perfluorovinyldiiron complex. *J. Organomet. Chem.*, 1997, **533**, 177-185.

125. J. Vela, J. M. Smith, Y. Yu, N. A. Ketterer, C. J. Flaschenriem, R. J. Lachicotte and P. L. Holland. Synthesis and reactivity of low-coordinate iron(II) fluoride complexes and their use in the catalytic hydrodefluorination of fluorocarbons. *J. Am. Chem. Soc.*, 2005, **127**, 7857-7870.

126. X. Xu, H. Sun, Y. Shi, J. Jia and X. Li. Imine-assisted C-F bond activation by electron-rich iron complexes supported by trimethylphosphine. *Dalton Trans.*, 2011, **40**, 7866-7872.

127. J. M. Bassett, M. Green, J. A. K. Howard and F. G. A. Stone. Chemistry of Low-Valent Metal Isocyanide Complexes .2. Oxidative Reactions of Pentakis(Tert-Butyl Isocyanide)Iron with Alkyl, Allyl, Benzyl, Fluoroalkyl, and Pentafluorophenyl Halides, and with Trimethyloxonium Tetrafluoroborate and Diphenylacetylene - Evidence for Isocyanide Insertion Reactions, and the Molecular-Structure of [Fe(Cnbut)3-[1-4-Eta-C(=Nbut)=C(Ph)C(Ph)=C(=Nbut)]]M. *Journal of the Chemical Society-Dalton Transactions*, 1980, 1779-1788.

128. G. A. Artamkina, A. Y. Milchenko, I. P. Beletskaya and O. A. Reutov. Transition-Metal Carbonylates in Nucleophilic Aromatic-Substitution .1. Influence of Ionic Association on the Rates of Reactions with Perfluoroaromatic Substrates. *J. Organomet. Chem.*, 1986, **311**, 199-206.

129. R. Chukwu, A. D. Hunter, B. D. Santarsiero, S. G. Bott, J. L. Atwood and J. Chassaignac. Organometallic Complexes with Electronic Bridges .7. Electrochemical, Spectroscopic, and Structural Studies of Monometallic and Bimetallic Complexes of Iron - X-Ray Crystal-Structures of Cpfe(Co)2-C6f5, 4-Cpfe(Co)2-C5f4n, and 1,4-C6f4(Cpfe(Co)2)2. *Organometallics*, 1992, **11**, 589-597.

130. A. N. Nesmeyanov, I. F. Leshcheva, I. V. Polovyanyuk, Y. A. Ustynyuk and L. G. Makarova. NMR study of some cyclopentadienyliron carbonyl derivatives. *J. Organometal. Chem.*, 1972, **37**, 159-165.

131. M. B. Yim and D. E. Wood. Free radicals in an adamantane matrix. XII. EPR and INDO study of .sigma.*-.pi.* crossover in fluorinated benzene anions. *J. Am. Chem. Soc.*, 1976, **98**, 2053-2059.